c-Myc- driven nuclear repositioning of chromosome 11 in mouse plasmacytomas and its clinical significance

by

Patrapim Sunpaweravong

A Thesis submitted to the Faculty of Graduate Studies of

The University of Manitoba

In partial fulfilment of the requirements of the degree of

MASTER OF SCIENCE

Department of Human Anatomy and Cell Science

University of Manitoba

Winnipeg

Abstract

Deregulation of c-Myc, a nuclear transcription and replication factor, leads to multiple changes in three-dimensional (3D) nuclear telomere organization as well as selective chromosome movement and overlap. c-Myc drives neoplastic transformation in various tumour types including the mouse plasmacytoma (PCT), a B lineage tumour resulting from c-Myc–activating chromosomal translocation. Human telomeres are found to attach to the nuclear matrix and the telomeric shelterin protein telomere repeat-binding factor 2 (TRF2) interacts with the nuclear matrix protein lamin A/C. Based on the above, the hypotheses of this thesis are that activation of c-Myc results in re-positioning of chromosome 11 in mouse PreB *v-abl/myc* cells, immortalized pre-B lymphocytes tranfected with c-Myc, and that the interaction between telomeres, TRF2, and lamin A/C is a potential mechanism enabling the Myc-dependent relocation of chromosome 11. Following c-Myc upregulation, the repositioning of chromosome 11 was demonstrated as early as at the hour 1 timepoint. Concomitantly, c-Myc-activated PreB *v-abl/myc* cells exhibited a significant decrease in TRF2 protein levels as measured by quantitative fluorescent immunohistochemistry and a higher frequency of shorter telomeres. Significant decrease in average fluorescent intensities of the nuclear matrix protein lamin A/C in concordance with TRF2 was observed as early as at the 20 minute timepoint post Myc-deregulation. Similar results were observed in cells being processed either with or without nuclear matrix preparation. These results indicate that interactions between telomeres, TRF2, and lamin A/C appear to be involved in the repositioning of chromosome 11 in mouse PreB *v-abl/myc* cells after c-Myc upregulation. In *v-abl/myc*-induced accelerated mouse PCT development, alterations of subcytoband 11E2 (syntenic with human chromosome 17q25) always occur and frequent aberrations of cytoband 17q25 in humans are observed in multiple tumour types. Therefore further investigation of the human chromosomal region 17q25.3 was conducted and revealed a potential role of this region in non-small cell lung cancer (NSCLC) tumorigenesis. 3D telomeric organization was also confirmed as a

potential tool to classify NSCLC patient subgroups. Overall, this study enhances our understanding of the role of c-Myc activation in chromosome 11 repositioning in mouse PreB *v-abl/myc* cells and a possible interaction between telomeres, TRF2, and lamin A/C underlying this phenomenon. Additionally, the importance of human 17q25.3 is confirmed as a potential region involved in NSCLC tumorigenesis. A utilizationof the 3D telomeric organization profiles is demonstrated a tendency to categorize NSCLC patients into different prognostic subgroups, underscoring a potential future value of its clinical application.

Acknowledgements

This study was supported by the Canadian Institutes of Health Research (CIHR). Patrapim Sunpaweravong received a studentship grant from the Faculty of Medicine, Prince of Songkla University, Songkhla, Thailand. The author thanks Mary Cheang, a senior biostatistician, for statistical analysis of the data.

List of Tables

List of Figures

List of Abbreviations

2D	two-dimensional
3D	three-dimensional
4-HT	4-hydroxytamoxifen
µg	microgram
µl	microlitre
µm	micron, micrometre
aa	amino acids
AC	adenocarcinoma
ALK	anaplastic lymphoma kinase
ALT	alternative telomere lengthening
A-MuLV	Abelson murine leukemia virus
ANC	active nuclear compartment
a-NHEJ	alternative nonhomologous end-joining
ANOVA	analysis of variance
ATM	ataxia telangiectasia mutated
ATP	adenosine triphosphate
ATR	ataxia telangiectasia and Rad3-related protein
BBF	breakage bridge fusion
BC	British Columbia
Bcl-2	B-cell lymphoma 2
Bcl-XL	B-cell lymphoma-extra large
b/HLH	basic helix-loop-helix
b/HLH/LZ	basic helix-loop-helix leucine zipper
BSA	bovine serum albumin

CA	California
CDC	chromatin domain cluster
Cdc45	cell division cycle 45
CDKN1A	cyclin-dependent kinase inhibitor 1 A
CDKN2B	cyclin-dependent kinase inhibitor 1 B
ChIP	chromatin immunoprecipitation
CGH	comparative genomic hybridization
c-Myc	cellular Myc
CNBP	cellular nucleic acid binding protein
c-NHEJ	classical nonhomologous end-joining
CO	Colorado
CSK	cytoskeleton
CT	chromosome territory
CTD	C- terminal domain
CT–IC	chromosome territory – interchromatin compartment
DAPI	4',6-diamidino-2-phenylindole
DBD	DNA-binding domain
DDW	double-distilled water
DHFR	dihydrofolate reductase
DIC	differential interference contrast
DNA	deoxyribonucleic acid
DNase I	deoxyribonuclease
DSB	double-strand break
E-box	enhancer box
EE	extrachromosomal element

EGFR	epidermal growth factor receptor
Egr1	early growth response protein 1
EGTA	ethylenebis- (oxyethylenenitrilo) tetraacetic acid
EML4	echinoderm microtubule-associated protein-like 4
ER	estrogen receptor
ERK	extracellular signal-regulated kinase
Fbw7	F-box and WD repeat domain-containing 7
FISH	fluorescence *in situ* hybridization
GSK3	glycogen synthase kinase-3
GTP	guanosine triphosphate
HATS	histone acetyltransferase
HCl	hydrochloric acid
HDR	homology-directed repair
H&E	haematoxylin and eosin
HGPS	Hutchinson Gilford Progeria Syndrome
HLH	helix-loop-helix
hnRNP	heterogeneous nuclear ribonucleoprotein
hTERT	human telomerase reverse transcriptase
HTH	helix-turn-helix
IC	interchromatin compartment
ICN	interchromatin network
Ig	immunoglobulin
IgH	immunoglobulin heavy chain locus
IL	Illinois
INC	inactive nuclear compartment

ITL	interstitial telomere loop
ITS	interstitial telomeric sequence
kb	kilobase
kbp	kilobase pair
LZ	leucine zipper
MAPK	mitogen-activated protein kinase
Max	Myc-associated factor X
Mb	megabase
mBANDing	multi-colour banding
MBI	Myc box-I
MBII	Myc box-II
MBIII	Myc box-III
MBD	Myc-binding domain
Mbp	mega base pair
Mdm2	mouse double minute 2
MEF	mouse embryonic fibroblast
$MgCl_2$	magnesium chloride
miRNA	microRNA
Miz1	Msx-interacting-zinc finger 1
ml	millilitre
mM	millimolar
MO	Missouri
mRNA	messenger RNA
MYCN	Myc – neuroblastoma
MYCL	Myc – lung cancer

NA	not available
NaCl	sodium chloride
NaSCN	sodium thiocyanate
neg	negative
NHE III1	nuclease hypersensitivity element III1
NHEJ	nonhomologous end-joining
NLS	nuclear localization signal
nm	nanometre
NSCLC	non-small cell lung cancer
NTD	N- terminal domain
ODC	ornithine decarboxylase
ON	Ontario
OR	Oregon
PARP	poly (ADP-ribose) polymerase 1
PBS	phosphate-buffered saline
PCT	plasmacytoma
PI3K	phosphatidylinositol-3-kinase
Pin1	peptidylprolylisomerase NIMA-interacting 1
Pipes	Piperazine-N, N-bis (2- ethane- sulfonic acid)
PMSF	phenylmethylsulfonyl fluoride
PNA	peptide nucleic acid
pos	positive
PR	perichromatin region
pre-RC	pre-replicative complexes
P-TEFb	positive transcription elongation factor b

Q-FISH	quantitative fluorescence *in situ* hybridization
RFU	relative fluorescence unit
RNA	ribonucleic acid
RNA pol II	RNA polymerase II
RNase A	ribonuclease A
RRD	relative radial distribution
RT	room temperature
RTL	relative telomere length
Ser	serine
SNP	single nucleotide polymorphism
SQ	squamous cell carcinoma
SSC	saline sodium citrate buffer
STORM	super-resolution fluorescence imaging method
TAD	transcription activation domain
TBP	TATA-box-binding protein
Thr	threonine
TIFF	Tag Image File Format
TKI	tyrosine kinase inhibitor
TRF1	telomere repeat-binding factor 1
TRF2	telomere repeat-binding factor 2
UFB	ultra-fine bridges
UK	United Kingdom
UV	ultraviolet
VEGF	vascular endothelial growth factor
wt	wild-type

Chapter I : Introduction

Molecular characterization and functions of c-Myc

The *c-myc* oncogene, the cellular homologue of the avian myelocytomatosis virus transforming sequence, is located on human chromosome 8q24 and encodes a nuclear transcription and replication factor (Kuzyk and Mai, 2014). Deregulated expression of the c-Myc protein is sufficient to drive cell proliferation and apoptosis (Liang et al., 2009). c-Myc induces genomic instability by altering the stability of multiple genes and genomic sites, while also affecting non-coding RNAs (Huppi et al., 2008; Huppi et al., 2011). Myc can induce DNA damage at early replication fragile and common fragile sites and such replication stress-induced damage can result in chromosomal rearrangements (Barlow et al., 2013). Deregulation of c-Myc leads to multiple changes in cellular nuclear organization. It was shown to remodel the nuclear architecture, to alter the position of telomeres and chromosomes, and to promote neoplastic transformation (Mai, 2010; Gadji et al., 2011).

The *c-myc* oncogene was discovered in Burkitt's lymphoma, a B-lymphocyte malignancy, in which reciprocal chromosome translocation, t(14;8), involving the *c-myc* oncogene on chromosome 8 and the immunoglobulin (*Ig*) heavy or light chain genes at chromosomes 2, 14, and 22 is characteristic. Cloning the break-point of the translocation chromosomes revealed *c-myc*, the cellular homologue to *v-gagmyc* in avian myelocytomatosis retrovirus MC29 which causes spontaneous myelocytomatosis, a type of leukemia occurring in chickens (Neel et al.,1982; Vennstrom et al., 1982). The *c-myc* oncogene consists of 3 exons and 2 introns (Fig. 1 a) (Watt et al., 1983; Chen BJ et al., 2014).

Figure 1.

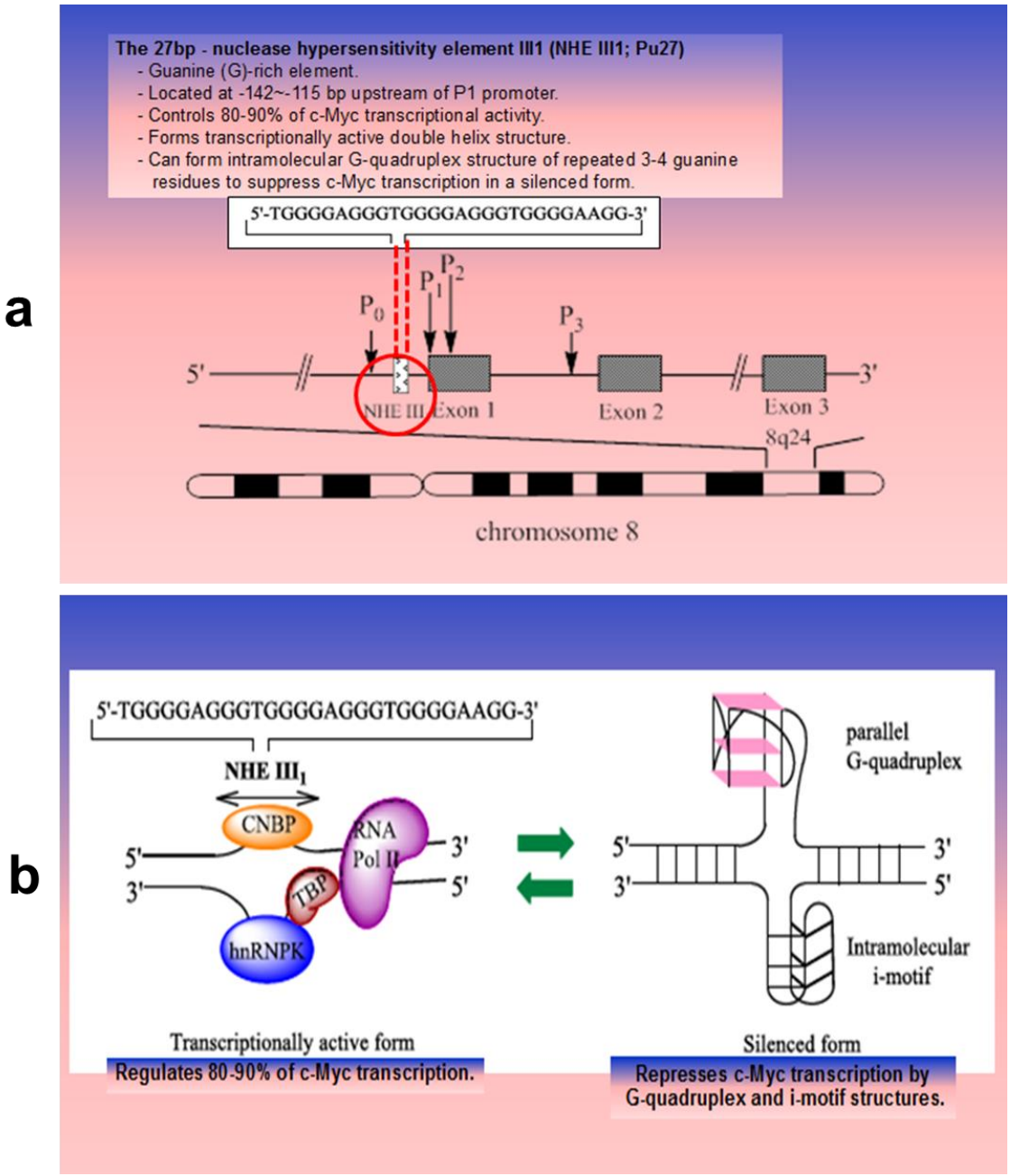

Figure 1. Structure of the *c-myc* gene. (a) *c-myc* gene structure; (b) equilibrium between two forms of NHE III 1 in a c-Myc gene. CNBP: cellular nucleic acid binding protein; hnRNP: heterogeneous nuclear ribonucleoprotein; NHE III1: nuclease hypersensitivity element III1; TBP: TATA-box-binding protein; RNA pol II: RNA polymerase II. (Adapted from Chen BJ et al., 2014).

The nuclease hypersensitivity element III1 (NHE III1) is a major regulator of *c-myc* transcription and controls 80-90% of the transcriptional activity of the *c-myc* gene (Islam et al., 2014). NHE III1 is located at -142~-115 bp upstream of the P1 promoter and forms a transcriptionally active double helix structure. An intramolecular G-quadruplex structure, consisting of repeated sequences with 3-4 guanine residues, can be formed by the guanine-rich strand of NHE III1, suppressing *c-myc* transcription in a silenced form (Fig. 1 b) (Cashman et al., 2008; Chen BJ et al., 2014).

c-myc encodes the c-Myc protein, a nuclear transcription and replication factor. The c-Myc protein harbours 2 sizes, 64 and 67 kDa phosphoproteins, both belonging to a basic helix-loop-helix leucine zipper (b/HLH/LZ) protein family and composed of 439 amino acids (aa), consisting of an N-terminal transactivation domain (NTD), a C-terminal domain (CTD), and a central region (Fig. 2) (Cashman et al., 2008; Chen BJ et al., 2014). The NTD contains a transcription activation domain (TAD) and 3 ~20 aa segments, which are Myc box-I (located at aa 45-63), -II (located at aa 129-143), and -III (located at aa 188-199). The Myc boxes are responsible for c-Myc regulation of transcription and transformation (Sakamuro and Prendergast, 1999; Delmore et al., 2011). The nuclear localization signal (NLS), an amino acid sequence of PAAKRVKLD responsible for protein import into the cell nucleus by nuclear transport, is located at aa 320-328 (Dang and Lee,1988). The CTD extends from aa 355-439 and is essential for the association with b/HLH/LZ-interacting proteins, especially the Myc-associated factor X (Max), the other central player of the network (Fig. 2). The c-Myc protein, mainly through its b/HLH domain and less importantly through the Myc-binding domain (MBD), can bind to DNA, while the LZ domain allows dimerization with Max. The Myc-Max heterodimerization plays a major role in transcription and is considered as a master regulatory factor of cell proliferation, metabolism, differentiation, and apoptosis (Pelengaris and Khan, 2003; Ponzielli et al., 2005; Cowling and Cole, 2006).

Figure 2.

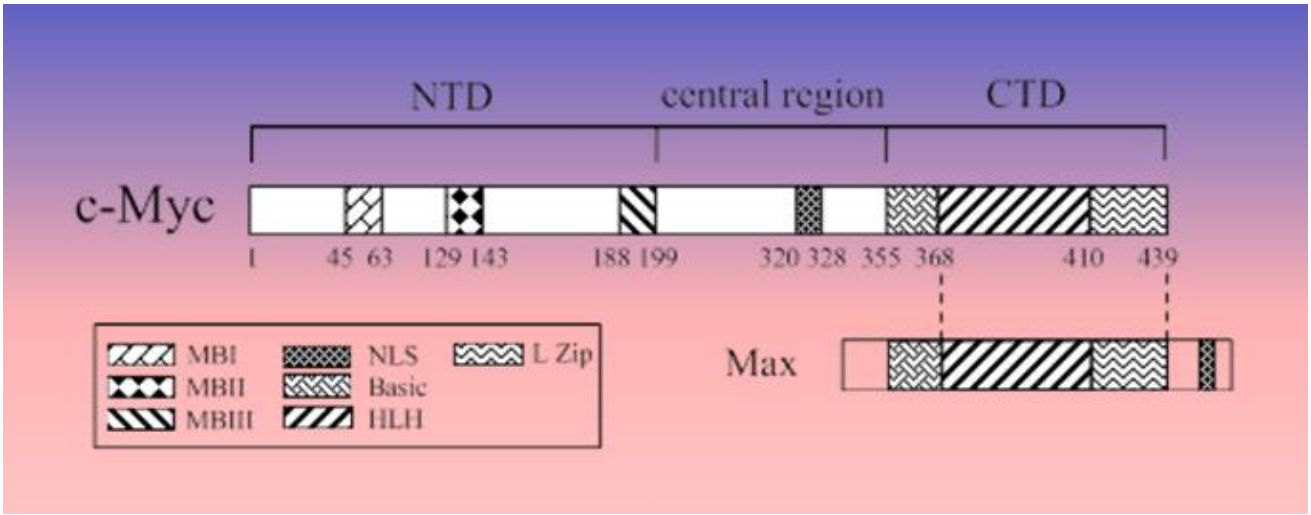

Figure 2. Structure of the c-Myc protein. NTD: N- terminal domain; CTD: C- terminal domain; MBI: Myc box-I; MBII: Myc box-II; MBIII: Myc box-III; NLS: nuclear localization signal; HLH: helix-loop-helix; L Zip: leucine zipper. (Chen BJ et al., 2014).

The c-Myc protein initiates its function by forming heterodimers with Max, which consequently bind to DNA sequences with the consensus CA(NN)TG, especially the conserved sequence element "CACGTG" termed enhancer boxes (E-boxes) at target promoters and regulates gene expression (Eilers and Eisenman, 2008). c-Myc activates transcription by recruitment of co-factors containing histone acetyltransferase (HATS) activity, which in turn mediates increased DNA accessibility. Therefore, in addition to its role as a classical transcription factor, c-Myc also functions to regulate the global chromatin structure by regulating histone acetylation both in gene-rich regions and at sites far from any known gene (Cotterman et al., 2008). To promote transcription elongation, Myc-Max, after binding to an E-box, recruits the elongation factor complex positive transcription elongation factor b (P-TEFb). The extreme amino-terminus of c-Myc binds cyclin T1, a part of the P-TEFb (Eberhardy and Farnham, 2002), which phosphorylates the CTD of RNA polymerase II (RNA pol II) at serine 2 and releases of RNA polymerase pausing, thereby promoting the transition from promoter binding to productive elongation (Fig. 3) (Tu et al.,

2015; Wolf et al., 2015). Therefore the release of RNA pol II from a paused position is a key mechanism of c-Myc's transcriptional activation (Rahl et al., 2010). Moreover, in addition to transcriptional activation of protein-encoding genes through RNA pol II, c-Myc also stimulates transcription by RNA polymerases I and III (for a review, see Campbell and White, 2014).

Figure 3.

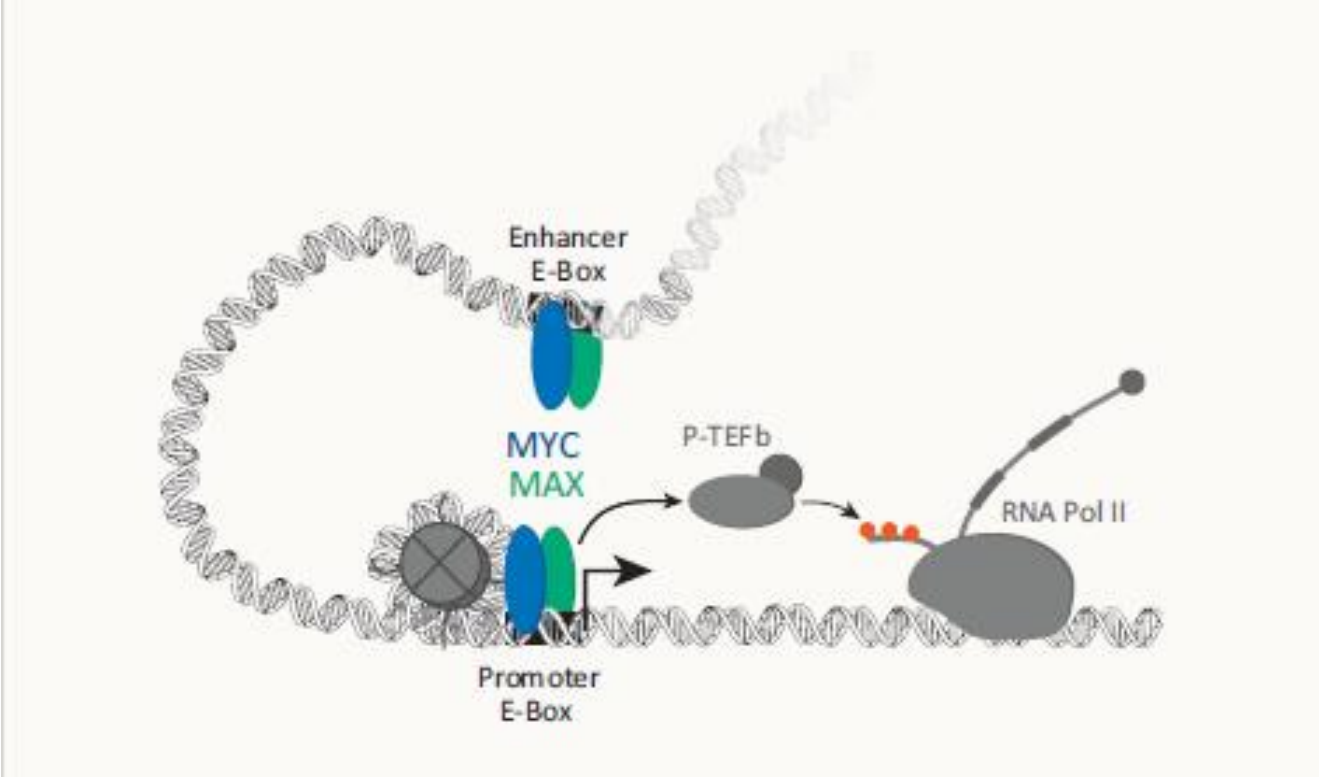

Figure 3. Schematic of transcription elongation-promoting activity of c-Myc. P-TEFb: positive transcription elongation factor b; RNA pol II: RNA polymerase II. (Wolf et al., 2015).

To date, c-Myc has been shown to alter the stability of multiple genes and genomic sites (for a review, see Conacci-Sorrell et al., 2014). c-Myc overexpression upregulates transcription of various genes (Campaner and Amati, 2012), overrides cell cycle checkpoints (Felsher and Bishop, 1999; Li and Dang, 1999; Robinson et al., 2009), and disrupts the repair of double-strand breaks (Karlsson et al., 2003; Li et al., 2012). More than 11% of all cellular loci are affected by c-Myc deregulation (Fernandez et al., 2003; Orian et al., 2003; Hulf et al., 2005), especially the c-

Myc/Max heterodimer complexes where the DNA binding of c-Myc together with its heterodimeric partner, Max, are a known hallmark of Burkitt's lymphoma (Li et al., 2003). It has been shown that more than 45% of all replication origins in human cells carry Myc-binding E-box motifs (Swarnalatha et al., 2012) and the c-Myc deregulation promotes the formation of telomeric aggregates which is dependent on a functional *myc* box II (Caporali et al., 2007). In addition, deregulated c-Myc also causes nuclear remodeling, altering the position and function of telomeres, as well as selective chromosome movement and overlap (Louis et al., 2005; Mai and Garini, 2005). Moreover, the conditional expression of the deleted box II mutant-Myc (D106-Myc) protein which could induce a lower level of apoptosis but higher level of genomic instability than its wild-type (wt) counterpart, was able to induce genomic instability within 48 hours, including structural and numerical aberrations, gene amplification, the formation of extrachromosomal elements (EEs), chromosomal breakage, increased aneuploidy, and polyploidization (Caporali et al., 2007).

Other transforming and more tissue-specific family members of c-Myc have been discovered in neuroblastoma (N-Myc) and lung cancer (L-Myc) (Tu et al., 2015). The 3 Myc proteins are encoded by 3 different Myc genes and are differentially expressed during development. However, the 3 Myc proteins are functionally equivalent in most biological systems (KC et al., 2014). Another additional form of c-Myc includes B-myc which is an endogenous, N-terminal homologue that lacks the C-terminal DNA binding and protein dimerization domain of c-Myc (Burton et al., 2006). Lastly, S-Myc, a Myc family protein which is closely related to N-Myc in its structure and is similar to c-Myc in its ability to induce apoptosis, is also considered one of the Myc protein members (Noguchi et al., 2000).

Roles of c-Myc in initiating and maintaining tumorigenesis

In cancers, deregulation of c-Myc protein expression is frequently caused by *c-myc* gene amplification and translocation. In addition, c-Myc activity deregulation can also occur from alterations in mitogenic signaling pathways that affect c-Myc mRNA or protein levels through

both transcriptional and post-transcription mechanisms (Kapeli and Hurlin, 2011; Chen Y et al., 2014). *c-myc* is one of the most frequently deregulated oncogenes in human cancers (Sewastianik et al., 2014). Alterations of c-Myc protein levels due to gene amplification, enhanced transcription, increased RNA or protein stability, chromosomal translocation, or viral insertion have been involved in the initiation and progression of more than 70% of all tumors studied to date (Ikegaki et al., 1989; Mitani et al., 2001; Kuzyk and Mai, 2014).

In Burkitt's lymphoma, the uncontrolled expression of c-Myc is caused by the juxtaposition from the translocation of the *myc* proto-oncogene to the *Ig* heavy or light chain locus regulatory elements. This particular t(14;8) translocation, though a defining hallmark of Burkitt's lymphoma, is not specific to only this hematologic malignancy. In addition, this translocation can be also found in diffuse large B-cell lymphoma and other lymphoid malignancies including B-cell lymphoma, unclassifiable plasma cell myeloma, mantle cell lymphoma, and plasmablastic lymphoma (Aukema et al., 2014). In mouse models, the *c-myc* gene which is located on chromosome 15 can induce leukemias, lymphomas, and plasmacytomas (PCTs). The typical chromosome translocations t(12;15) in murine PCTs and analogous t(14;8) in Burkitt's lymphomas characterize certain B lymphoid tumors associated with the *c-myc* oncogene and the *Ig* heavy chain loci (Adams et al., 1985). However, in other mouse models of lymphomagenesis or leukemogenesis, cooperation of *c-myc* oncogene with other deregulated pathways, for example, inactivation of the p53 pathway, structural alterations of Bcl-2 family members, or increased PI3K activity, accelerates tumorigenesis (Adams and Cory, 1992; Yu and Thomas-Tikhonenko, 2002; Park et al., 2005).

Studies have successfully demonstrated that c-Myc deregulation causes genomic instability by using c-Myc-inducible cell lines and *in vivo* using the mouse model of PCT, a B-lineage tumour resulting from c-Myc–activating chromosomal translocation. c-Myc target genes have also been identified including *dihydrofolate reductase* (*DHFR*) (Mai, 1994; Mai et al., 1996b),

ribonucleotide reductase R2 (Kuschak et al., 1999), and *ornithine decarboxylase* (*ODC*) (George et al., 1996; Mai and Mushinski, 2003; Kuttler and Mai, 2006). In the *v-abl/myc* virus-induced fast-growing mouse PCT model, accelerated tumor development was associated with duplication of subcytoband 11E2 of mouse chromosome 11, supporting the importance of subregion 11E2 in accelerated PCT development and the cooperation with c-Myc that apparently facilitates the fast-onset PCT (Wiener et al., 2010).

Although *c-myc* is one of the most commonly activated oncogenes involved in tumorigenesis, *c-myc* activation alone generally cannot induce cellular proliferation or neoplastic transformation of most normal human cells (Felsher et al., 2000). In most normal cells, c-Myc protein activation alone is restrained from causing tumorigenesis through several genetic and epigenetically controlled checkpoint mechanisms which are proliferative arrest, apoptosis, and cellular senescence. The genetic events known to frequently synergize with c-Myc to induce cellular proliferation as well as malignant transformation mainly include the overexpression of Bcl-2, loss of p53, or loss of p19ARF (Schmitt and Lowe, 2001; Gabay et al., 2014). Additionally, for c-Myc to induce tumorigenesis, toxins or carcinogens associated with the activation of cellular proliferation also facilitate the process (Beer et al., 2008).

In some experimental mouse models, c-Myc-induced tumorigenesis was found to be reversible (Felsher and Bishop, 1999; Pelengaris et al., 2002; Marinkovic et al., 2004). The suppression of c-Myc has been shown to reverse tumorigenesis in a wide variety of hematopoietic malignancies including T- and B-cell lymphoma and leukemia, epithelial tumors (hepatocellular, breast, squamous carcinoma), and mesenchymal tumors (osteogenic sarcoma) (Felsher and Bishop, 1999; Pelengaris et al., 2002; Marinkovic et al., 2004). However, c-Myc-induced tumorigenesis is not always reversible. In some genetic contexts, c-Myc suppression resulted in the initial regression of a tumor that subsequently recurred. The introduction of additional genetic events, such as a mutant Ras, can abrogate the reversibility of c-Myc-induced breast adenocarcinoma (D'Cruz et al., 2001).

Similarly, in c-Myc-induced lymphoma model, loss of p53 expression also prevents the tumor from being reversible (Giuriato et al., 2006).

Activation of c-Myc has also been found to be associated with global changes in cancer cells metabolism, making tumors particularly susceptible to the inhibition of enzymes being essential for metabolism (Dang et al., 2009; O'Shea and Ayer, 2013). c-Myc promotes cellular growth by activating genes related to ribosomal and mitochondrial biogenesis, glucose and glutamine metabolism as well as lipid synthesis, resulting in the metabolic reprogramming essential for cancer cell adaptation to tumor microenvironment (Morrish et al., 2009; Wahlstrom and Henriksson, 2015). The suppression of c-Myc may, therefore, induce tumor regression by acutely disrupting the ability of tumor cells to maintain sufficient metabolism to sustain survival and/or by directly regulating death signaling (Morrish and Hockenbery, 2014).

Role of c-Myc in chromosome organization

The term chromosome territory (CT) describes a specific order that chromosomes assume in the 3D space of the nucleus. It represents a non-random territorial organization of chromosomes in the interphase of eukaryotic cells (Cremer and Cremer, 2010). Different models of nuclear organization have been proposed to date. Two opposing chromosome architecture models are the chromosome territory – interchromatin compartment (CT–IC) and interchromatin network (ICN) models (Cremer and Cremer, 2010). The CT-IC model proposes that CTs are composed of " ~ 1 Mbp chromatin domains", made up by " ~ 100 kbp chromatin loop domains" (Branco and Pombo, 2006) whereas the IC domain/compartment extends into the interior of CT and contacts the surface of the 100 kbp domains where active genes are located (Branco and Pombo, 2006). The ICN model proposes that chromatin fibers/loops from the same CT, as well as from the neighboring, can intermingle and make contact in a rather uniform way (Cremer and Cremer,

2010). This model assumes that there is no free inter-chromatin space and the chromatin loops may expand from an individual CT to meet loops from another CT.

Recently, Cremer and colleagues publsihed new insights into the CT-IC model and demonstrated the spatio-temporal relationships between chromatin and nuclear machineries (Cremer et al., 2015). By using electron and super-resolved fluorescence microscopes, the authors introduced 2 spatially co-aligned, active and inactive nuclear compartments (ANC and INC). The ANC, which is the major site of RNA synthesis and is enriched in active RNA pol II, splicing speckles, and histone signatures for transcriptionally competent chromatin, consists of the transcriptionally active periphery of chromatin domain clusters (CDCs), called the perichromatin region (PR) and the interchromatin compartment (IC). The IC, which is connected to nuclear pores, controls nuclear import and export functions. The inactive compartment, INC, is formed by the compact, transcriptionally inactive core of CDCs and carries marks for repressed chromatin (Hübner et al., 2015; Cremer et al., 2015). Furthermore, in a live cell experiment, the authors examined the effects of chromatin decondensation triggered by hypotonic conditions on the appearance of IC lacunae in granulocytes, a state which could be restored within 1 minute after reincubation in a normotonic medium (Hübner et al., 2015).

Chromosome repositioning has been demonstrated during the differentiation of human T-cells (Kim et al., 2004a), adipocytes (Kuroda et al., 2004), and keratinocytes (Marella et al., 2009). Moreover, Mehta and colleagues have reported that, upon serum removal from the culture medium, chromosomes of primary human fibroblasts altered their positions within 15 minutes (Mehta et al., 2010). The authors proposed that the chromosome repositioning is probably dependent on nuclear myosin 1β (Mehta et al., 2010). A large-scale spatial repositioning of CTs can be induced by DNA damage and is a reversible process following a damage-repair response (Mehta et al., 2013). Mehta and colleagues investigated the relation between CT organization and DNA damage response by analyzing the positions of all human chromosomes by 2D-FISH

following DNA damage induced by H_2O_2 treatment. They found that although most chromosomes did not alter their localization within interphase nuclei following damage, a few gene-dense chromosomes including chromosomes 17, 19, and 20 repositioned from the nuclear interior to the periphery, whereas vice versa, chromosomes 12 and 15 repositioned towards the interior of the nucleus. They observed that the CT repositioning was a reversible process which was dependent upon double-strand break recognition and damage sensing and concluded that the process might be a fundamental aspect of cellular damage response (Mehta et al., 2013).

When *v-abl* and *c-myc* genes are overexpressed in precursor pre-B cells, instead of lymphoma occurrence as when *v-abl* is overexpressed alone (Weissinger et al., 1993; Risser et al., 1978), this combination induces PCTs. Mouse PCT, similar to rat immunocytoma and human Burkitt lymphoma, is a B lineage tumour resulting from c-Myc–activating chromosomal translocation (Adams et al., 1983; Klein, 1983; Cory, 1986; Pear et al., 1988). In more than 90% of tumors, c-Myc translocates to the immunoglobulin heavy chain locus (*IgH*) and after their juxtaposition, the *IgH* acts as an enhancer to promote *c-myc* gene expression in B cells resulting in tumour development (Potter and Wiener, 1992). This pathway was confirmed in a transgenic mouse model. In brief, the authors transfected pre-B cells derived from mice harboring Eμ-myc, a transgenic DNA sequence isolated from a mouse PCT in which a normal *myc* gene had been translocated to the *IgH* enhancer (Corcoran et al., 1985), with *v-abl* and transferred the cells to compatible mice, inducing them to develop PCTs (Sugiyama et al.,1989; Sugiyama et al., 1990). Furthermore, the authors demonstrated the ability of the same pre-B cells to develop lymphomas in the same hosts when *v-abl* is not coexpressed (Adams et al., 1985; Alexander et al., 1989). Rosenbaum and his colleagues analyzed the cytogenetic and molecular profiles of spontaneous PCTs in *v-abl* transgenic mice and found that *c-myc* gene was translocated to the *IgH* and constitutively expressed (Rosenbaum et al., 1990).

To date, 2 types of mouse PCTs, fast-onset and slow-onset, can be experimentally induced. In fast-onset PCTs, the mice are initially induced by injection of pristane into the peritoneum, followed by the transfection with Abelson murine leukemia virus (A-MuLV). Both *c-myc* and *v-abl* genes are overexpressed in these mice with a mean latency of 36 days for tumour development (Largaespada et al., 1992; Park et al., 2007). Sixty-one percent of these mice exhibit trisomy of chromosome 11 which is a second event of chromosomal aberration in addition to *Ig/myc* juxtaposition (Ohno et al., 1984). In BALB/c or BALB/c congenic mice induced by pristane pretreatment, followed by a helperfree *v-abl/myc* retrovirus, up to 100% of chromosome 11 changes were demonstrated (Largaespada et al., 1992; Wiener et al., 1995; Wiener et al., 2010). In contrast, in slow-onset PCTs in which only pristane is injected into the peritoneum, trisomy 11 is found at a low frequency (7.1%). The inflammatory process is initiated and the mice slowly develop PCTs in their peritoneum with a mean latency of 145 - 220 days (Ohno et al., 1979; Wiener et al., 1980; Largaespada et al., 1992; Wiener et al., 1995; Park et al., 2007). In these mice, mostly the translocation of chromosome T(12;15) occurs and generates c-Myc upregulation which is an early initiating event in malignant transformation (Potter and Wiener, 1992).

In the *v-abl/myc* virus- induced fast-onset PCT model, Wiener and colleagues found that the accelerated tumor development is usually associated with chromosome 11 trisomy (Wiener et al., 1995) and a duplication of subcytoband 11E2 (Wiener et al., 2010). Contrastingly, in the slow-growing pristane only–induced PCTs, both copies of chromosome 11 are normal based on mBANDing (Wiener et al., 2010). Furthermore pristane only–induced tumors did not develop duplications of chromosome 11 or of 11E2 bands, supporting the importance of subregion 11E2 in accelerated PCT development and the cooperation with c-Myc that apparently triggers the fast-onset PCT (Wiener et al., 2010).

Furthermore, Kuzyk and Mai reported an association of the *v-abl/myc*-induced accelerated mouse PCT development with the selected telomere length changes and aberrant 3D nuclear

telomere organization (Kuzyk and Mai, 2012). They found that fast-onset PCTs had a significantly different 3D telomere profile and that the translocation chromosome carrying 11E2 is the only chromosome with telomere lengthening, compared with primary B cells of wild-type littermates with and without rcpT(X;11). The finding supports the concept of individual telomere lengthening of chromosomes that are functionally important for the tumorigenic process, or reflecting that tumor cells might utilize a chromosome-specific telomere lengthening mechanism to protect key genes responsible for their tumorigenesis (Kuzyk and Mai, 2012).

c-Myc deregulation can alter the positions of chromosomes. In PreB *v-abl/myc* cells, immortalized mouse B lymphocytes stably transfected with Myc-ER chimera, an expression vector with which c-Myc protein can be activated by 4HT (Littlewood et al., 1995; Mai et al., 1999), changes in chromosome positioning measured by chromosomal overlaps were observed in nuclei of c-Myc deregulated cells for chromosomes 5 and 13, 7 and 10, and 7 and 17 over a 96-hour period (Louis et al., 2005). The study emphasized the role of c-Myc in regulating chromosome organization and nuclear remodeling.

Telomeres and telomeric shelterin proteins

Telomeres are the sequence of $(TTAGGG)_n$ repeats which specify mammalian chromosome ends and protect them from fusion, degradation, recombination, and DNA damage repair. Human telomeres form a complex with 6 telomere-specific shelterin protein subunits including telomere repeating factor 1 (TRF1), TRF2, TIN2, Rap1, TPP1, and POT1 (Fig. 4; from Moon and Jarstfer, 2007).

Figure 4.

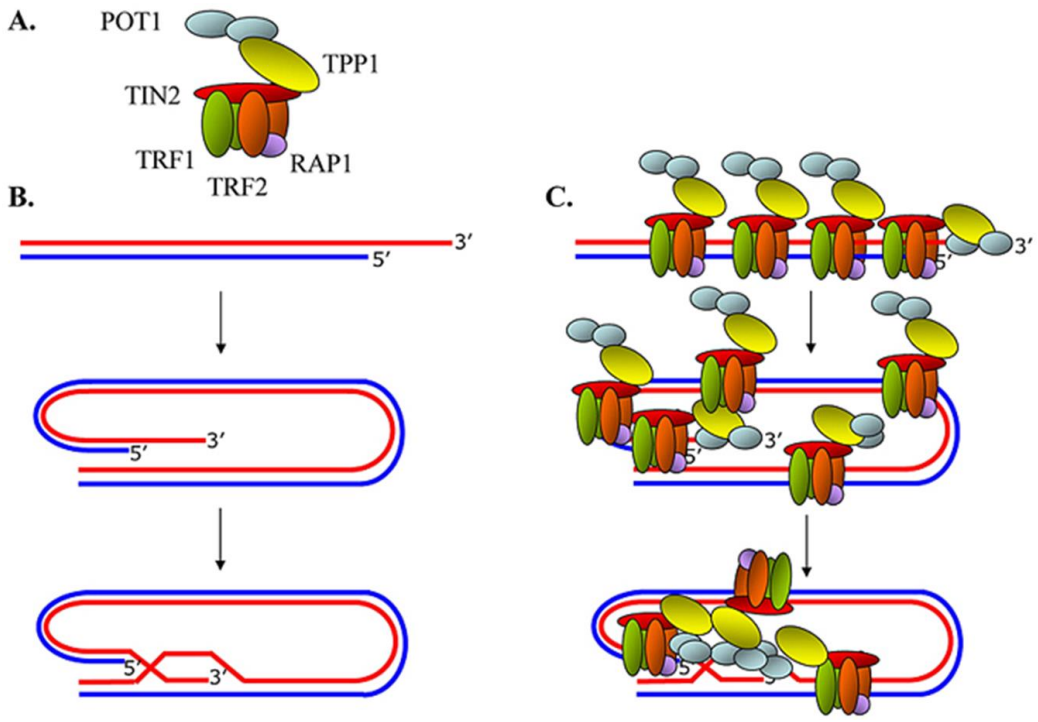

Figure 4. Structure of the telomeric shelterin protein complex. The telomere forms a t-loop, a lasso-like structure under the direction of the shelterin protein subunits. (a) Six shelterin subunits, TRF1, TRF2, TPP1, POT1, TIN2, and RAP1 form a telomere-protection shelterin complex in mammalians. (b) Human telomeres configurate in a t-loop structure characterized by insertion of the 3' overhang into a region of double-stranded telomeric DNA. (c) The shelterin complex caps the telomeric DNA repeats $(TTAGGG)_n$ in part by inducing t-loop formation (Moon and Jarstfer, 2007).

TRF1 was the first mammalian telomeric protein identified and was isolated based on its *in vitro* specificity for double-stranded $(TTAGGG)_n$ repeats (Zhong et al., 1992; Chong et al., 1995). TRF2 was later identified as a TRF1 paralog in the database (Bilaud et al., 1997; Broccoli et al., 1997). After that TIN2 was revealed in two-hybrid screens, a technique utilized to reveal protein-

protein interactions (Young, 1998), with TRF1, then Rap1 with TRF2, (Kim et al., 1999; Li et al., 2000). TPP1 (TINT1, PTOP, PIP1) was identified from searches for TIN2-interacting proteins (Houghtaling et al., 2004; Liu et al., 2004b; Ye et al., 2004b), whereas POT1, the most conserved component of shelterin, was revealed based on its homology sequence to telomere end-binding factors in unicellular eukaryotes (Baumann and Cech, 2001). In mice, 2 POT1 paralogs, POT1a and POT1b were identified (Hockemeyer et al., 2006).

In experiments examining fractionated nuclear extracts, all 6 shelterin proteins were identified in a single complex, confirming their interaction as a telomeric shelterin complex (Liu et al., 2004a; Ye et al., 2004a). TRF1, TRF2, and POT1 are major shelterin subunits that directly recognize $(TTAGGG)_n$ repeats and interconnect with the other 3 shelterin proteins, TIN2, TPP1, and Rap1. The shelterin protein complex possesses multiple $(TTAGGG)_n$ recognition folds making it extremely specific to telomeric $(TTAGGG)_n$ repeats. TRF1 and TRF2 have single Myb-type helix-turn-helix (HTH) DNA-binding domains (DBDs), each of which binds to the sequence 5′-YTAGGGTTR-3′ in duplex DNA (Bianchi et al., 1999; Court et al., 2005; Hanaoka et al., 2005). TRF2, similar to TRF1, forms homodimers and higher order oligomers, bringing multiple DBDs to the complex. TRF2 is able to involve a large DNA sequence. POT1, the most conserved component of shelterin with strong $(TTAGGG)_n$ sequence specificity interacts with single-stranded 5′-(T)TAGGGT TAG-3′, at a 3′ end and at internal positions (Lei et al., 2004; Loayza et al., 2004). POT1 also influences the maintenance of telomeric DNA by telomerase and protecting the 5′ end of the chromosome. TRF1, TRF2, and POT1 are interconnected through protein-protein interactions, providing the shelterin complex the unique capacity to distinguish telomeric DNA from other DNA ends, with at least five DNA-binding domains, with 2 each in TRF1 and TRF2 and 1 in POT1.

Mouse telomeres contain POT1a and POT1b. Both distinct POT1 proteins are required in mice to prevent a DNA damage signal at chromosome ends, endoreduplication, and senescence.

Hockemeyer and colleagues demonstrated that both proteins had distinct functions. Only POT1a was required to repress a DNA damage signal at telomeres whereas POT1b specifically regulated the amount of single-stranded DNA at the telomere terminus (Hockemeyer et al., 2006). TIN2 acts as the core element of shelterin complex and tethers TPP1/POT1 to TRF1 and TRF2. TIN2 also links TRF1 to TRF2 which promotes stabilization of TRF2 on telomeres (Liu et al., 2004a; Ye et al., 2004a).

In mammalian cells, the telomeric DNA at the ends of chromosomes require telomere end protection from 6 distinct double-strand break (DSB) processing pathways including classical Ku70/80- and DNA-ligase-4- dependent nonhomologous end-joining (c-NHEJ), microhomology-dependent alternative NHEJ (a-NHEJ) mediated by PARP1 and DNA ligase 3, homology-directed repair (HDR), CtIP-dependent 5' end resection, ATM signaling, and ATR kinase. Among these 6 pathways, TRF2 protects telomeres from the DNA damage repair mechanism by c-NHEJ and ATM kinase signaling (van Steensel et al., 1998; Karlseder et al., 1999; Smogorzewska and de Lange, 2002a; Smogorzewska et al., 2002b; Celli and de Lange, 2005; Denchi and de Lange, 2007). Reduction in TRF2 leads to activation of an ATM kinase cascade and frequent c-NHEJ which facilitates fusion of chromosome ends (Doksani et al., 2013).

Distinct effects of shelterin in telomere protection have been identified. The shelterin protein subunits recognize telomeric DNA and remodel it into a t-loop formation, a tucked-in large duplex lasso structure taking place at the end of telomeres, which presumably results in concealing the chromosome end from the DNA damage repair machinery (Griffith et al., 1999; Stansel et al., 2001). The 3′ end of telomeres harbours a long single-stranded sequence of $(TTAGGG)_n$ repeats and this 3′ overhang has been postulated to insert into the double-stranded telomeric DNA where the C-strand is base-paired and the G-strand is displaced (Makarov et al., 1997). Various sizes of t-loops, from 1-25 kb, have been observed in human cells. T-loops, at first, were demonstrated in purified telomeric restriction fragments from human and mouse cells (Griffith et al., 1999).

Griffith and colleagues, using electron microscopy (EM) to study isolated telomeric DNA, demonstrated a t-loop configuration of telomeres as a lariat structure formed through the insertion of the telomeric 3' overhang into the double-stranded telomeric repeat sequences. The t-loop structure has been proposed to enable a blockage of DNA damage repair reactions since it can sequester the end of a telomere making it inaccessible from the process activation (de Lange, 2009). The method of interstrand cross-links with psoralen and UV needs to be applied in order to observe t-loops in protein-free DNA, otherwise the branch migration can dissociate these formations. The lasso structures of t-loops were also identifiable in telomeric chromatin being isolated without the use of psoralen, by which method the nucleosomes on the t-loop and the adjacent tail DNA were also revealed (Nikitina and Woodcock, 2004).

In vitro experiments have suggested that TRF2 promotes t-loop formation by mediating DNA strand invasion of the telomere end and stabilizing the t-loop configuration (Griffith et al., 1999; Stansel et al., 2001; Fouche´ et al., 2006; Amiard et al., 2007; Poulet et al., 2009; Nora et al., 2010). To date, however, there is still only limited *in vivo* evidence to clearly reveal the existence of t-loop formation or the role of TRF2 in this configuration or maintenance. T-loop configuration of chromosome ends has been exhibited by using super-resolution imaging including the super-resolution fluorescence imaging method (STORM) (Doksani et al., 2013). Doksani and colleagues, to identify t-loop structures in fixed mouse splenocytes, used a peptide nucleic acid (PNA) FISH probe complementary to the $(TTAGGG)_n$ repeats and labeled with a photoswitchable dye, then performed images with 3D STORM. STORM relies on stochastic switching and high-precision localization of individual photoswitchable fluorescent probes to achieve imaging with subdiffraction- limit resolution (Rust et al., 2006). With this technique, they could image the telomeric DNA *in situ* and directly visualized the t-loop structure in chromatin. However, only 22.7% of the scored telomeres were found in the t-loop configuration (Doksani et al., 2013). The question regarding the small number of t-loops structure reported from this study representing the

real occurrence of t-loop formation in live cells, or possibly being underestimated due to the stringent scoring criteria remains opened. The authors also revealed that, among the telomeric shelterin protein subunits, TRF2 was the key component required for the configuration / maintenance of t-loops (Doksani et al., 2013). When TRF2 is present, it facilitates a configuration of chromosome ends into t-loop structures, hiding away telomeres from the activation of the free-DNA repair machinery, c-NHEJ and ATM signaling. Conditional deletion of TRF2, not TRF1, Rap1, or POT1 subunits, decreased the frequency of t-loop appearances (Doksani et al., 2013).

The mechanism underlying telomeric t-loop formation still remains to be determined. Experiments performed *in vitro* have demonstrated that the DNA remodeling activities of shelterin subunits, TRF2 in particular, contribute to t-loop formation (Griffith et al., 1999; Stansel et al., 2001). For example, despite the lack of a recognizable helicase domain in TRF2 and although not an efficient reaction, purified TRF2 is able to generate t-loop formation without ATP requirement. *In vivo*, TRF2 is expected to require other cofactors to initiate t-loop formation. However, unanswered questions regarding the uncertainty of t-loop formation remain. For example, the definitive structure of t-loop has still not been revealed, neither has the role of shelterin proteins in t-loop formation been tested *in vivo*. Moreover, whether the t-loop is the only or major structure of protected chromosome ends is still not clearly established.

In addition to TRF2, other telomeric shelterin protein subunits have been reported as potentially involved in generating the telomere folding structures. TRF1 demonstrated its DNA remodeling activity by looping, bending, and base-pairing the telomeric repeat sequences *in vitro*, therefore TRF1 could also be *in vivo* folding the telomere and stimulating the formation of t-loops. (Bianchi et al., 1997; Bianchi et al., 1999; Griffith et al., 1998). Kim and colleagues found that TIN2, the analog of TRF1, enhanced TRF1's architectural effects on t-loop formation (Kim et al., 2003).

When telomeric dysfunction occurs, upon an inhibition of telomeric shelterin subunits or by telomere attrition resulting in the loss of telomere protection, the DNA damage response pathways

are activated to repair the damage. Telomeres can lose their protection with or without the obvious change in DNA structure. When telomeres become unprotected, the DNA sequences have access to associate with DNA damage response factors (de Lange, 2004). Consequently, ATM kinase is activated, leading to a p53-dependent cell cycle arrest in the G1/S phase, which results in apoptosis or senescence. When ATM is not present, it has been proposed that the ATR kinase substitutely induces cell cycle arrest. In p53-deficient human cells, p16 can also be induced upon telomere dysfunction and result in proliferation inhibition (Jacobs and de Lange, 2004).

Shelterin proteins protect telomeres by preventing them from the pathway that alerts cells to DNA damage and inhibition of shelterin activates the DNA damage response. Inhibition of TRF2 with TRF2ΔBΔM, a dominant-negative allele which heterodimerizes with the TRF2, blocks its binding activity to DNA and results in the activation of the ATM kinase pathway which leads to an upregulation of p53 and a p21-mediated G1/S arrest (van Steensel et al., 1998; Karlseder et al., 1999; de Lange, 2002). Experiments with a TRF2 knockout mouse model have also confirmed the TRF2-depleted activation of ATM and p53-dependent cell cycle arrest (Celli and de Lange, 2005).

Rationale to study the 17q25.3 region and 3D telomere organization in NSCLC patients

Non-small cell lung cancer (NSCLC) is the leading cause of cancer related death in Canada and worldwide. In Canada, it was estimated that there were 49,225 new lung cancer cases in 2015 and the 1-, 3-, 5- , and 10-year relative survival ratios for this cancer were only 40%, 22%, 17%, and 13%, respectively, from the years 2006-2008 (Canadian Cancer Statistics, 2015). Since the survival of NSCLC patients remains unfavorable, a better understanding of its molecular biology and causality, along with advances in diagnostic methods and multidisciplinary therapeutic approaches, are needed to improve patient survival. Both endogenous and exogenous factors contribute to NSCLC tumorigenesis. Cigarette smoking has been recognized as the exogenous factor most related to NSCLC. However, smoking-naïve NSCLC patients have also been

diagnosed, which supports the significance of triggering differential endogenous molecular mechanisms that can lead to cancer cell formation. Furthermore, racial differences of NSCLC biology across human populations have been observed; however, data of the cytogenetic disparities are needed to better understand the disease and ultimately lead to the development of more effective therapeutic approaches.

c-myc is well established as an oncogene involved in the initiation and progression of NSCLC (Chen et al., 2012). Gains in the copy numbers of *myc* were found to be associated with lung adenocarcinoma in never smokers (El-Telbany and Ma, 2012). In a c-Raf-driven mouse model for NSCLC, addition of c-Myc induced immediate acceleration of tumor growth and macrometastasis in liver and lymph nodes (Rapp et al., 2009). Increased activation of Myc has been observed in lung squamous cell carcinomas, compared to premalignant lesions within the same patients, highlighting the significance of this molecule during stepwise lung carcinogenesis (Ooi et al., 2014).

Advances in NSCLC biology research have revealed cellular pathways and molecules related to cancer development and proliferation, making it possible to utilize targeted therapeutic strategies for patients. The novel receptor tyrosine kinase inhibitors (TKIs) that have been approved to treat NSCLC patients include erlotinib and gefitinib (which target the epidermal growth factor receptor (EGFR)) and crizotinib (which targets rearranged anaplastic lymphoma kinase (ALK)). Monoclonal antibodies such as cetuximab (targeting EGFR) and bevacizumab (targeting vascular endothelial growth factor (VEGF)) (El-Telbany and Ma, 2012) are also used for NSCLC treatment. To date, evidence from phase III clinical trials have clearly demonstrated EGFR TKIs as the best first-line therapy in *EGFR*-mutated patients. In *ALK*-translocated NSCLC, a phase III trial established the superiority of a multi-target TKI, including ALK, crizotinib, when compared to standard second-line chemotherapy (Minuti et al., 2014). In patients with acquired resistance to EGFR TKIs or crizotinib, novel agents targeting EGFR or ALK are under investigation

particularly to provide personalized therapy to NSCLC patients for achieving better outcomes (Minuti et al., 2014).

Recently, a major improvement in NSCLC patient survival resulted from the implementation of molecularly targeted therapy with anti-EGFR inhibitors. EGFR is a key transmembrane tyrosine kinase receptor in signaling transduction pathways, upon which its activation can trigger anti-apoptotic signaling, proliferation, angiogenesis, invasion, metastasis, and drug resistance, leading to development and progression of human epithelial cancers, including NSCLC (Nurwidyan et al., 2014). In western countries, approximately 15% of patients with lung adenocarcinoma harbour activating *EGFR* mutations whereas 20-40% of East Asian populations with NSCLC have positive *EGFR* mutations (El-Telbany and Ma, 2012; Liao et al., 2013). EGFR inhibitors have shown benefits in treating NSCLC patients, especially those who have an *EGFR* mutation and/or amplification (Mok et al., 2009; Fukuoka et al., 2011). *EGFR* mutational status has been well established as a biological marker to predict response after anti-EGFR targeted therapy in advanced NSCLC patients.

Gains of chromosome 17q25 have been reported in several types of human cancers including NSCLC (Choi et al., 2006; Bermudo et al., 2008; Zack et al., 2013). Kuzyk and colleagues studied 2 neuroblastoma cell lines and 16 primary neuroblastomas and found a frequent gain of 17q25.3 in high MYCN protein expressing neuroblastoma cells with and without MYCN gene amplification. They also found a strong correlation between 17q25.3 gains and MYCN protein levels in neuroblastoma tissue, suggesting that 17q25.3 and MYCN protein levels are strong correlative biomarkers for aggressive neuroblastomas (Kuzyk et al., 2015). Cytoband 17q25.3 in humans is syntenic to the 11E2 region in mice and the 10q32 region in rats (Koelsch et al., 2005). Studies in animal models have shown that these syntenic regions show gains associated with accelerated tumor development. Therefore, a cross-species association between this oncogenic region and tumour aggressiveness seems apparent.

Recent advances in nuclear remodeling studies have been made possible with the development of confocal microscopy and optical sectioning, providing higher resolution 3D images (Gadji et al., 2011). 3D nuclear organization imaging technology enables a comprehensive and quantitative analysis of nuclei and their morphology, including specific regions of interest including telomeres. 3D nuclear telomere architecture has been investigated in various cancers, revealing its potential as a molecular biomarker to categorize patients based on various clinical features. For example, promising results with 3D nuclear organization profiling as a novel molecular diagnostic target to differentiate patient subgroups have been demonstrated in multiple cancer types including Hodgkin lymphoma, multiple myeloma, acute myeloid leukemia, glioblastoma, and prostate cancer (Gadji et al., 2010; Gadji et al., 2012; Knecht et al., 2012; Adebayo et al., 2013; Klewes et al., 2013).

Chapter II : Rationale, Hypothesis, and Objectives

Mouse chromosome 11 cytoband E2, syntenic with human chromosome 17q25, harbours commonly amplified genes in mouse PCT. In humans, allelic aberrations on chromosome region 17q25 have been reported in various types of cancers, supporting the importance of this region in tumorigenesis. Based on the synteny of mouse subcytoband 11E2 and human chromosome 17q25, frequent aberrations of cytoband 17q25 in humans, and the alteration of subcytoband 11E2 in *v-abl/myc*-induced accelerated mouse PCT development, the thesis was conceived to study this region to better understand its roles in tumor development and progression.

Deregulation of c-Myc promotes the formation of telomeric aggregates and accelerated PCT development is usually associated with duplication of cytoband 11E2, telomere length changes in translocation chromosomes carrying 11E2, and aberrant 3D nuclear telomere organization. Moreover, c-Myc deregulation can alter the positions of chromosomes in PreB *v-abl/myc* cells, and this research therefore explored whether c-Myc-driven chromosome 11 nuclear repositioning occurs in mouse PCT. If the alteration of nuclear positions/orientation of chromosome 11 and/or of cytoband 11E2 was observed after c-Myc activation, this would confirm the significance of chromosome 11 repositioning and/or of cytoband 11E2 orientation as a potentially causal involvement for v-*abl/myc*-induced PCT development.

Telomere and telomeric proteins form a shelterin complex and their interactions are important for telomere function in protecting chromosome ends from degradation, fusion, recombination, and DNA damage repair (de Lange, 2005). Human telomeres are known to attach to the nuclear matrix and the telomeric position of the $(TTAGGG)_n$ repeats is required for their interaction with the nuclear matrix (de Lange, 1992). Telomeric shelterin subunits, TRF2 in particular, contribute to t-loop formation and telomere configuration (Doksani et al., 2013). Taken together, a study to identify whether a detachment of telomeric shelterin proteins from the nuclear matrix occurs in mouse PreB *v-abl/myc* cells after c-Myc activation would potentially reveal the cause and

consequence-relationship between c-Myc driven chromosome 11 repositioning and fast-onset PCT development.

NSCLC remains a devastating disease characterized by clinical and molecular heterogeneity, therefore molecularly-personalized approaches to improve response and survival are needed. Molecular therapy targeting EGFR has improved survival outcome in *EGFR*-mutated NSCLC patients. Characterization of 3D nuclear organization enables a comprehensive analysis of nuclei and their morphology and quantification of regions of interest including telomeres. 3D telomere architecture has been investigated in numerous cancers which have confirmed its potential as a molecular biomarker for distinguishing patients with various clinical features (Gadji et al., 2010; Gadji et al., 2012). Gains of chromosome 17q25 have been reported in several types of human cancers, including NSCLC (Choi et al., 2006; Bermudo et al., 2008; Zack et al., 2013), but its clinical significance in NSCLC remains unknown. Cytoband 17q25.3 in humans is syntenic to the regions 11E2 in mice and 10q32 in rats, and studies in animal models have revealed that these regions are gained and associated with accelerated tumour development (Helou et al., 2001; Wiener et al., 2010). Based on pre-clinical and clinical evidence of this region's association with tumorigenesis, a hypothesis that 17q25.3 copy gains may also be an indicator of tumor progession and agressiveness in NSCLC patients was established to be further explored in this thesis. The study compared disparities in 3D telomeric organization with different NSCLC patient backgrounds, clinical parameters, cytoband 17q25.3 aberration, and *EGFR* mutational status.

The hypotheses of this thesis were: (1) c-Myc deregulation induces chromosome 11 nuclear repositioning in PreB *v-abl/myc* cells; (2) detachment of the telomeric shelterin protein TRF2 from the nuclear matrix protein lamin A/C occurs after c-Myc activation in PreB *v-abl/myc* cells and is a potential mechanism underlying chromosome 11 repositioning and fast-onset PCT development; and (3) cytoband 17q25.3 (syntenic to mouse subcytoband 11E2) aberrations and the 3D nuclear

telomeric organization profile in NSCLC patients correlate with tumor aggressiveness and prognoses.

The objectives of this thesis were to:

- determine whether c-Myc deregulation drives chromosome 11 repositioning in PreB *v-abl/myc* cells
- determine the interactions between TRF2, telomeres, and nuclear matrix protein lamin A/C after c-Myc activation, in order to reveal the cause and consequence-relationship between chromosome 11 repositioning and fast-onset PCT development
- explore the correlation and clinical application of human chromosomal cytoband 17q25.3 aberration and the 3D nuclear telomeric organization in NSCLC patients. Taking these parameters together with clinical data, categorization of NSCLC patients might be made possible according to the aggressiveness of their tumours. The application of this molecular evaluation basis to better determine their appropriate treatment modality and to estimate their prognoses was warranted.

Chapter III : Materials and Methods

Cell culture and conditional c-Myc activation

PreB *v-abl/myc* cells are precursor pre-B lymphocytes which are immortalized and stably transfected with a highly plasmacytomagenic retroviral construct consisiting of *v-abl* retrovirus and a conditional MycER^{TM} vector (Largaespada et al., 1992). The PreB *v-abl/myc* cells demonstrate changes in the E1/E2 bands of chromosome 11, similar to those reported in *v-abl/myc*-induced PCT. Therefore they are appropriate cells to be used to study *v-abl/myc*-dependent tumorigenesis in mouse B cells (Benedek et al., 2004). Optimal cell culture conditions for PreB *v-abl/myc* cells have been described (Mai et al., 1999), with cell viability confirmed by hemocytometer counts using trypan blue (Gibco, Palsley, Scotland, UK). Activation of c-Myc in PreB *v-abl/myc* cells was done through MycER^{TM} as described previously (Littlewood et al., 1995). In brief, PreB *v-abl/myc* cells were split 24 hours before the MycER^{TM} activation, followed by treatment with 100 nM 4-hydroxytamoxifen (4HT) (Sigma, St. Louis, MO) to 10^5 cells per ml. Non-4HT treated PreB *v-abl/myc* cells served as negative controls and were cultivated in ethanol, the solvent used to dissolve 4HT (Adams et al., 1985; Chiang et al., 2003; Littlewood et al., 1995). Analyses of c-Myc-induced changes in chromosome positioning and 3D telomere organization were carried out after a single addition of 4HT that was left in the culture medium until its biological effects subsided (Vafa et al., 2002; Hironaka et al., 2003). Following the 4HT treatment, the nuclei were analyzed over time periods that were expected to reveal chromosome 11 movements (0, 6, 12, 24, 48 and 72 hours). MycER^{TM} activation was determined by fluorescent immunohistochemistry.

Three different PreB *v-abl/myc* cell harvesting schemes after MycER^{TM} activation were performed. First, a determination of the earliest time point of c-Myc-induced changes in mouse chromosome 11 positioning was carried out after a single addition of 4HT (Grenman et al., 1988a; Grenman et al., 1988b; Mandlekar et al., 2000), then the chromosome positioning was localized by

using chromosome paints (Applied Spectral Imaging (ASI; Vista, CA)) mouse chromosome 11-Cy3 paint; chromosome 10 served as a negative control (mouse chromosome 10-FITC paint); chromosomes 5 and 7 served as positive controls (mouse chromosome 5-Cy3 paint; mouse chromosome 7-FITC paint). Pre B *v-abl/myc* nuclei were examined at 0, 6, 12, 24, 48, and 72 hours over a 3-day period. When the earliest time point revealing the repositioning of chromosome 11 was identified, a second time course was performed. At this second scheme of cell harvesting, c-Myc in PreB *v-abl/myc* cells was activated by the addition of 4HT, then analyzed over the time period that was expected to reveal the first observation of chromosome 11 repositioning (0, 1, 2, 3, 4, 5, and 6 hours). Lastly, the third time course of cell harvesting was conducted. Cells were harvested at 20, 40 and 60 minutes after a single addition of 4HT and processed in the experiments to study the interactions between TRF2, telomeres, and nuclear matrix protein lamin A/C, with the aim of attempting to examine the mechanism potentially responsible for c-Myc activated mouse chromosome 11 repositioning in Pre B *v-abl/myc* cells. Positionings of all chromosomes were analyzed using 3D measurements by a fully automated program described in the "chromosome paints" and "3D image acquisition and analyses" sections.

Immunofluorescence

MycER^{TM} activation was determined by fluorescent immunochemistry which was performed as described in a previously estabilished protocol (Fukasawa et al., 1997). Immunofluorescence for c-Myc was performed on cytocentrifuged cells. In brief, PreB *v-abl/myc* cells were fixed on slides with 3.7% formaldehyde in phosphate-buffered saline (PBS) for 20 minutes. The fixed cells were washed 3 times with 1x PBS at 5 minutes each time and then permeabilized with 0.2% Triton X-100 in DDW, followed by 3 times of 1x PBS wash. The cells were then blocked with 3% bovine serum albumin (BSA) in 4x SSC for 30 minutes. c-Myc activation was revealed by using a primary rabbit polyclonal anti-c-Myc antibody (N262; Santa Cruz Biotechnology, Santa Cruz, CA) at a

dilution of 1:200 for 30 minutes and with a secondary anti-rabbit IgG antibody coupled to Alexa 488 (Abcam, Toronto, ON, Canada) at a dilution of 1:10,000 for 30 minutes.

TRF2 was revealed by rabbit polyclonal antibodies against TRF2 (Novus, NB 110-57130; Novus Biologicals, Littleton, CO) at a dilution of 1:500 for 1 hour. The secondary antibody was chicken anti-rabbit IgG antibody coupled to the Alexa 488 (Molecular Probes, Eugene, OR) at a dilution of 1:1,000 for 45 minutes. The primary antibody for lamin A/C (N-18, sc-6215; Santa Cruz Biotechnology, Santa Cruz, CA) was an affinity-purified goat polyclonal antibody at a dilution of 1:500 for 1 hour. The secondary antibody was a donkey anti-goat IgG antibody (Abcam, Toronto, ON, Canada) coupled to Cy3 at a dilution of 1:1,000 for 45 minutes. Coimmunofluorescence for TRF2 and lamin A/C was conducted to localize the distribution of TRF2, in correlation with lamin A/C, following the above-mentioned protocol. Nuclei were counterstained with 4',6-diamidino-2-phenylindole (DAPI). Analysis was performed through a Zeiss AxioImager Z1 microscope (Zeiss, Toronto, Canada). Images were acquired with a cooled AxioCam HR B&W camera (Zeiss, Toronto, Canada).

Fluorescence in situ hybridization (FISH)

Chromosome paints

c-Myc in PreB *v-abl/myc* cells was activated by the addition of 4HT, then the interphase nuclei were analyzed over a time period that was expected to reveal putative chromosome 11 repositioning, using chromosome painting. Chromosome 10 served as a negative control and chromosomes 5 and 7 as positive controls, since their repositioning had been observed previously (Louis et al., 2005). In brief, the slides were equilibrated in 2x SSC at RT for 10 minutes, followed by treatment with RNAse A 100 µg/ml in 2x SSC at 37°C for 1 hour. The slides were washed 3 times, 5 minutes per time, with shaking in 2x SSC at RT. The slides were then incubated in freshly prepared 0.01M HCl with 50 µg/ml pepsin for 10 minutes at 37°C. After washing the slides in 1x

PBS twice at 5 minutes per time, they were rotatorily pretreated in 1xPBS/50mM $MgCl_2$ for 5 minutes at RT, followed by postfixation in 1% formaldehyde in 1xPBS/50mM $MgCl_2$ for 10 minutes at RT, then washed in 1xPBS. Next the slides were dehydrated in ethanol (3 times at 70%, 90%, and 100% for 3 minutes each at RT, then let air dry. The slides were then prewarmed at 70°C for 5 minutes and immediately transferred to be incubated in 70% deionized formamide / 2x SSC (pH 7.0), at 70°C for 2 minutes for denaturation, followed by dehydration in cold ethanol (70%, 90%, and 100%) for 3 minutes each at -20°C. Next, Q-FISH was performed using chromosome paint probes (Applied Spectral Imaging (ASI; Vista, CA)) including mouse chromosomes 5 (labeled with Cy3), 7 (FITC), 10 (FITC), and 11 (Cy3). The chromosome paint probes were pretreated by incubation at 85°C for 7 minutes for denaturation, then transferred to an incubator at 37°C for 30 minutes for annealing. The chromosome paint probes were then applied onto the slides. The areas were then covered with cover slips and sealed with rubber cement and incubated for 16 hours at 37°C. After hybridization, the slides were washed in the following sequence: 50% formamide / 2x SSC at 45°C 3 times, 5 minutes per time, 4xSSC / 0.1% Tween 20 at 45°C 2 times at 5 minutes per time, and finally 1x SSC at 45°C for 2 minutes. The cells were then counterstained with DAPI and mounted with VectaShield® (Vector Laboratories, Burlington, Ontario, Canada). Three independent experiments were conducted. 3D image acquisition of painted interphase nuclei was then performed in at least 30 nuclei per each 3 independent experiments. Automated measurements of relative radial distribution (RRD) representing the positions of each chromosome were performed after 3D image acquisition and constrained iterative deconvolution. The positioning of all chromosomes was analyzed using 3D measurements by a fully automated program developed by Dr. Christiaan Righolt in Dr. Sabine Mai's lab as follows.

The 3D measurements were fully automated in a three-step procedure. First, the nucleus and chromosomes were automatically detected. Second, the relative radial position of each

chromosome copy was determined. And third, these measurements were all collected for each group, plotted as a cumulative distribution and statistically tested with the two-sample, two-sided Kolmogorov-Smirnov test. All image processing for these 3D measurements was done with the DIPimage program (Hendriks et al., 1999), a toolbox for Matlab. The regions of interest were automatically detected from the deconvolved images. This segmentation of the image process consists of two parts: the segmentation of the nucleus and the segmentation of four chromosome copies, two each for both chromosome 10 and 11. The image of the nucleus is non-linearly processed in several steps to reduce background intensity and clip extreme values. The resulting image is thresholded with the isodata algorithm (Ridler and Calvard, 1978) to yield an initial binary representation of the nucleus. The filled convex hull of this initial result is taken as the region of interest (mask) representing the nucleus. Both chromosome channels are segmented in the same way from their respective images. The image is first band-filtered with a difference of Gaussians filter, the negative values arising from this filter are clipped to 0. The product of the original image and the clipped band-pass filtered image is subsequently thresholded over the nuclear mask with the isodata algorithm. Potential holes within connected regions are filled and the two largest connected, detected regions are determined to be the chromosomal masks for each chromosome channel.

The relative radial position is measured for each chromosome copy. The eigenvalues of the moment of inertia tensor of the nuclear mask are determined first, the shape of the nucleus is now approximated by an ellipsoid. The eigenvalues of the moment of inertia tensor are known algebraically for an ellipsoid as a function of the length of the semi-axes – the off-diagonal elements are 0 for an ellipsoid when the semi-axes coincide with the cardinal directions of the coordinate system. These equations are then solved to yield the semi-axes in the rotated coordinate system of the nucleus around the center of mass of the nuclear mask. The relative radial position of each chromosome copy is now given by calculating the center of mass of each chromosomal mask

in the rotated coordinate system of the nuclear mask after the ellipsoid is normalized to the unit sphere.

The different orientations of chromosomes were compared to each other using all of the following tests: Chi-Square, Likelihood Ratio Chi-Square, Continuity Adj Chi-Square and Mantel Haenszel Chi-Square analyses (Schmälter et al., 2014). RRD observed for control and c-Myc-activated Pre B *v-abl/myc* cells were compared over time by two-way analysis of variance (ANOVA). In addition, statistical analyses were performed for the difference of RRD of each pair of chromosomes, which were chromosomes 5 vs. 7 (served as positive controls), and chromosomes 10 (served as negative control) vs. 11, over the experimental period. *P* values of < 0.05 were considered significant.

ImmunoFISH

The cells were seeded on slides and fixed in 3.7% formaldehyde / 1x PBS for 20 minutes at RT, followed by a rotatory wash with 1x PBS twice, for 5 minutes each time, at RT. The cells were then permeabilized with 0.1% Triton X-100 in DDW at RT for 12 minutes without shaking, followed by 3 rotatory five-minute washes with 1x PBS. Blocking with 4% BSA / 4x SSC for 30 minutes at RT was applied, followed by an incubation with a primary antibody (Rabbit polyclonal TRF2; Novus (NB 110-57130)) (Novus Biologicals, Littleton, CO) in 4% BSA / 4x SSC with 1:500 dilution for 1 hour at 37°C in a humidified atmosphere. Then another round of 3 washes with 1x PBS was performed, followed by an application of a secondary antibody (goat anti-rabbit; Alexa 488, Abcam, Toronto, ON, Canada) in 4% BSA / 4x SSC with 1:1000 dilution for 45 minutes at 37°C in a humidified atmosphere. Three five-minute washes with shaking in 1x PBS at RT were performed. Next, Q-FISH was performed by applying a Cy3-labeled PNA telomere probe (Dako, Glostrup, Denmark) onto the slides. The areas were then covered with 25x25 mm cover slips and sealed with rubber cement. The slides were further processed by using Hybrite® (Vysis;

Abbott Diagnostics, Des Plains, IL) for denaturation at 80°C for 3 minutes, then hybridized for 2 hours at 30°C. After hybridization, the slides were rotatorily washed in a sequence of 70% deionized formamide / 10 mM Tris (pH 7.4) at RT 2 times, 15 minutes each, 1xPBS at RT for 1 minute, 0.1x SSC at 55°C for 5 minutes, and 2x SSC / 0.05% Tween 20 at RT 2 times, 5 minutes each. The primary and secondary antibodies from the immunofluorescence steps were then reapplied as described above, to improve the quality of the signals. The slides were then washed 3 times with 1x PBS and counterstained with DAPI and mounted with Vectashield®. Three independent experiments were performed.

3D image acquisition and analyses

Imaging of interphase nuclei was performed with a Zeiss DECON-1 microscope (Zeiss, Toronto, ON, Canada). Images were acquired by using AXIOVISION 4.8 (Zeiss, Toronto, ON, Canada) with a deconvolution module in multichannel mode. For every fluorochrome, the 3D image consists of a stack of 60 images with a sampling distance of 200 nm along the z and 106 nm in the x, y directions. The constrained iterative algorithm option was used (Schaefer et al., 2001). At least 30 nuclei were analyzed for each time point.

Quantifications of telomeres and TRF2 were performed using the program Teloview^{TM} (Chuang et al., 2004; Vermolen et al., 2005). The program is designed by choosing a simple threshold for the signals (telomeres or TRF2) so that a binary image is found. Based on a detection of the corresponding image, the centre of gravity of intensities is calculated for every object which results in a set of coordinates (x, y, z) denoted by crosses on the screen. Calculation of the integrated intensity of each telomere is made and is proportionated to the telomere length (Poon et al., 1999). Determination of the integration region is conducted by growing a sphere on top of the found coordinate. After every growth step (iteration), the sum under this volume (the telomere or TRF2) is subtracted by the sum just surrounding it (background level). In cases when the growth of

the sphere does not result in an integrated intensity increase, the algorithm stops and the integrated intensity of the telomere with an automatic background correction is obtained (Louis et al., 2005). Telomeric profiles consist of:

Telomere aggregates: Defined as clusters of telomeres that are found in close association and cannot be further resolved as separate entities at an optical resolution limit of 200 nm (Vermolen et al., 2005).

Telomere length: The following criteria was applied to determine telomere length. Telomeres with a relative fluorescent intensity (x-axis) ranging from 0 to 4,000 units were classified as very short, intensity from 4,000 to 7,000 units defined as short, intensity from 7,000 to 12,000 units as mid-sized, and intensity more than 12,000 units as large.

Telomere volume: Total telomere volume is the sum of all very short, short, mid-sized, and large telomeres and aggregates within one cell.

Nuclear volume: The nuclear volume was calculated according to the 3D nuclear DAPI staining as previously described (Sarkar et al., 2007).

a/c ratio: a/c ratio is a mean of defining progression through cell cycle in interphase cells (Gadji et al., 2010).

Nuclear matrix preparation

To investigate the detachment mechanism of the telomeric shelterin complex from the nuclear matrix, a nuclear matrix preparation procedure (He et al., 1990; Nickerson et al., 1997) was applied to the PreB *v-abl/myc* cells with and without c-Myc activation. To visualize the nuclear matrix component and its interactive structure, the nuclear matrix preparation protocol was applied, following the previously established protocol**.** The nuclear matrix preparation for mouse PreB *v-abl/myc* cells was adapted from He and colleagues. (He et al., 1990). Pre B *v-abl-myc* cells were seeded onto slides and fixed with 3.7% formaldehyde in 1x PBS for 30 minutes at RT. The slides

were washed twice, 2 minutes each time, in 1x PBS at 4°C, and then incubated on ice for 5 minutes with cytoskeleton (CSK) buffer containing 10 mM Pipes (Piperazine-N, N-bis (2- ethane-sulfonic acid) (pH 6.8), 300 mM sucrose, 100 mM NaCl, 3 mM $MgCl_2$, 1 mM EGTA (Ethylenebis- (oxyethylenenitrilo)) tetraacetic acid, 0.5% (v/v) thiodiglycol, 1 mM phenylmethylsulfonyl fluoride (PMSF), in 0.25% Triton X-100. They were then given a 5 minute-wash with shaking in 1x PBS at 4°C, followed by incubation on ice for 30 minutes with 3.7% formaldehyde in CSK buffer. After that, the slides were washed 4 times, 5 minutes each at 4°C, with digestion buffer containing 10 mM Pipes (pH 6.8), 300 mM sucrose, 50 mM NaCl, 3 mM $MgCl_2$, 1 mM EGTA, in 0.5% Triton X-100, followed by a 5-minute wash, with shaking, in 1x PBS at 4°C. Then the slides were rotatorily treated at 37°C for 1 hour, with DNAase I (D 5025; Sigma Aldrich, St. Louis, MO) in 1x reaction buffer containing 20 mM Tris – HCl (pH 8.3) and 2 mM $MgCL_2$. The final concentration of DNase I was 0.5mg/ml and the optimum concentration and time of DNAse I digestioin were confirmed by a quantification of DAPI intensity. The slides were then washed for 5 minutes at RT, gently shaking, with 0.25 M ammonium sulfate in digestion buffer, followed by 2 M NaCl in digestion buffer, and 2 additional washes with digestion buffer. Then a 5 minute-wash with shaking in 1x PBS at 4°C was done, followed by incubation on ice for 30 minutes with 3.7% formaldehyde in CSK buffer. After that the slides were washed 3 times, 5 minutes each with a rotator, in 1x PBS at 4°C and further processed with immunoFISH or co-immunofluorescence protocols. Coimmunofluorescence staining of TRF2 and lamin A/C and immunoFISH of TRF2 and telomere were conducted in parallel in c-Myc-activated and – inactivated PreB *v-abl/myc* cells undergoing nuclear matrix preparation. Image capture and analyses of the immuno-FISH in c-Myc-activated PreB *v-abl/myc* cells were conducted during that time period of chromosome repositioning.

Patient samples

Tissue sections, 5 µm in thickness, of archival formalin-fixed paraffin-embedded tissue from 18 primary human NSCLC patients were obtained from the BC Cancer Research Centre (Vancouver, British Columbia, Canada). Tumor areas were specified using haematoxylin and eosin (H&E) stained sections. Quantitative fluorescence *in situ* hybridization (Q-FISH) telomere experiments were performed without knowledge of the clinical characteristics of the patients in a blinded manner.

3D nuclear telomere experiments

Tissue specimens underwent 3D fixation to prepare interphase nuclei for Q-FISH experiments. In summary, paraffin embedded tissue specimens were deparaffinized by xylene 2 times for 15 minutes each and rehydrated in an ethanol series (100%, 70%, 50%, and 30%) for 5 minutes at each strength. Then the slides were incubated in 1M NaSCN at 80°C for 20 minutes and washed in 1x PBS twice for 5 minutes each at RT. Then the slides were incubated in 3.7% formaldehyde/1×PBS for 30 minutes and washed while shaking in 1×PBS 3 times for 5 minutes each, followed by 10 minutes of pepsin (50 µg/ml) / 0.01 M HCl treatment at 37°C. The slides were then washed once while shaking in 1×PBS for 5 minutes before being incubated in 3.7% formaldehyde/1×PBS for 10 minutes. 8 µl of PNA telomeric probe (Dako, Glostrup, Denmark) was applied onto each slide. To denature nuclear DNA and the probe, the slides were incubated at 80°C for 3 minutes followed by hybridization at 30°C for 2 hours using a Hybrite (Vysis; Abbott Diagnostics, Des Plains, IL). The slides were then washed while shaking twice for 15 minutes in 70% formamide/10mM Tris (pH-7.4), followed by in 1×PBS at RT for 1 minute, and in 0.1×SSC at 55°C for 5 minutes. The slides were washed while shaking in 2×SSC/0.05% Tween-20 twice for 5 minutes each at RT. After that the slides were counterstained with DAPI (1 µg/ml) and incubated in the dark for 3 minutes. The slides were finally air-dried and mounted with Vestashield® for analyses.

Image acquisition

The slides were imaged using an AxioImager Z2 microscope (Zeiss, Toronto, ON, Canada) and an AxioCam HR charge-coupled device (Zeiss, Toronto, ON, Canada). The DAPI filter was used to detect nuclear DNA staining and the Cy3 filter to detect telomeric probe signals. Eighty Z-stacks were acquired at a sampling distance of x, y: 102 nm and z: 200 nm for each slice of the stack. The acquired images were deconvolved using AxioVision 4.8 software (Zeiss, Toronto, ON, Canada) and a constrained iterative algorithm. Deconvolved images were converted into TIFF files and exported into TeloView^{TM} software for the analyses of telomeres, as previously described.

3D FISH of cytoband 17q25.3

Tissue specimens from the primary NSCLC patients underwent FISH with a 17q25.3 cytoband probe (G101024R-8, Agilent Technologies Inc., Santa Clara, CA) according to the manufacturer's instructions. A 17p11.2 cytoband probe (G100020G-8, Agilent Technologies Inc., Santa Clara, CA) was used as a control region for chromosome 17. After de-paraffinization with xylene and dehydration with ethanol, the slides were fixed in formaldehyde/magnesium chloride for 10 minutes, then washed 3 times in 2x SSC. The slides were then incubated in 1% RNAase/2xSSC at 37°C for 1 hour. After 3 rinses with 2x SSC, they underwent a protease pre-treatment in pepsin/0.01 M HCl at 37°C for 10 minutes and subsequent 2x SSC washes. The probes were mixed with FISH hybridization buffer and DDW, then denatured for 5 minutes at 80°C before being applied to the slide's area of interest, covered and sealed with rubber cement. The slide with probe was then denatured at 78°C for 3 minutes and incubated overnight at 37°C. The slides were washed in 2x SSC/0.05% Tween 20 and 4x SSC at 55°C, counterstained with DAPI and mounted in Vectashield®. Image acquisition was performed using a DAPI filter for nuclear staining, a Cy3 filter for detection of 17q25.3, and a FITC filter for 17p11.2 signals. For 3D images, 40 z-stacks at a sampling distance of x, y: 106 nm and z: 200 nm for each slice of the stack, were acquired. The

acquired 3D images were deconvolved then the copy numbers of 17q25.3 and 17p11.2 in at least 100 non-overlapping intact interphase nuclei from each tissue sample were analyzed visually, to determine the average copy numbers and average ratios of cytoband 17q25.3 to cytoband 17p11.2. The following criteria to classify a gain of cytoband 17q25.3 or chromosome 17 were implemented.

Copy gains of cytoband 17q25.3 : Gains were deemed in tissue specimens when the analysed nuclei presented an average ratio between the cytoband 17q25.3 and the reference 17p11.2 probe (i.e. 17q25.3/17p11.2) ≥1.5. Clonal gains were defined when the criteria were unmet, but ≥10 % of the analysed nuclei demonstrated a 17q25.3/17p11.2 probe ratio ≥1.5 (adapted from Bermudo et al., 2008).

Chromosome 17 copy gains : Gains of chromosome 17 were deemed when the analysed nuclei presented an average copy number ≥3 for both 17q25.3 and 17p11.2 cytobands, and the 17q25.3/17p11.2 ratio was <1.5.

Comparative genomic hybridization (CGH) and single nucleotide polymorphism (SNP) arrays data

CGH and SNP array data were obtained from the BC Cancer Research Centre (Vancouver, British Columbia, Canada)**.** Sixteen CGH and 11 SNP array data sets were available for the 18 NSCLC tumours. CGH and SNP arrays were conducted and processed as previously described (Lockwood et al., 2012; Thu et al., 2012). CGH arrays were processed to generate segmentation files representing copy number gains and losses for each tumour assayed (Lockwood et al., 2012). SNP arrays were conducted according to the manufacturer's instructions, and processed using Partek Genomics Suite Software as previously described (Thu et al., 2012). The copy number status of genes encompassed by the FISH probes interrogating 17p11.2 (RAI1 and SREBF1) and 17q25.3 (ANAPC11, ARHGDIA, ASPSCR1, CCDC57, DCXR, DUS1L, FASN, GPS1, LRRC45,

MAFG, NOTUM, NPB, P4HB, PCYT2, PYCR1, RAC3, RFNG, SIRT7, STRA13) were assessed in the segmented copy number profiles generated. For CGH data, genes with $\log_2$ ratios > 0.1 or < -0.1 were considered gained or lost, respectively, while genes with $\log_2$ ratios between -0.1 and 0.1 were considered copy neutral. For SNP data, genes with calculated copy numbers > 2.3 were considered gained, < 1.7 were considered lost, and between 1.7 and 2.3 were considered copy neutral. Tumour copy number statuses for the 17q25.3 and 17p11.2 cytobands as a whole were determined based on the copy numbers of genes comprising the region for each tumour; the copy numbers were found the same for all genes in each region within individual tumours. Q-FISH of the cytoband 17q25.3 region of interest using cytoband 17p11.2 as the control region was conducted for all 18 tumours without knowledge of the CGH and/or SNP array copy number calls.

Statistical analysis

As previously described, the different orientations of chromosomes were compared to each other using Chi-Square, Likelihood Ratio Chi-Square, Continuity Adj Chi-Square and Mantel Haenszel Chi-Square analyses (Schmälter et al., 2014). RRDs of Pre B *v-abl/myc* cells were compared over time by two-way ANOVA. TeloView™ software was used to quantify nuclear telomeric organization profiles and to compare parameters including the number of telomeres, signal intensity (the telomere length), number of telomere aggregates, a/c ratios (indicating the phase of the cell cycle), and nuclear volume. Differences in telomeric parameters between subgroups were compared using the Chi-squared test. Telomeric and fluorescence parameters between subgroups were compared over time by two-way ANOVA. Multiple comparisons using the least-square means test were performed in which interaction effects between two factors were found to be significant. *P*-values of <0.05 were considered statistically significant. Kaplan-Meier survival analyses were computed using SPSS for Windows (version 16.0; SPSS Inc., Chicago, IL) to obtain mean survival times of NSCLC patients in each subgroup.

Chapter IV : Results

Activation of c-Myc results in chromosome 11 repositioning in mouse PreB *v-abl/myc* cells

To investigate whether c-Myc upregulation affected the 3D positioning of mouse chromosome 11 in the interphase nuclei of Pre B *v-abl/myc* cells, the effect of conditional c-Myc expression in the immortalized mouse Pre B *v-abl/myc* cells, stably transfected with MycER^{TM}, was examined. After MycER^{TM} activation with 4HT, nuclear c-Myc signals were observed in Pre B *v-abl/myc* cells more predominantly, compared to the non-4HT treated control cells (hour 0) (Fig. 5). Pre B *v-abl/myc* cells with MycER^{TM} activation revealed more Myc immunofluorescence staining (green colour: FITC) at hours 2, 4, and 6 than the control (hour 0).

Figure 5.

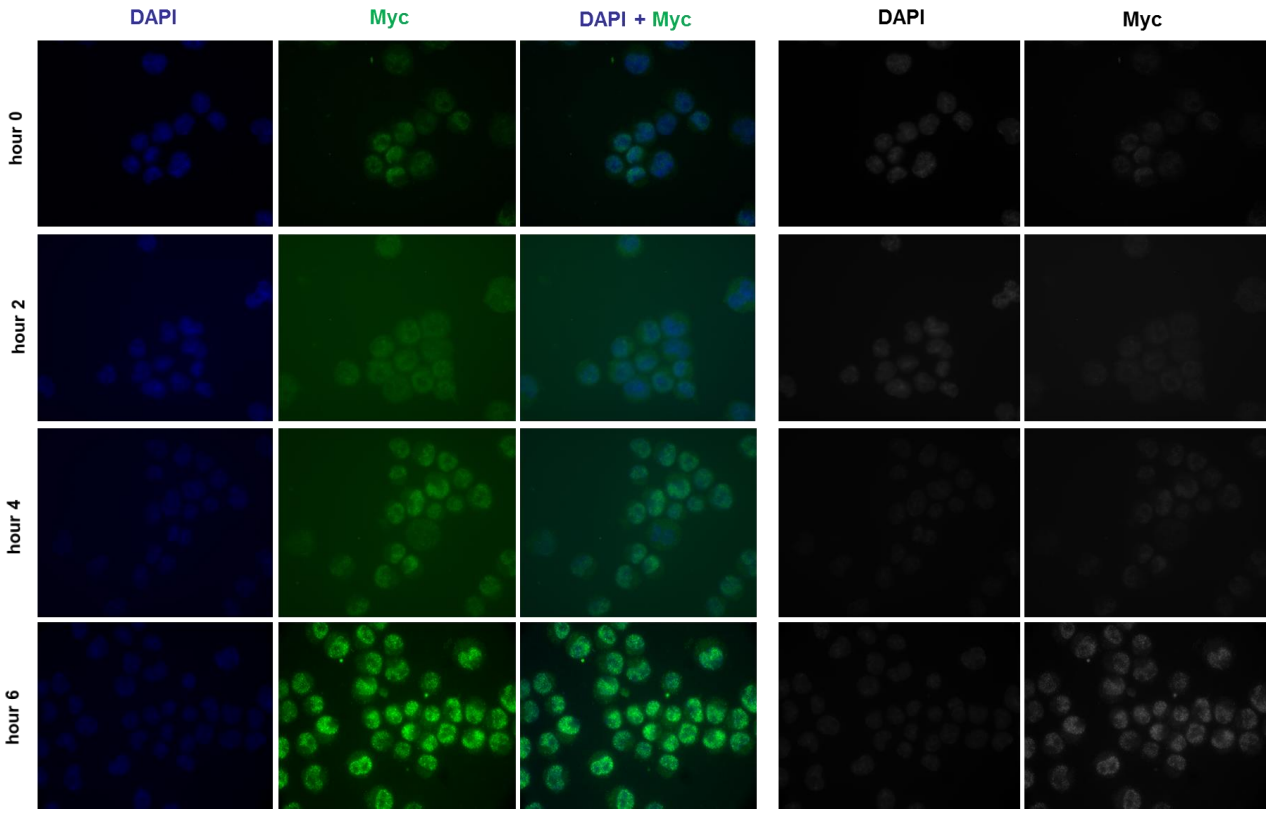

Figure 5. Immunofluorescence staining of c-Myc in PreB *v-abl/myc* cells after c-Myc activation demonstrated with high objective (63×), at hours 0 to 6. The last 2 columns depict cells in gray

scale to better reveal the localization and intensity of c-Myc proteins. Pre B *v-abl/myc* cells with MycER^{TM} activation (at hours 2, 4, and 6) reveal higher levels of Myc immunofluorescence staining (green colour: FITC) than the control (hour 0).

The relative radial distribution (RRD) of each chromosome copy was automatedly determined using the 3D measurements from the nuclear segmentation program. Fig. 6 illustrates a computerized image from the nuclear segmentation automated program of mouse chromosomes 10 and 11 in interphase Pre B *v-abl/myc* nucleus.

Figure 6.

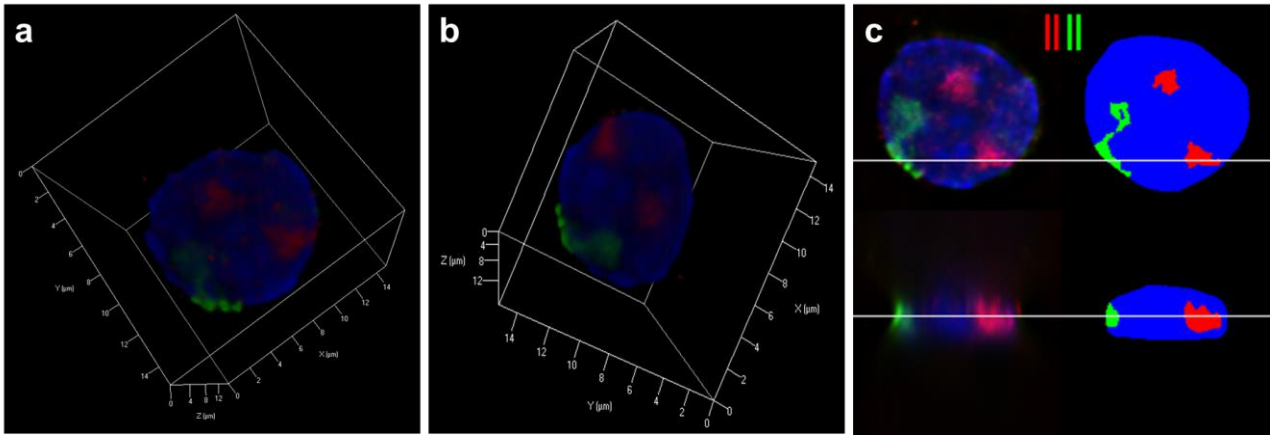

Figure 6. Chromosome paints in PreB *v-abl/myc* cells. (a) and (b) Representative images of PreB *v-abl/myc* cells underwent FISH analysis displayed in different dimensions with high objective (63×). Chromosomes (blue) were hybridized with chromosome paint probes for mouse chromosomes 11 (red) or 10 (green, the negative control). At least 90 interphase nuclei each of Myc- or non-Myc-activated cells from 3 independent experiments were examined for each time point for positioning of chromosomes 11 and 10. (c) Positioning analyses of chromosomes 11 and 10 using a RRD were carried out through a specifically-developed computerized program.

Three different time courses of Pre B *v-abl/myc* cell harvesting schemes after MycER^{TM} activation were performed. First, a determination of the earliest time point of c-Myc-induced change of position in mouse chromosome 11 was carried out at 0, 6, 12, 24, 48, and 72 hours; *i.e.* over a 3-day period. The earliest time point revealing the repositioning of chromosome 11 was identified at hour 6. Nuclear repositioning of chromosome 11 was demonstrated more frequently and in a higher degree of statistical significance in c-Myc- driven mouse PreB *v-abl/myc* cells compared to the cells without c-Myc activation (Table 1) and to chromosome 10 of c-Myc-induced PreB *v-abl/myc* cells (Tables 1, 2, and 3, and Fig. 7).

Table 1. RRD of mouse chromosomes 11 and 10 in PreB *v-abl/myc* cells in the first scheme of cell harvesting

Time points compared	c-Myc-activated Chr 11 (p-value)	c-Myc-inactivated Chr 11 (p-value)	c-Myc-activated Chr 10 (p-value)	c-Myc-inactivated Chr 10 (p-value)
0 vs. 6 hr	0.41 vs. 0.55 (0.02)	0.41 vs. 0.44 (0.24)	0.46 vs. 0.62 (0.0008)	0.62 vs. 0.51 (0.02)
0 vs. 12 hr	0.41 vs. 0.41 (0.92)	0.41 vs. 0.54 (0.04)	0.46 vs. 0.55 (0.04)	0.62 vs. 0.55 (0.10)
0 vs. 24 hr	0.41 vs. 0.50 (0.09)	0.41 vs. 0.51 (0.11)	0.46 vs. 0.55 (0.04)	0.62 vs. 0.57 (0.16)
0 vs. 48 hr	0.41 vs. 0.32 (0.009)	0.41 vs. 0.48 (0.17)	0.46 vs. 0.49 (0.59)	0.62 vs. 0.54 (0.05)
0 vs. 72 hr	0.41 vs. 0.39 (0.45)	0.41 vs. 0.46 (0.83)	0.46 vs. 0.48 (0.62)	0.62 vs. 0.47 (0.001)
6 vs. 12 hr	0.55 vs. 0.41 (7.52e-005)	0.44 vs. 0.54 (0.001)	0.62 vs. 0.55 (0.06)	0.51 vs. 0.55 (0.37)
6 vs. 24 hr	0.55 vs. 0.50 (0.70)	0.44 vs. 0.51 (0.01)	0.62 vs. 0.55 (0.14)	0.51 vs. 0.57 (0.13)
6 vs. 48 hr	0.55 vs. 0.32 (1.00e-006)	0.44 vs. 0.48 (0.27)	0.62 vs. 0.49 (0.0004)	0.51 vs. 0.54 (0.05)
6 vs. 72 hr	0.55 vs. 0.39 (0.0001)	0.44 vs. 0.46 (0.39)	0.62 vs. 0.48 (5.85e-007)	0.51 vs. 0.47 (0.36)
12 vs. 24 hr	0.41 vs. 0.50 (0.005)	0.54 vs. 0.51 (0.16)	0.55 vs. 0.55 (0.90)	0.55 vs. 0.57 (0.89)
12 vs. 48 hr	0.41 vs. 0.32 (0.0006)	0.54 vs. 0.48 (0.03)	0.55 vs. 0.49 (0.22)	0.55 vs. 0.54 (0.27)
12 vs. 72	0.41 vs. 0.39	0.54 vs. 0.46	0.55 vs. 0.48	0.55 vs. 0.47

hr	(0.60)	(0.03)	(0.003)	(0.009)
24 vs. 48 hr	0.50 vs. 0.32 (5.64e-005)	0.51 vs. 0.48 (0.17)	0.55 vs. 0.49 (0.11)	0.57 vs. 0.54 (0.24)
24 vs. 72 hr	0.50 vs. 0.39 (0.005)	0.51 vs. 0.46 (0.21)	0.55 vs. 0.48 (0.003)	0.57 vs. 0.47 (0.004)
48 vs. 72 hr	0.32 vs. 0.39 (0.009)	0.48 vs. 0.46 (0.37)	0.49 vs. 0.48 (0.14)	0.54 vs. 0.47 (0.007)

Table 1. The median values of mean RRD of chromosomes 11 and 10 in PreB *v-abl/myc* cells with and without c-Myc activation at different time points. The red numbers indicate where a statistically significant difference ($P < 0.05$) was observed.

Table 2. RRD of mouse chromosome 11 in c-Myc-activated PreB *v-abl/myc* cells

Time point	Median values of mean RRD	*P* -value
h0 vs. h6	0.41 vs. 0.55	0.02
h6 vs. h12	0.55 vs. 0.41	7.52e-005
h12 vs. h24	0.41 vs. 0.50	0.005
h24 vs. h48	0.50 vs. 0.32	5.64e-005
h48 vs. h72	0.32 vs. 0.39	0.009

Table 2. Median values of mean RRD of mouse chromosome 11 in c-Myc activated PreB *v-abl/myc* cells at each time point. The red numbers indicate where a statistically significant difference ($P < 0.05$) was observed.

Table 3. RRD of mouse chromosome 10 in c-Myc-activated PreB *v-abl/myc* cells

Time point	Median values of mean RRD	*P* -value
h0 vs. h6	0.46 vs. 0.62	0.0008
h6 vs. h12	0.62 vs. 0.55	0.06
h12 vs. h24	0.55 vs. 0.55	0.90
h24 vs. h48	0.55 vs. 0.49	0.11
h48 vs. h72	0.49 vs. 0.48	0.14

Table 3. Median values of mean RRD of mouse chromosome 10 in c-Myc activated PreB *v-abl/myc* cells at each time point. The red numbers indicate where a statistically significant difference ($P < 0.05$) was observed.

Figure 7.

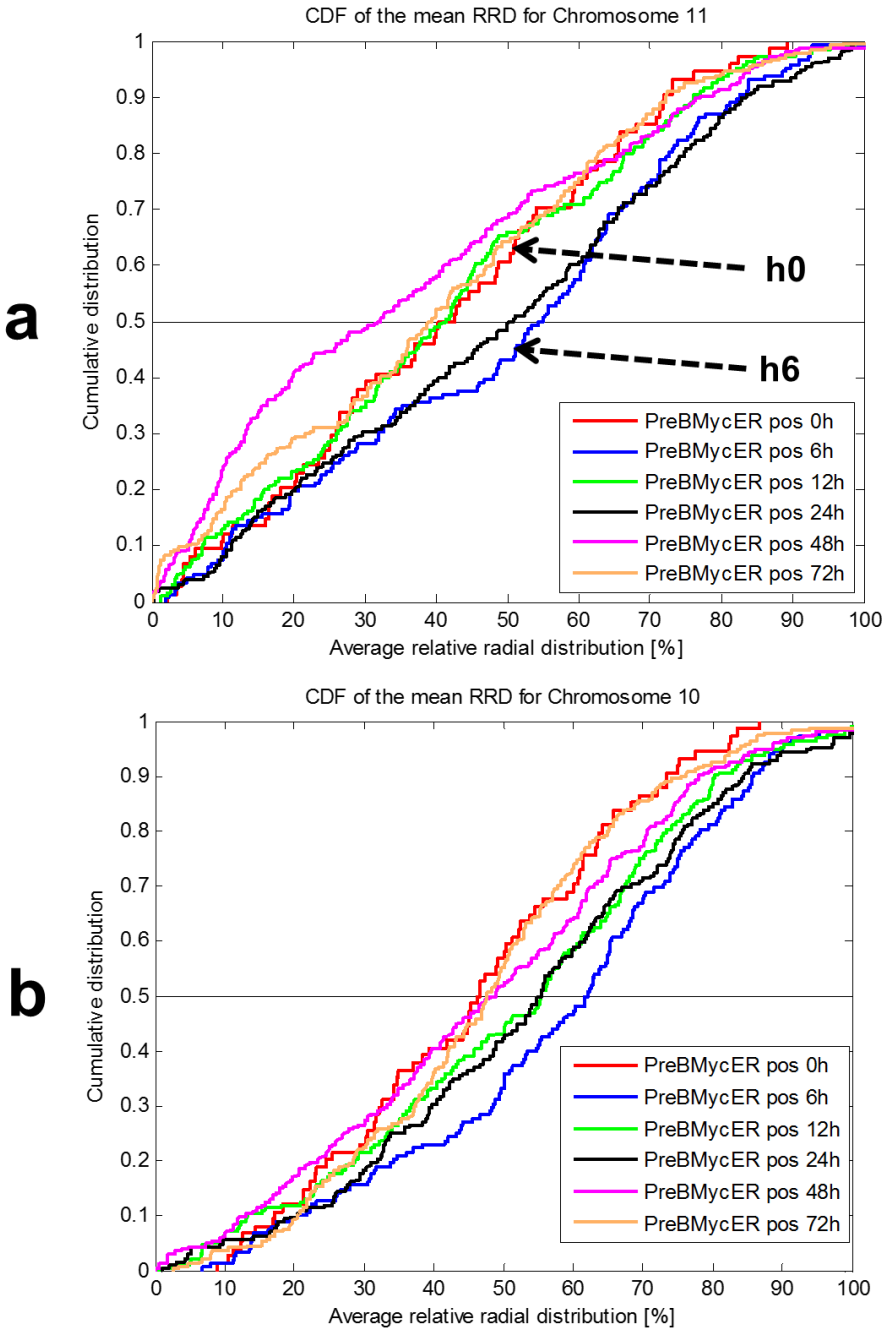

Figure 7. Quantification of average RRD of mouse chromosome 11 (a) in PreB *v-abl/myc* cells that underwent Myc activation at different time points. The mouse chromosome 10 (b) serves as a negative control. The repositioning of chromosome 11 was observed as early as at hour 6 after Myc activation (marked with black arrows in (a)) with a statistically significant difference ($P < 0.05$), by two-way ANOVA.

Chromosomes 5 and 7 served as positive controls and the repositioning of the respective chromosomes were observed in a distinct manifestation (Tables 4 and 5). The repositioning of chromosome 5 was observed as early as at hour 6 after Myc activation whereas the repositioning of chromosome 7 was observed only at hour 12 after Myc activation.

Table 4. RRD of mouse chromosome 5 in c-Myc-activated PreB *v-abl/myc* cells

Time point	Median values of mean RRD	*P* -value
h0 vs. h6	0.49 vs. 0.42	0.01
h0 vs. h12	0.49 vs. 0.36	9.45e-005
h0 vs. h24	0.49 vs. 0.32	5.19e-005
h0 vs. h48	0.49 vs. 0.53	0.67
h0 vs. h72	0.49 vs. 0.33	1.31e-005

Table 4. Median values of mean RRD of mouse chromosome 5 in c-Myc activated PreB *v-abl/myc* cells at each time point. The red numbers indicate where a statistically significant difference ($P < 0.05$) was observed.

Table 5. RRD of mouse chromosome 7 in c-Myc-activated PreB *v-abl/myc* cells

Time point	Median values of mean RRD	*P* -value
h0 vs. h6	0.36 vs. 0.46	0.07
h0 vs. h12	0.36 vs. 0.48	0.02
h0 vs. h24	0.36 vs. 0.32	0.26
h0 vs. h48	0.36 vs. 0.44	0.19
h0 vs. h72	0.36 vs. 0.31	0.31

Table 5. Median values of mean RRD of mouse chromosome 7 in c-Myc activated PreB *v-abl/myc* cells at each time point. The red numbers indicate where a statistically significant difference ($P < 0.05$) was observed.

At the second scheme of cell harvesting, c-Myc in PreB *v-abl/myc* cells was activated then analyzed over the time period that was expected to reveal the first observation of chromosome 11 repositioning. Following the second time course for cell harvesting every 1 hour for 6 hours, the repositioning of chromosome 11 in PreB *v-abl/myc* cells was observed as early as hour 1 after Myc activation. Nuclear repositioning of chromosome 11 was demonstrated more frequently in c-Myc-driven mouse PreB *v-abl/myc* cells, compared to the cells without c-Myc activation (Table 6 and Fig. 8) and to the chromosome 10 of c-Myc-induced PreB *v-abl/myc* cells (Table 6). Evaluation of the 3D positioning of mouse chromosome 11, in nuclei of non-MycER^{TM}-activated cells was conducted as a control and revealed a less significant pattern of chromosome repositioning (Table 6 and Fig. 8).

Table 6. RRD of mouse chromosomes 11 and 10 in PreB *v-abl/myc* cells in the second scheme of cell harvesting

Time points compared	c-Myc-activated Chr 11 (p-value)	c-Myc inactivated Chr 11 (p-value)	c-Myc-activated Chr 10 (p-value)	c-Myc-intivated Chr 10 (p-value)
0 vs. 1 hr	0.46 vs. 0.47 (0.03)	0.42 vs. 0.48 (0.35)	0.40 vs. 0.47 (0.34)	0.45 vs. 0.47 (0.48)
0 vs. 2 hr	0.46 vs. 0.54 (0.02)	0.42 vs. 0.48 (0.08)	0.40 vs. 0.51 (0.02)	0.45 vs. 0.45 (0.96)
0 vs. 3 hr	0.46 vs. 0.51 (0.07)	0.42 vs. 0.44 (0.06)	0.40 vs. 0.38 (0.60)	0.45 vs. 0.46 (0.26)
0 vs. 4 hr	0.46 vs. 0.57 (0.03)	0.42 vs. 0.51 (0.04)	0.40 vs. 0.48 (0.16)	0.45 vs. 0.62 (0.0002)
0 vs. 5 hr	0.46 vs. 0.39 (0.04)	0.42 vs. 0.42 (1.00)	0.40 vs. 0.41 (0.56)	0.45 vs. 0.44 (0.15)
0 vs. 6 hr	0.46 vs. 0.48 (0.53)	0.42 vs. 0.51 (0.04)	0.40 vs. 0.51 (0.008)	0.45 vs. 0.47 (0.87)
1 vs. 2 hr	0.47 vs. 0.54 (0.02)	0.48 vs. 0.48 (0.73)	0.47 vs. 0.51 (0.28)	0.47 vs. 0.45 (0.38)
1 vs. 3 hr	0.47 vs. 0.51 (0.003)	0.48 vs. 0.44 (0.65)	0.47 vs. 0.38 (0.14)	0.47 vs. 0.46 (0.64)
1 vs. 4 hr	0.47 vs. 0.57 (0.01)	0.48 vs. 0.51 (0.48)	0.47 vs. 0.48 (0.96)	0.47 vs. 0.62 (0.0001)
1 vs. 5 hr	0.47 vs. 0.39 (0.02)	0.48 vs. 0.42 (0.48)	0.47 vs. 0.41 (0.09)	0.47 vs. 0.44 (0.39)
1 vs. 6 hr	0.47 vs. 0.48 (0.02)	0.48 vs. 0.51 (0.61)	0.47 vs. 0.51 (0.22)	0.47 vs. 0.47 (0.60)
2 vs. 3 hr	0.54 vs. 0.51 (0.56)	0.48 vs. 0.44 (0.73)	0.51 vs. 0.38 (0.002)	0.45 vs. 0.46 (0.59)
2 vs. 4 hr	0.54 vs. 0.57 (0.65)	0.48 vs. 0.51 (0.49)	0.51 vs. 0.48 (0.21)	0.45 vs. 0.62 (0.0005)
2 vs. 5 hr	0.54 vs. 0.39 (3.57e-006)	0.48 vs. 0.42 (0.13)	0.51 vs. 0.41 (0.003)	0.45 vs. 0.44 (0.82)
2 vs. 6 hr	0.54 vs. 0.48 (0.16)	0.48 vs. 0.51 (0.52)	0.51 vs. 0.51 (0.32)	0.45 vs. 0.47 (0.97)
3 vs. 4 hr	0.51 vs. 0.57 (0.33)	0.44 vs. 0.51 (0.16)	0.38 vs. 0.48 (0.17)	0.46 vs. 0.62 (0.001)
3 vs. 5 hr	0.51 vs. 0.39 (0.0001)	0.44 vs. 0.42 (0.12)	0.38 vs. 0.41 (0.58)	0.46 vs. 0.44 (0.68)
3 vs. 6 hr	0.51 vs. 0.48 (0.20)	0.44 vs. 0.51 (0.15)	0.38 vs. 0.51 (0.002)	0.46 vs. 0.47 (0.76)
4 vs. 5 hr	0.57 vs. 0.39 (0.0001)	0.51 vs. 0.42 (0.05)	0.48 vs. 0.41 (0.06)	0.62 vs. 0.44 (0.0003)
4 vs. 6 hr	0.57 vs. 0.48 (0.10)	0.51 vs. 0.51 (0.70)	0.48 vs. 0.51 (0.45)	0.62 vs. 0.47 (0.0007)
5 vs. 6 hr	0.39 vs. 0.48 (0.003)	0.42 vs. 0.51 (0.12)	0.41 vs. 0.51 (0.0006)	0.44 vs. 0.47 (0.65)

Table 6. The median values of mean RRD of chromosomes 11 and 10 in PreB *v-abl/myc* cells with and without c-Myc activation at time points 0 to 6 hr. The repositioning of chromosome 11 was observed as early as hour 1 after Myc activation (highlighted in yellow). The red numbers indicate where a statistically significant difference ($P < 0.05$) was observed. Nuclear repositioning of chromosome 11 was demonstrated more frequently in c-Myc- driven mouse PreB *v-abl/myc* cells, compared to the cells without c-Myc activation and to the chromosome 10 of c-Myc-induced PreB *v-abl/myc* cells.

Figure 8.

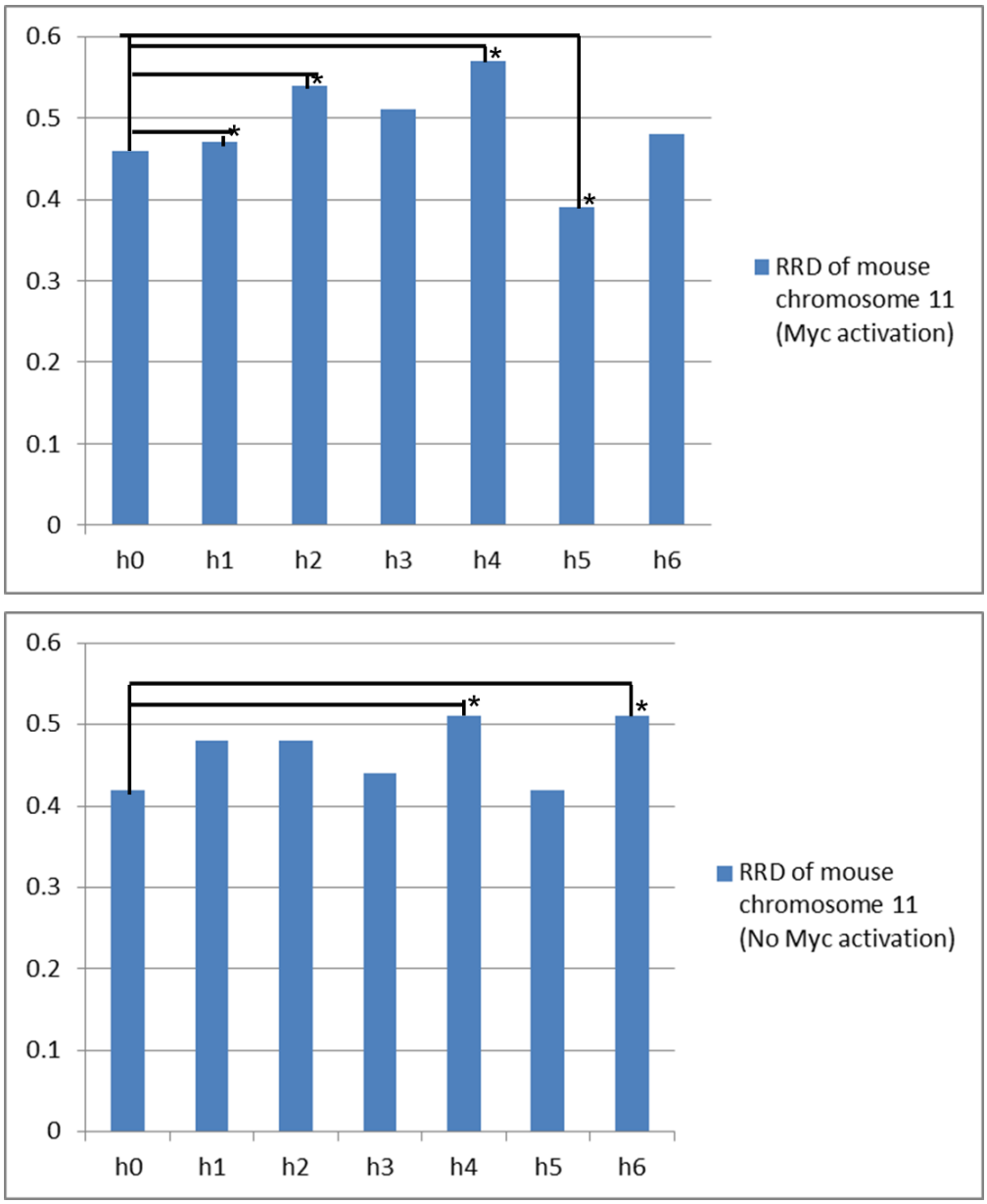

Figure 8. Comparisons between PreB *v-abl/myc* cells with and without Myc activation demonstrate the median values of average RRD of mouse chromosome 11 at the time points hours 0-6. The repositioning of chromosome 11 was observed as early as at hour 1 after Myc activation. The symbol * indicates where a statistically significant difference ($P < 0.05$) was observed. Evaluation of the 3D positioning of mouse chromosome 11 in nuclei of non-MycER^{TM}-activated cells was conducted as a control and revealed a less frequent significant pattern of chromosome repositioning.

Lastly, cells were harvested every 20 minutes for 60 minutes after MycER^{TM} activation and the interactions between TRF2, telomeres, and nuclear matrix protein lamin A/C examined. This was to identify the mechanism potentially responsible for c-Myc activated mouse chromosome 11 repositioning in Pre B *v-abl/myc* cells and the nuclear matrix preparation protocol was implemented into this part of the study.

Nuclear matrix preparation in PreB *v-abl/myc* cells

Processing of PreB *v-abl/myc* cells through a nuclear matrix preparation protocol was applied to better visualize the nuclear matrix component and its interactive structure. This procedure was implemented into the experiments mainly to investigate the detachment mechanism of telomeric shelterin complex from the nuclear matrix. PreB *v-abl/myc* cells were processed for nuclear matrix preparation by high-salt extraction and DNaseI treatment. Digestion of DNA material by DNAseI was confirmed by quantification of DAPI intensity (Table 7).

Table 7. Quantification of DAPI in PreB *v-abl-myc* cells in nuclear matrix preparation

Timepoint	Mean DAPI intensity (RFU ±S.D.)	Level of decreased DAPI from h0
0 min (h0)	8787.01 ± 2126.33	0%
30 min	7139.39 ± 2529.44	18.75%
45 min	5975.40 ± 2011.97	32.0%
1 h	905.96 ± 304.76	89.69%
1 h 15 min	685.10 ± 198.84	92.20%
1 h 30 min	1031.37 ± 388.61	88.26%
1 h 45 min	829.45 ± 203.38	90.56%
2 h	829.51 ± 231.20	90.56%

Table 7. Quantification of mean DAPI intensity per cell in PreB *v-abl-myc* cells undergoing nuclear matrix preparation, through relative fluorescence units (RFU). At least 30 PreB *v-abl-myc* cells from each timepoint of DNaseI treatment were examined to determine the appropriate

duration for DNaseI digestion. Markedly decreased and sustainable DAPI intensity, representing the optimum time of DNaseI treatment, was identified at 1 hour of incubation. The final concentration of DNaseI was 0.5 mg/ml at the temperature of 37°C.

Table 7 exhibits DAPI intensities quantified by average fluorescence intensity before and after the digestion at different timepoint with DNAseI. The final concentration of 0.5 mg/ml for DNaseI at 37°C was determined to be an appropriate condition to use for the experiments of nuclear matrix preparation for PreB *v-abl/myc* cells. By using differential interference contrast (DIC), an imaging technique enabling better detection of non-stained cells, PreB *v-abl/myc* cells processed through the nuclear matrix preparation could be demonstrated more clearly as shown in Fig. 9.

Figure 9.

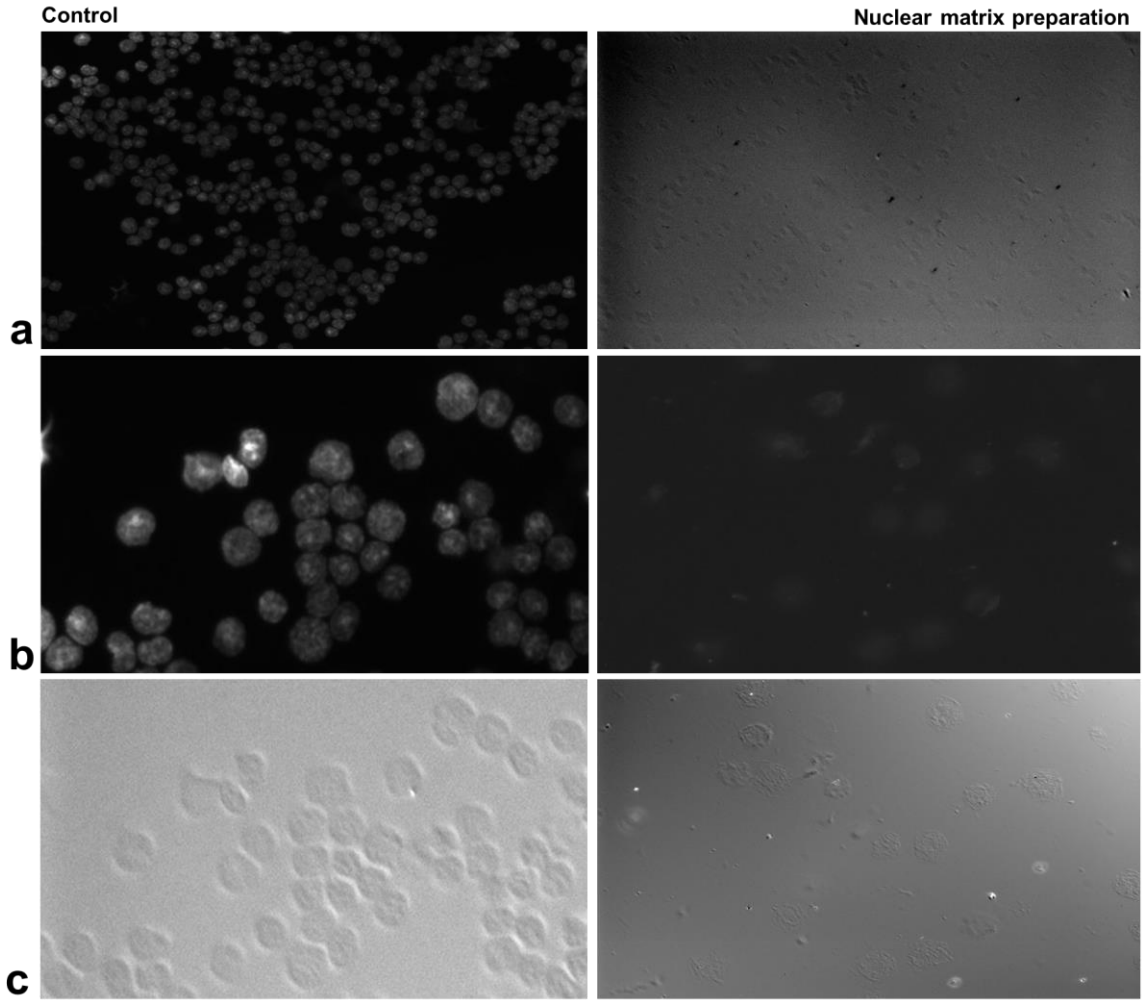

Figure 9. Nuclear matrix preparation in PreB *v-abl/myc* cells demonstrated with low objective (20×) in (a) and high objective (63×) in (b) and (c). DAPI images with no DNaseI digestion were shown in (a) and (b). Differential interference contrast (DIC) was applied in (c) to better identify cells that underwent nuclear matrix preparation. The DNaseI final concentration was 0.5 mg/ml for a digestion time of 1 hour at the temperature of 37°C.

Alterations of TRF2, telomeres, and lamin A/C upon c-Myc induction

To investigate the potential mechanism underlying the phenomenon of chromosome 11 repositioning in Pre B *v-abl/myc* cells after c-Myc upregulation, immunofluorescence revealing

TRF2 and lamin A/C, and immunoFISH investigating TRF2 and telomeres were conducted (Figs. 10-13).

Figure 10.

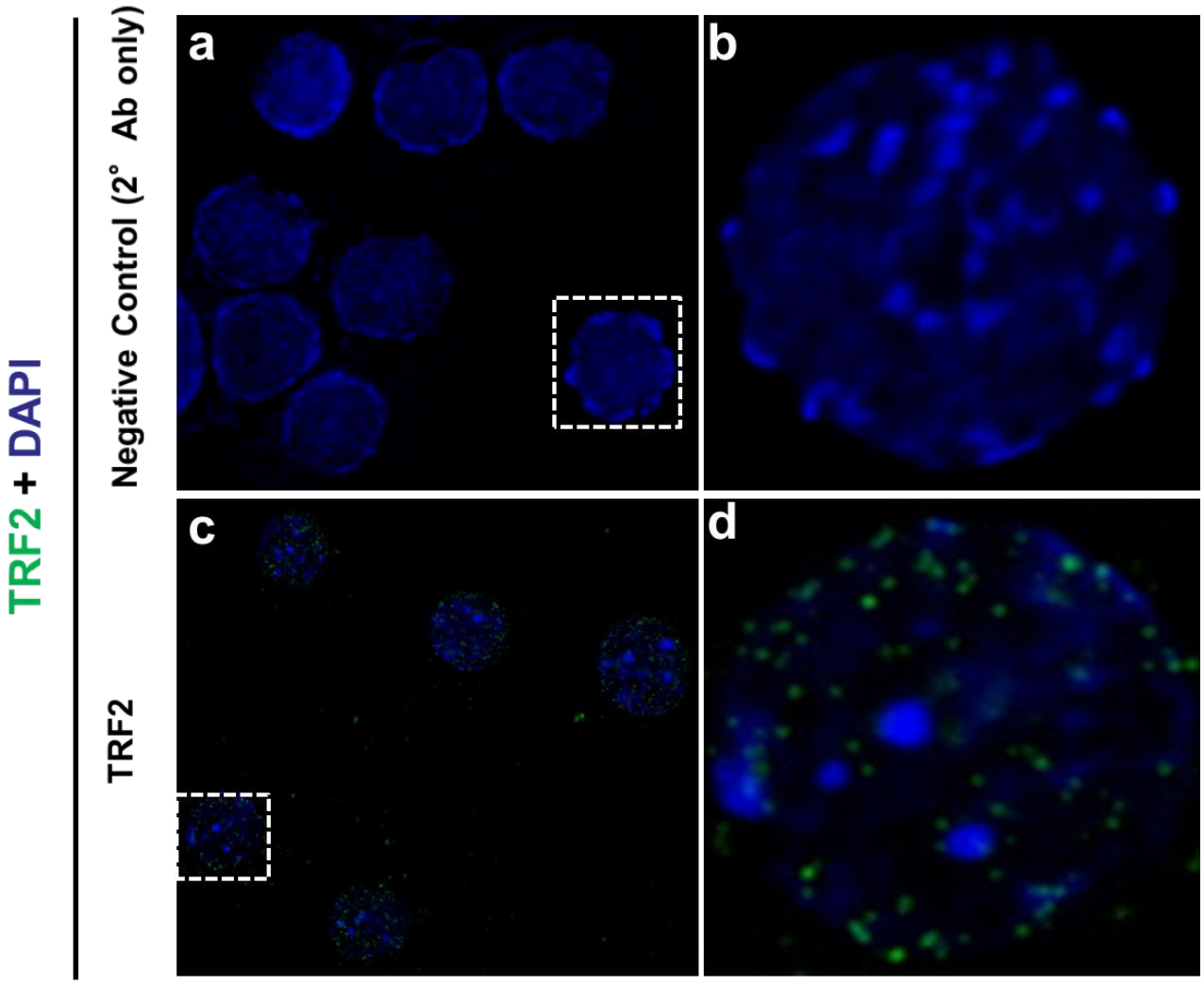

Figure 10. Assessing TRF2 expression in PreB *v-abl/myc* cells (63×, objective). PreB *v-abl/myc* cells underwent immunofluorescence for TRF2 antibody depiction: a, b negative controls (secondary antibody only). c, d TRF2 (green signals). The chromosomes were stained with DAPI (blue). Representative nuclei are outlined in white and enlarged in b, d. Note that the image represents a single section on the z axis.

Figure 11.

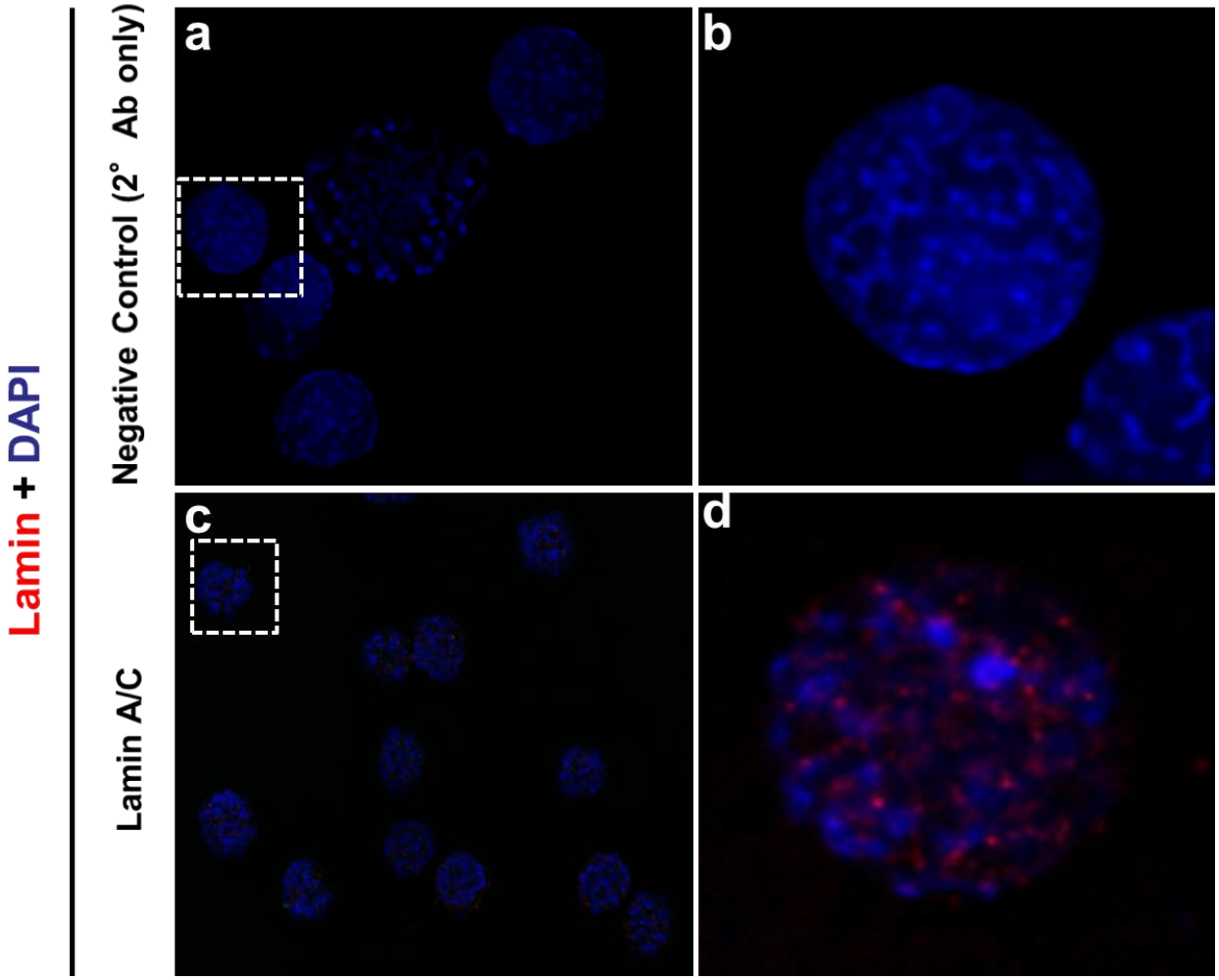

Figure 11. Assessing lamin A/C expression in PreB *v-abl/myc* cells (63×, objective). PreB *v-abl/myc* cells underwent immunofluorescence for lamin A/C antibody depiction: a, b negative controls (secondary antibody only). c, d lamin A/C (red signals). The chromosomes were stained with DAPI (blue). Representative nuclei are outlined in white and enlarged in b, d. Note that the image represents a single section on the z axis.

Figure 12.

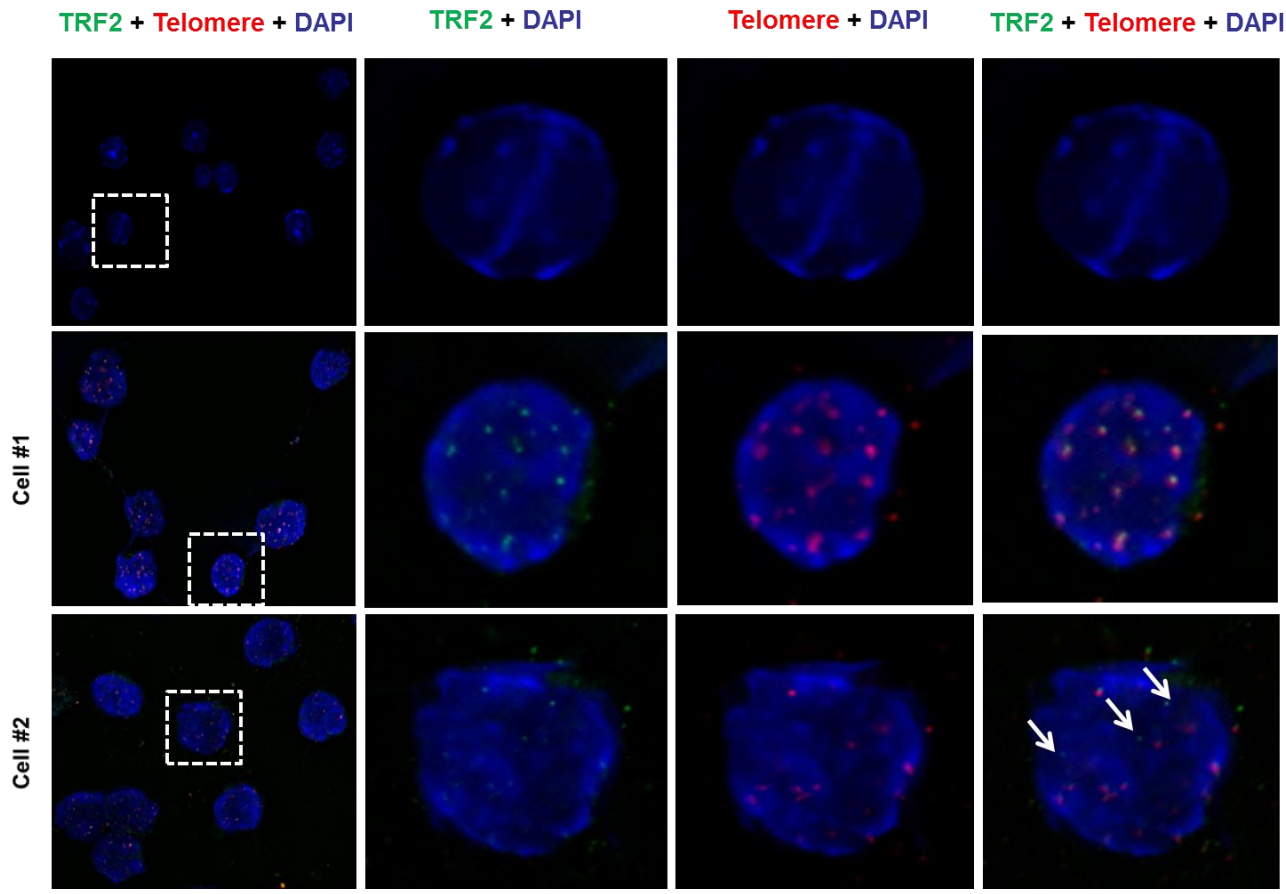

Figure 12. Representative images of TRF2 (green) and telomeres (red) in PreB *v-abl/myc* cells by immunostaining-FISH with an anti-TRF2 antibody and a telomeric PNA probe. The chromosomes were stained with DAPI (blue). Excess TRF2 signals not aligning with telomeres are marked by white arrows. Note that the image represents a single section on the z axis.

Figure 13.

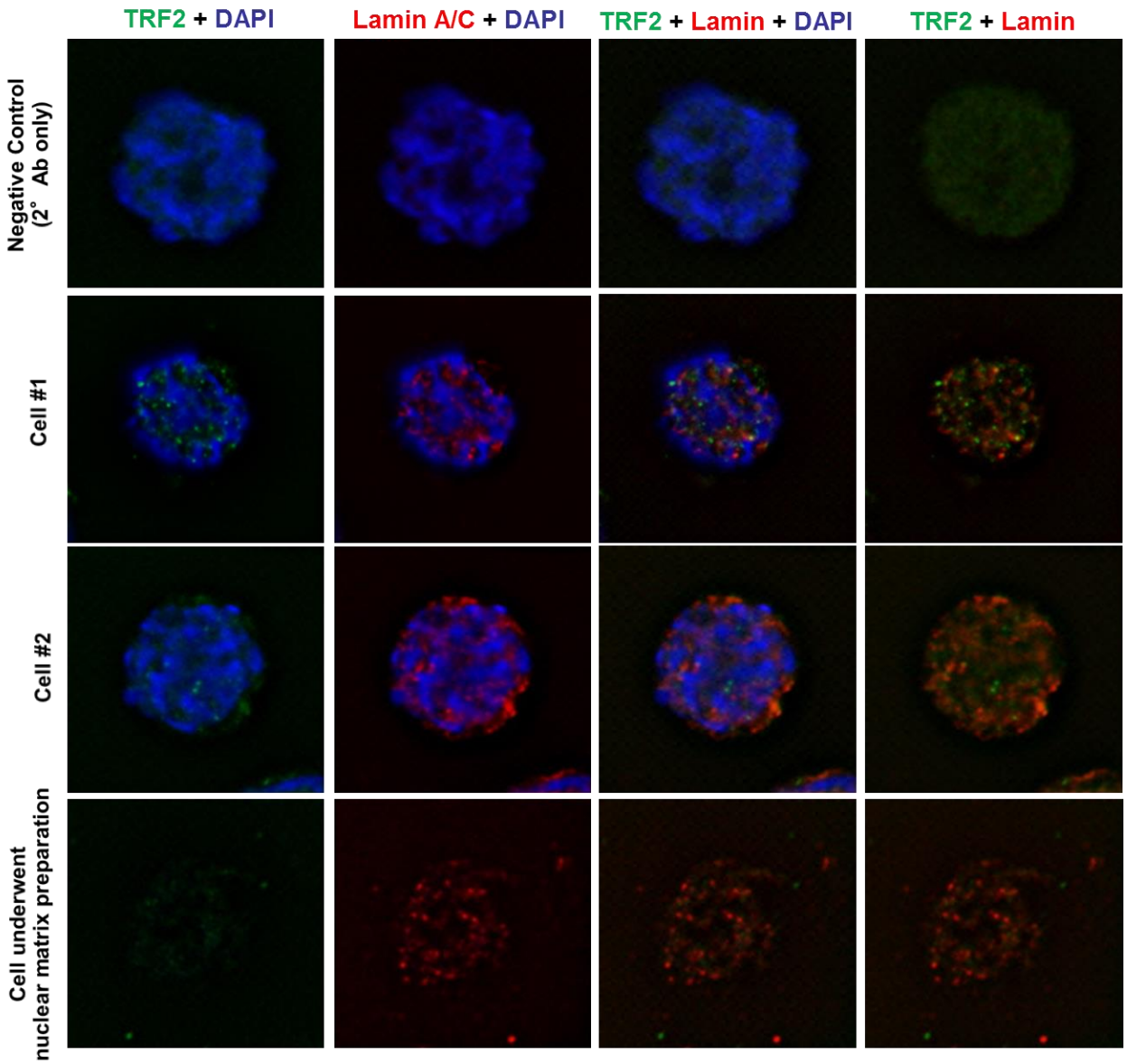

Figure 13. Representative images of TRF2 (green) and lamin A/C (red) in PreB *v-abl/myc* cells by co-immunofluorescence staining with anti-TRF2 and anti-lamin A/C antibodies. The chromosomes were stained with DAPI (blue). The top panel represents a negative control with secondary antibody only. The bottom panel represents a single PreB *v-abl/myc* cell that underwent nuclear matrix preparation followed by co-immunofluorescence staining. Note that the image represents a single section on the z axis.

The objective of this section of the thesis was to determine whether c-Myc upregulation, which was shown to result from chromosome 11 repositioning in the previous experiments, would potentially result from a detachment of the telomere / TRF2 complex from the nuclear matrix lamin A/C. Figs. 14 and 15 depict the number and intensities of telomeres and TRF2 signals in cells processed through a regular procedure (Fig. 14) and through nuclear matrix preparation (Fig. 15). Statistically significant decreases of TRF2 intensities in parallel with significantly increased numbers of lower intensity telomeres, representing telomeres shorter in length, were observed in PreB *v-abl-myc* cells within the first hour after Myc induction (Figs. 14 and 15). An increase in the total number of telomeric signals in PreB *v-abl/myc* cells at minute 20 after c-Myc induction was also observed (Figs. 14 and 15).

Figure 14.

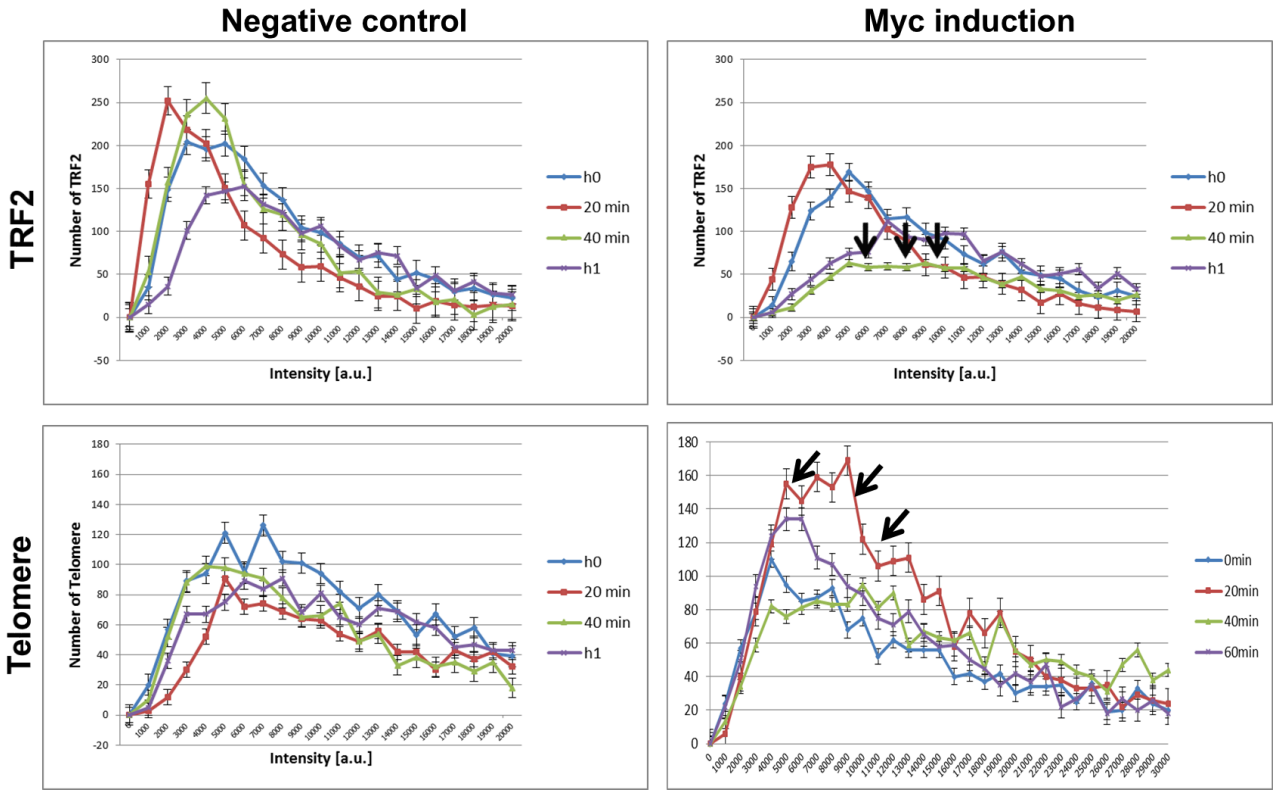

Figure 14. Quantification of telomeric signal intensities associated with the TRF2 protein. At least 90 PreB *v-abl-myc* cells from 3 independent experiments were examined for this association. Statistically significant decreases of TRF2 intensities ($P < 0.0001$) in parallel with significantly increased numbers of lower intensity telomeres ($P < 0.0001$), representing telomeres shorter in length, were observed in PreB *v-abl-myc* cells within the first hour after Myc induction, as marked by black arrows.

Figure 15.

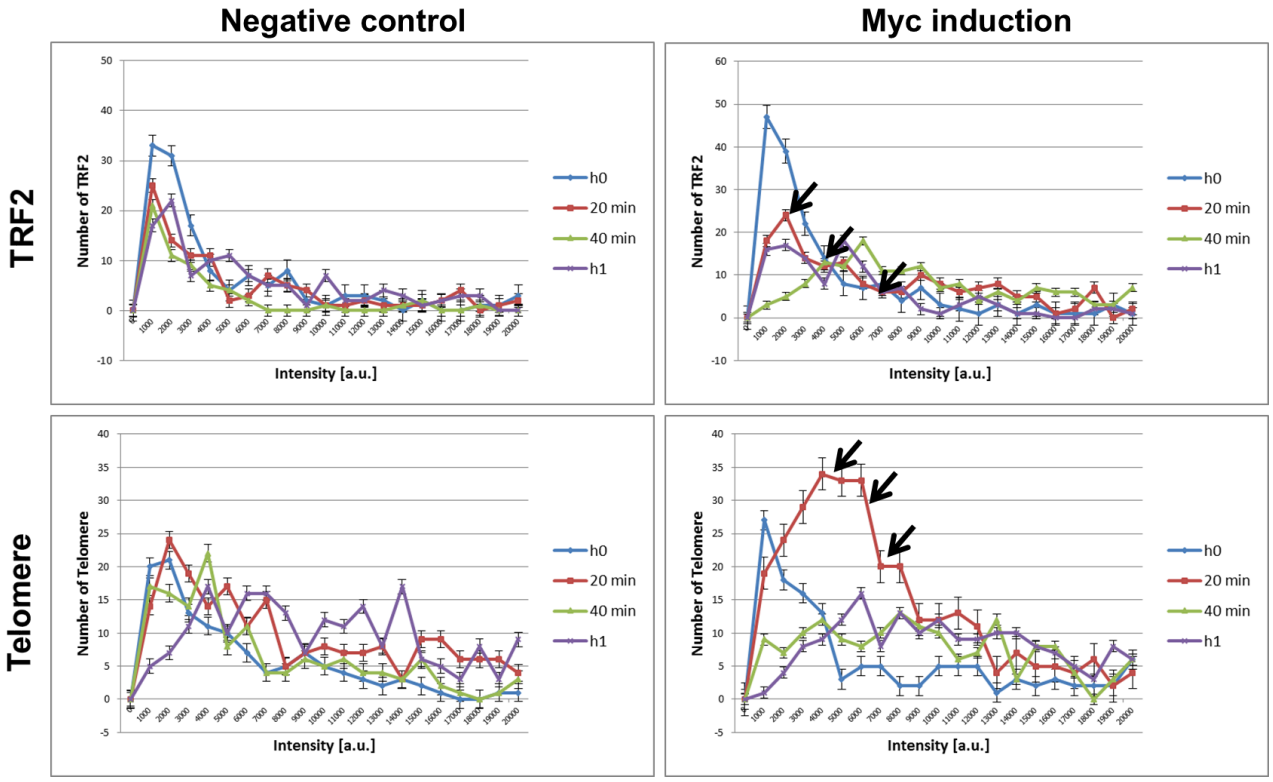

Figure 15. Quantification of telomeric signal intensities associates with TRF2 proteins in PreB *v-abl-myc* cells which underwent nuclear matrix preparation. At least 90 PreB *v-abl-myc* cells from 3 independent experiments were examined for this association. Similar to the regular experiments, statistically significant decreases of TRF2 intensities ($P < 0.001$) in parallel with significantly increased number of lower intensity telomeres ($P < 0.0001$), representing telomeres shorter in length, were observed in PreB *v-abl-myc* cells as early as at 20 minutes after Myc induction, as marked by black arrows.

Comparison of the telomeric intensity distribution in which intensity correlating to telomere length revealed that at the 20-min timepoint after c-Myc activation, significantly more shorter telomeres were present than when c-Myc had not been induced. The TRF2 signal intensity decreased significantly after c-Myc activation compared to the control timepoint. A similar pattern

of alterations in telomeres and TRF2 intensities was demonstrated in PreB *v-abl/myc* cells after DNAseI digestion in cells being processed with the nuclear matrix preparation protocol. The experiments were repeated 3 times independently (Figs. 14 and 15).

ImmunoFISH for TRF2 and telomeres revealed the disappearance of TRF2-associated telomere spots as shown in Fig. 12, reflecting the occurrence of non-telomere-binding TRF2 in some PreB *v-abl/myc* cells.

TRF2 signals were evaluated by using Teloview^{TM} and TRF2 aggregation was defined, with the same criteria of telomeric aggregates, as clusters of TRF2 that are found in close association and cannot be further resolved as separate signals at the optical resolution limit of 200 nm (Mai and Garini, 2006). Quantification of TRF2 signal intensity and aggregation (Figs.16-19), as well as an evaluation of fluorescence signal intensities for TRF2, lamin A/C, and DAPI (Table 8 and Fig. 20), were conducted, through relative fluorescence units (RFU).

Figure 16.

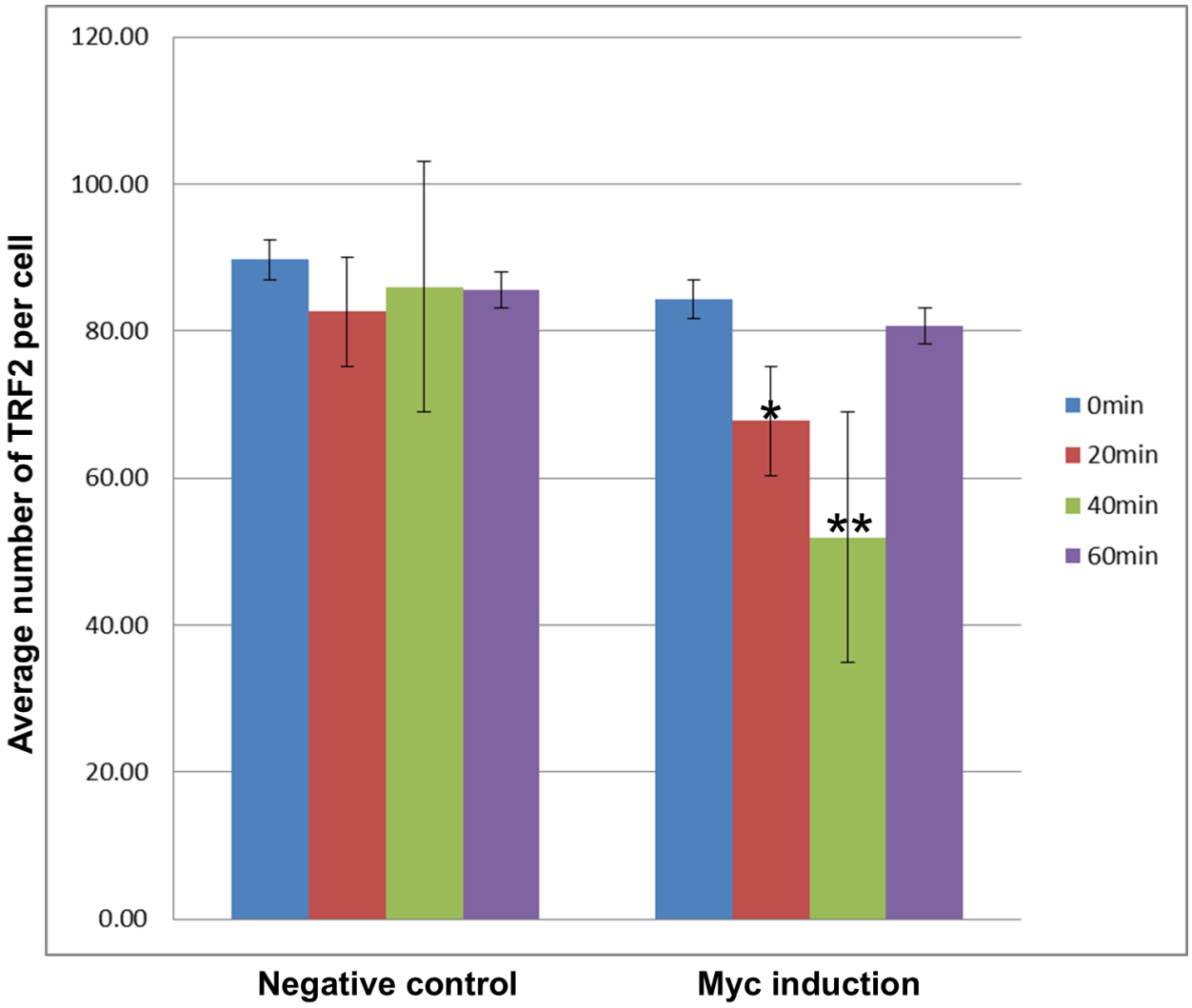

Figure 16. Quantification of TRF2 signal intensity per cell in PreB *v-abl-myc* cells. At least 90 PreB *v-abl-myc* cells from 3 independent experiments were examined for the average number of TRF2 signals per cell using TeloView^{TM}. Marked alterations of TRF2 numbers were observed in PreB *v-abl-myc* cells at 20 and 40 minutes after Myc induction, as marked by * $P = 0.001$ and ** $P < 0.001$.

Figure 17.

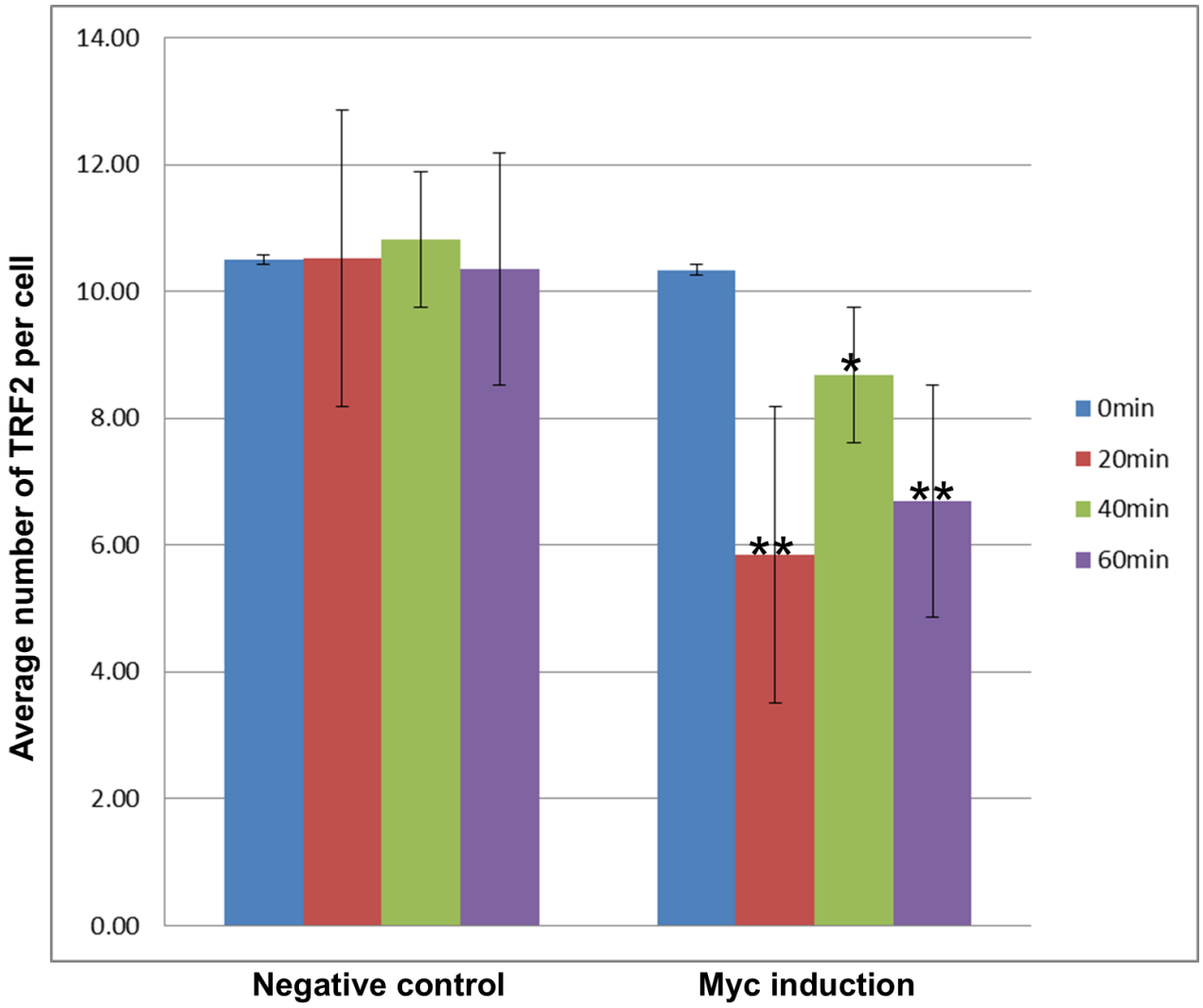

Figure 17. Quantification of TRF2 signal intensity per cell in PreB *v-abl-myc* cells underwent nuclear matrix preparation. At least 90 PreB *v-abl-myc* cells from 3 independent experiments were examined for the average number of TRF2 signals per cell using TeloView^{TM}. Marked alterations of TRF2 numbers were observed in PreB *v-abl-myc* cells at 20, 40, and 60 minutes after Myc induction, as marked by * $P = 0.001$ and ** $P < 0.001$.

Figure 18.

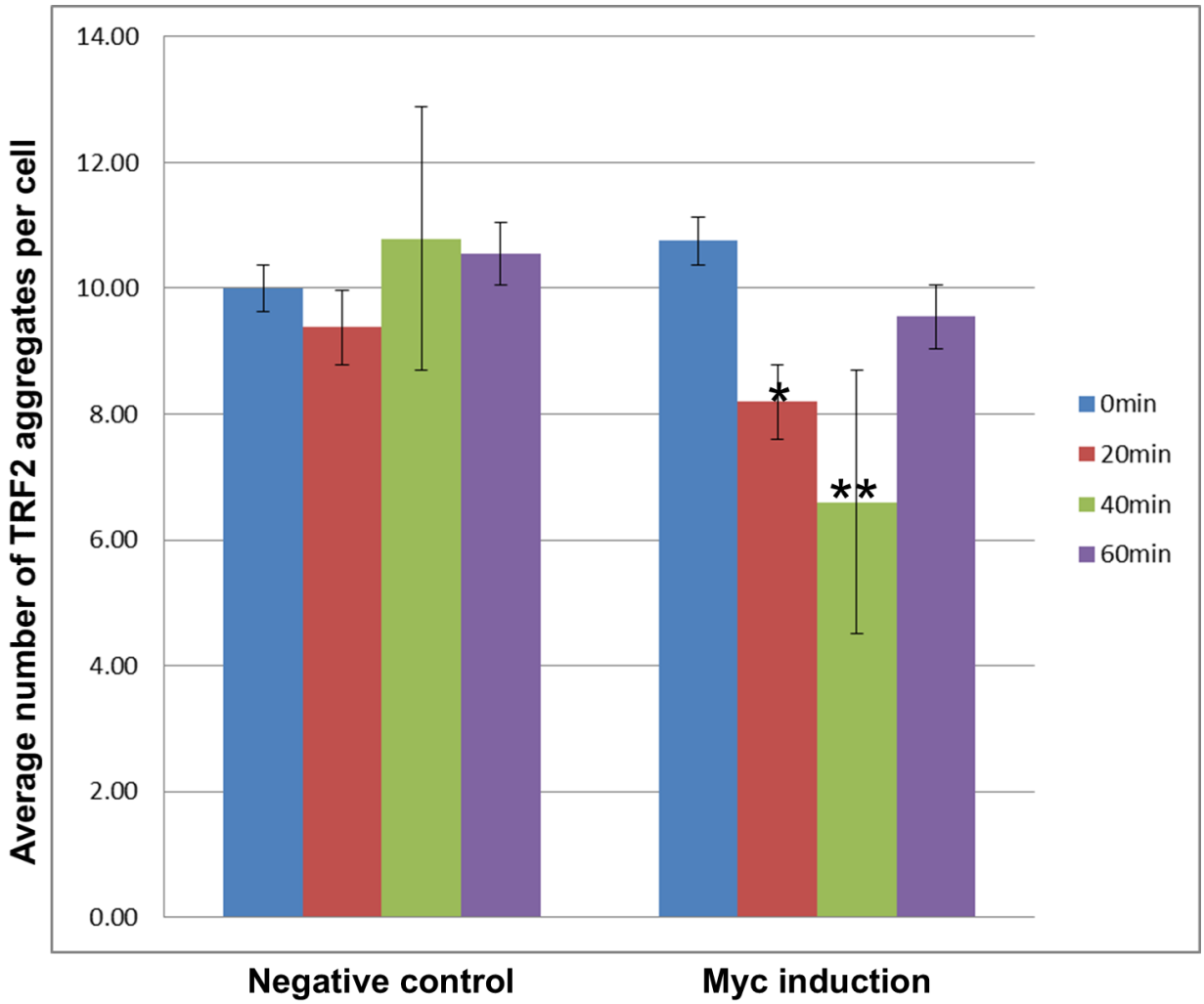

Figure 18. Quantification of TRF2 aggregates per cell in PreB *v-abl-myc* cells. At least 90 PreB *v-abl-myc* cells from 3 independent experiments were examined for TRF2 aggregation using TeloView^{TM}. Marked alterations of TRF2 aggregates were observed in PreB *v-abl-myc* cells at 20 and 40 minutes after Myc induction, as marked by * $P = 0.001$ and ** $P < 0.001$.

Figure 19.

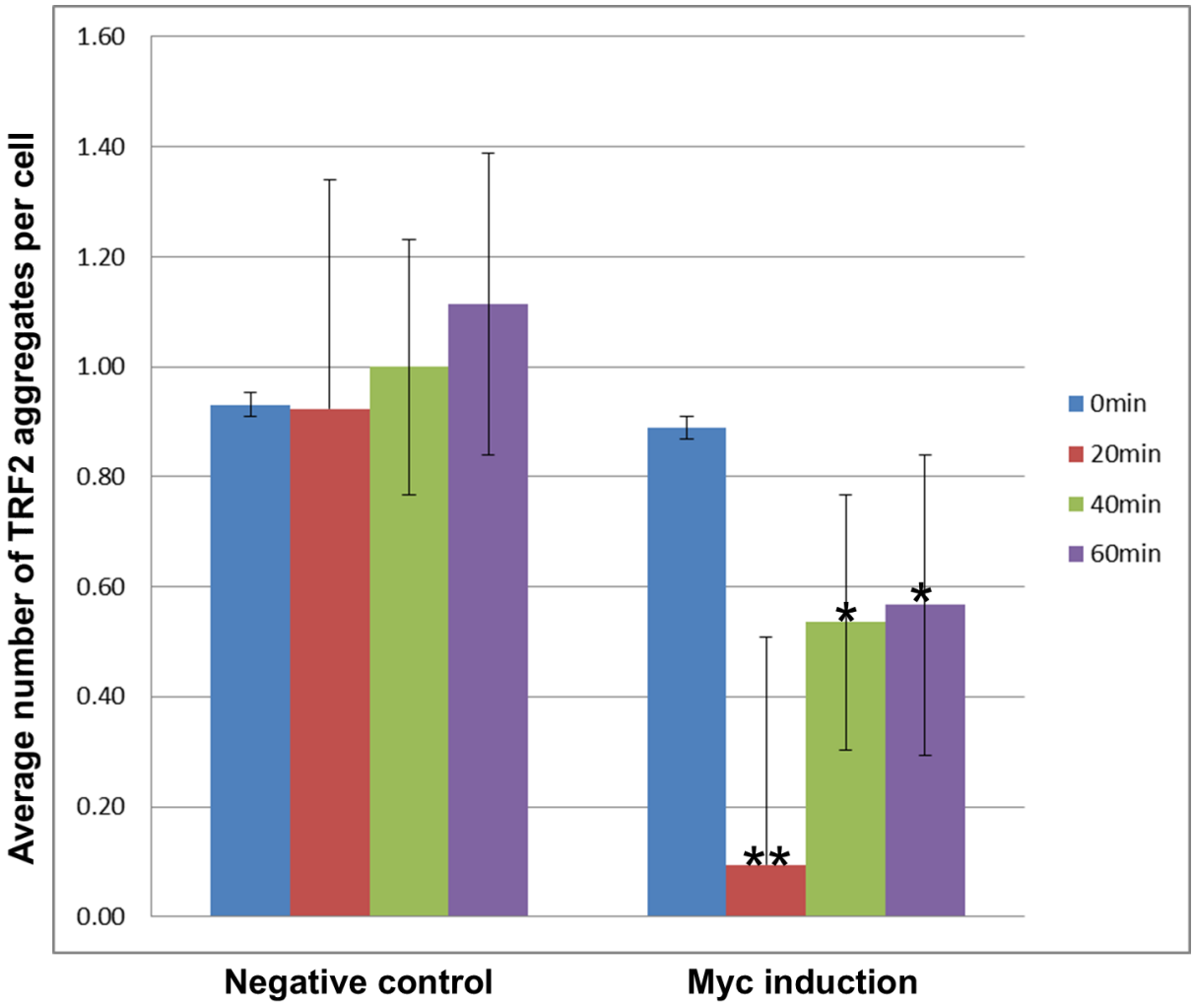

Figure 19. Quantification of TRF2 aggregates per cell in PreB *v-abl-myc* cells underwent nuclear matrix preparation. At least 90 PreB *v-abl-myc* cells from 3 independent experiments were examined for TRF2 aggregation using TeloView^{TM}. Marked alterations of TRF2 aggregates were observed in PreB *v-abl-myc* cells at 20, 40, and 60 minutes after Myc induction, as marked by * $P < 0.001$ and ** $P < 0.0001$.

After DNAseI digestion, TRF2 and lamin A/C intensities decreased significantly but a certain amount of proteins were still maintained along with the nuclear matrix, confirming the existence of TRF2 / telomere complex anchored to the nuclear matrix. TRF2 aggregation decreased significantly after c-Myc activation (Figs. 18 and 19), in parallel with a decrease in fluorescence intensities for lamin A/C and TRF2 (Tables 8 and 9, and Figs. 16, 17, 20, and 21), indicating an alteration in interacting expression between lamin A/C and TRF2 in the nucleus following c-Myc induction. Quantification of lamin A/C intensities per single signal of TRF2 in PreB *v-abl-myc* cells undergoing nuclear matrix preparation was conducted and revealed a statistical significance of reduction in lamin A/C intensities surrounding single signal of TRF2 (Fig. 22). Compared to minute 0, statistical significance of reduction in lamin A/C intensities surrounding single TRF2 signals was observed in PreB *v-abl-myc* cells at 20 ($P = 0.005$), 40 ($P < 0.005$), and 60 ($P < 0.005$) minutes after Myc induction.

Table 8. Quantification of fluorescence intensity for TRF2, lamin A/C, and DAPI in PreB *v-abl-myc* cells

Average fluorescence signals		Negative control (RFU ±S.D.)	Myc induction (RFU ±S.D.)
TRF2:	0 min	7777.01 ± 3156.34	8798.37 ± 2428.0
	20 min	7868.90 ± 2735.42	6478.58 ± 3606.0
	40 min	8183.07 ±3394.0	5099.79 ± 2304.5
	60 min	8768.97 ± 3737.42	5164.45 ± 2645.73
Lamin A/C:	0 min	5124.78 ± 2713.97	5542.14 ± 4501.60
	20 min	5498.55 ± 2372.80	3768.15 ± 2919.36
	40 min	6598.65 ± 4648.02	1958.85 ± 1973.13
	60 min	6798.69 ± 4589.34	2552.34 ± 2070.49
DAPI:	0 min	21281.04 ± 10484.89	20805.15 ± 10951.09
	20 min	21371.24 ± 10715.76	20877.93 ± 9439.04
	40 min	20037.56 ± 10342.18	19349.18 ± 10506.02
	60 min	20628.03 ± 10858.17	19571.24 ± 11458.39

Table 8. Quantification of fluorescence intensity per cell for TRF2, lamin A/C, and DAPI in PreB *v-abl-myc* cells through relative fluorescence units (RFU). At least 90 PreB *v-abl-myc* cells from 3

independent experiments were examined for the association between TRF2 and lamin A/C proteins. Marked decreases in fluorescence intensities, reflecting the expression levels, of TRF2 and lamin A/C were observed in PreB *v-abl-myc* cells as early as 20 minutes after Myc induction.

Figure 20.

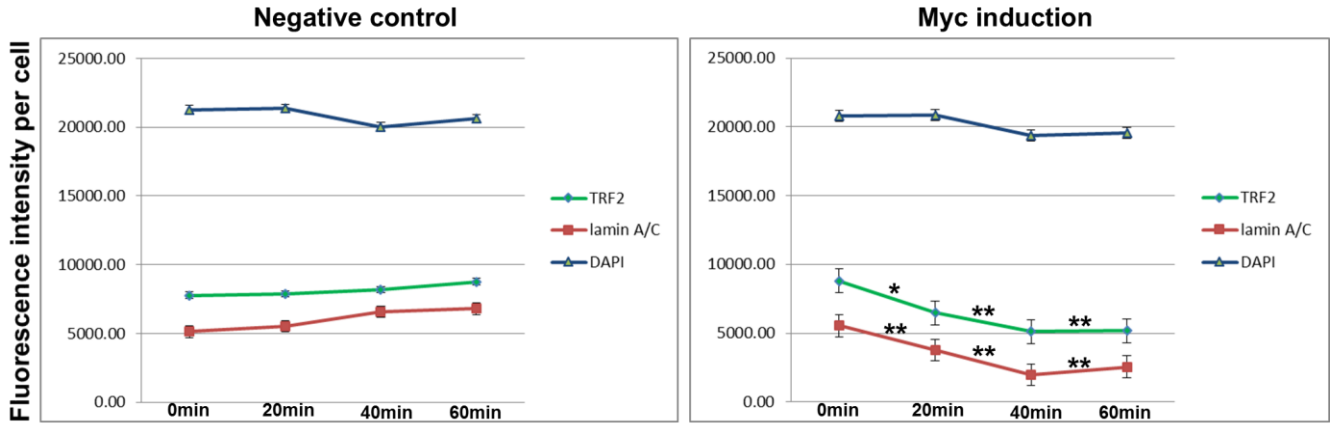

Figure 20. Quantification of fluorescence intensity per cell for TRF2, lamin A/C, and DAPI in PreB *v-abl-myc* cells through relative fluorescence units (RFU). At least 90 PreB *v-abl-myc* cells from 3 independent experiments were examined for the association between TRF2 and lamin A/C proteins. Marked decreases in fluorescence intensities, reflecting the expression levels, of TRF2 and lamin A/C were observed in PreB *v-abl-myc* cells as early as 20 minutes after Myc induction. Statistical significance is shown with the symbols * representing $P = 0.0001$ and ** $P < 0.0001$.

Table 9. Quantification of fluorescence intensities for TRF2, lamin A/C, and DAPI in PreB *v-abl-myc* cells undergoing nuclear matrix preparation

Average fluorescence signals		Negative control (RFU ±S.D.)	Myc induction (RFU ±S.D.)
TRF2:	0 min	2065.51 ± 1019.86	2654.07 ± 3621.62
	20 min	2005.42 ± 1806.24	1267.40 ± 526.65
	40 min	2152.68 ± 690.14	1457.36 ± 715.70
	60 min	1942.76 ± 418.72	1117.38 ± 615.75
Lamin A/C:	0 min	4379.00 ± 1819.52	4168.43 ± 2855.72
	20 min	4500.22 ± 3173.26	3933.02 ± 1986.34
	40 min	4459.24 ± 1047.23	2494.80 ± 1285.60
	60 min	4227.14 ± 1393.66	2886.62 ± 1454.08
DAPI:	0 min	5498.78 ± 922.11	5491.51 ± 1410.57
	20 min	5236.42 ± 1885.71	5512.80 ± 2423.76
	40 min	5886.43 ± 4161.29	5332.77 ± 4248.71
	60 min	5602.02 ± 3683.26	5643.49 ± 4725.88

Table 9. Quantification of fluorescence intensity per cell for TRF2, lamin A/C, and DAPI in PreB *v-abl-myc* cells undergoing nuclear matrix preparation, through relative fluorescence units (RFU). At least 90 PreB *v-abl-myc* cells from 3 independent experiments were examined for the association between TRF2 and lamin A/C proteins. Marked decreases in fluorescence intensity, reflecting the expression level, of TRF2 and lamin A/C were observed in PreB *v-abl-myc* cells as early as 20 minutes after Myc induction.

Figure 21.

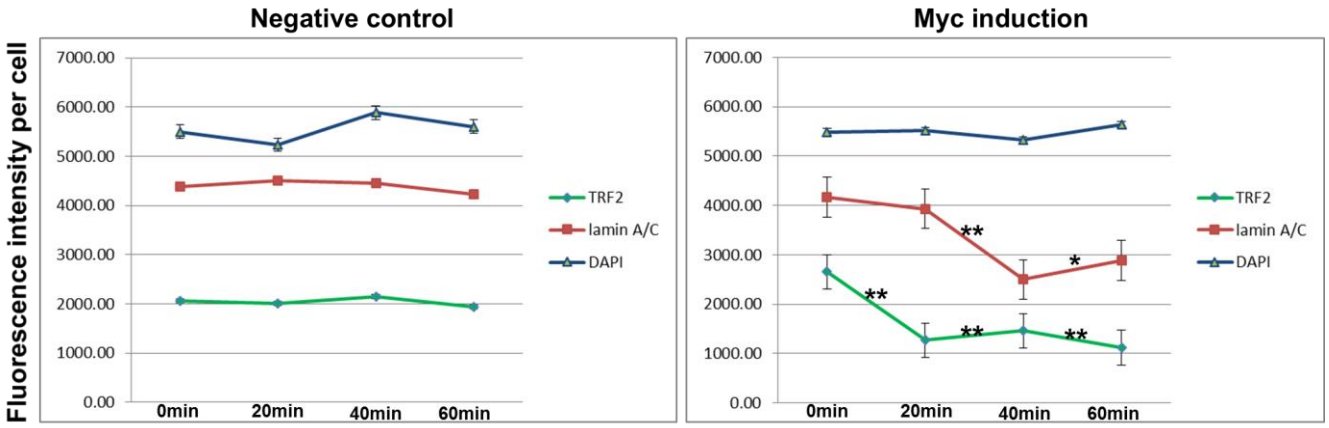

Figure 21. Quantification of fluorescence intensity per cell for TRF2, lamin A/C, and DAPI in PreB *v-abl-myc* cells undergoing nuclear matrix preparation, through relative fluorescence units (RFU). At least 90 PreB *v-abl-myc* cells from 3 independent experiments were examined for the association between TRF2 and lamin A/C proteins. Marked decreases in fluorescence intensity, reflecting the expression level, of TRF2 and lamin A/C were observed in PreB *v-abl-myc* cells as early as 20 minutes after Myc induction. Statistical significance is shown with the symbols * representing $P = 0.01$ and ** $P < 0.01$.

Figure 22.

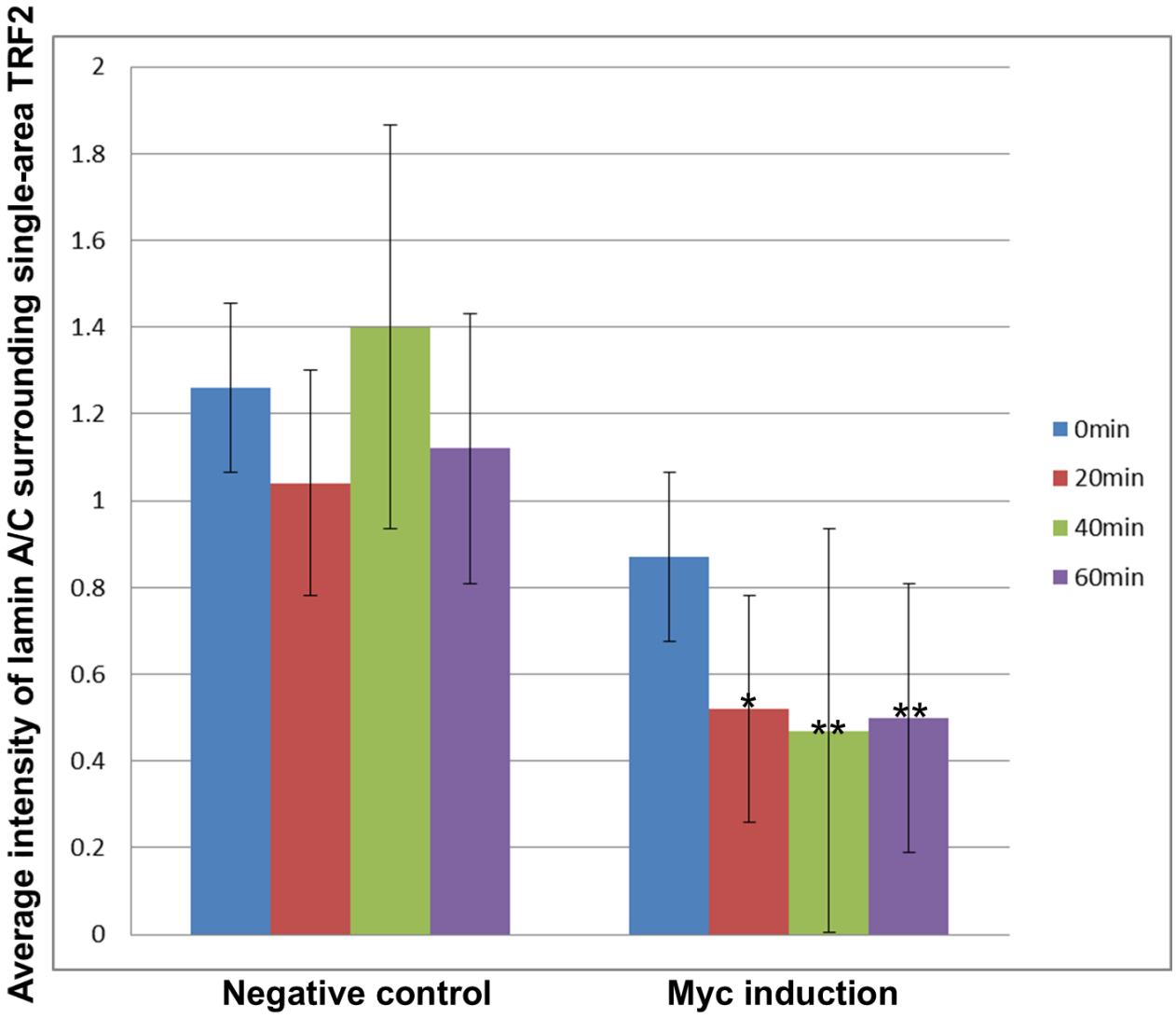

Figure 22. Quantification of lamin A/C intensity per single signal of TRF2 in PreB *v-abl-myc* cells undergoing nuclear matrix preparation. At least 90 PreB *v-abl-myc* cells from 3 independent experiments were examined. Compared to minute 0, statistical significance of reduction in lamin A/C intensities surrounding single TRF2 signals was observed in PreB *v-abl-myc* cells at 20 (P = 0.005), 40 ($P < 0.005$), and 60 ($P < 0.005$) minutes after Myc induction. * represents $P = 0.005$ and ** $P < 0.005$.

Characterization of cytoband 17q25.3 in NSCLC

Of the 18 patients with NSCLC who underwent surgical resections as primary treatment, 8 patients (44.44%) were smokers and 5 patients (27.78%) harboured the EGFR mutation. Four patients (22.22%) had squamous cell carcinoma histology whereas the rest were adenocarcinomas. The clinical characteristics of the NSCLC patients are described in Table 10.

Table 10. Clinical characteristics of 18 non-small cell lung cancer patients

Case No.	Sex	Age (years)	Smoking	EGFR mutation	Histology	Stage	Overall survival (months)	Survival outcome
1	F	73	No	pos	AC	IB	93	Alive
2	M	79	No	NA	AC	IIIB	7	Deceased
3	F	77	No	pos	AC	IIB	46	Deceased
4	M	74	No	pos	AC	IB	59	Deceased
5	F	70	No	pos	AC	IIIA	4	Deceased
6	F	82	No	pos	AC	IIB	98	Alive
7	F	75	No	neg	AC	IB	60	Deceased
8	F	39	No	neg	AC	IA	91	Alive
9	F	77	No	neg	AC	IB	13	Deceased
10	F	71	No	neg	AC	IB	26	Deceased
11	M	45	Yes	NA	AC	IA	86	Alive
12	F	67	Yes	neg	AC	IA	17	Deceased

13	F	57	Yes	neg	AC	IIB	86	Alive
14	F	73	Yes	NA	AC	IIIA	27	Deceased
15	M	58	Yes	NA	SQ	IA	98	Alive
16	M	67	Yes	NA	SQ	IB	63	Deceased
17	M	72	Yes	NA	SQ	IB	93	Alive
18	F	76	Yes	NA	SQ	IIIB	86	Alive

Table 10. Clinical characteristics of 18 non-small cell lung cancer patients. Pos, positive; Neg, negative; NA, not available; AC, adenocarcinoma; SQ, squamous cell carcinoma (Sunpaweravong et al., 2016).

To examine whether cytoband 17q25.3 was amplified in the 18 NSCLC cases, Q-FISH was performed to investigate the 17q25.3 copy number (Fig. 23), and was then compared to CGH and/or SNP array copy number data for the same tumours.

Figure 23.

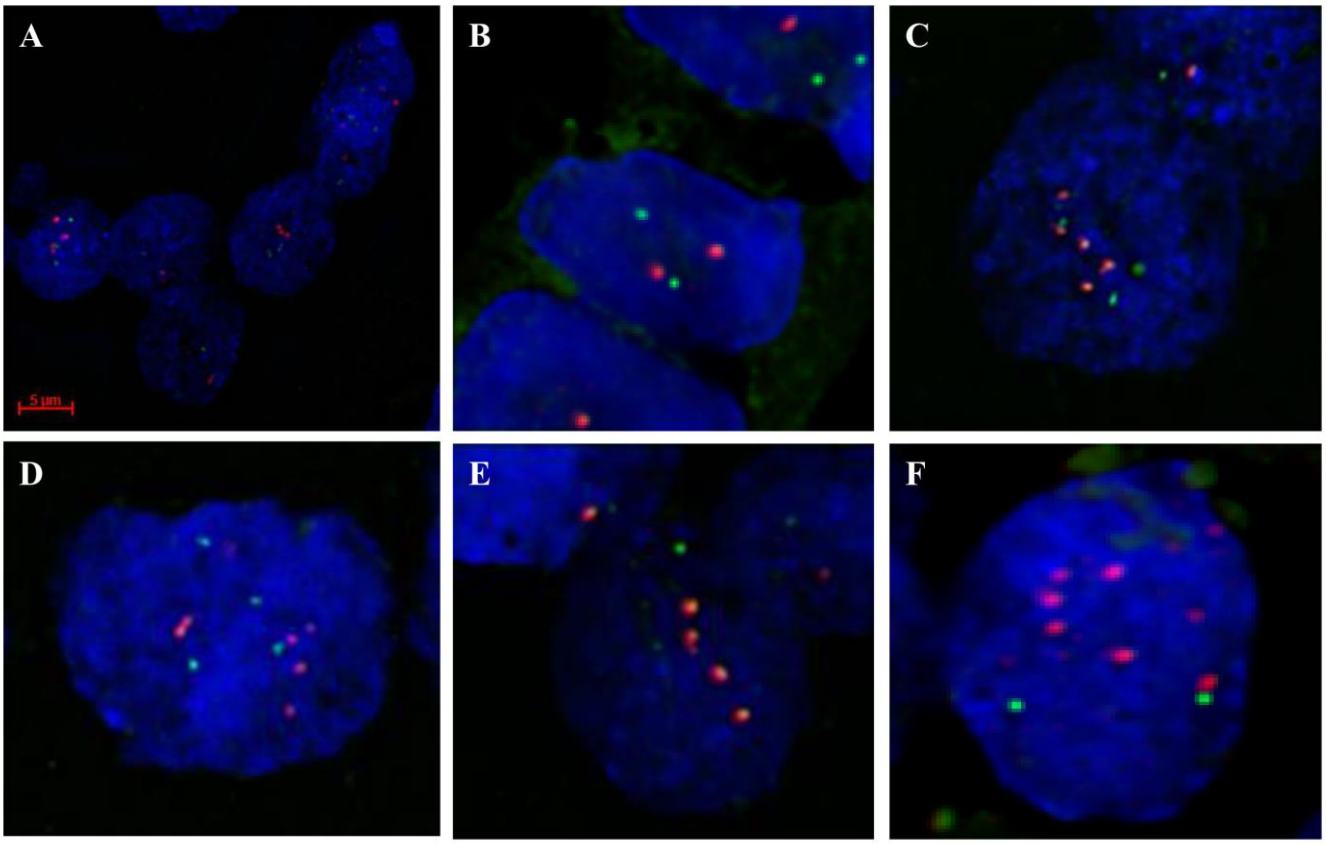

Figure 23. 17q25.3 (red) and 17p11.2 (green) signals in NSCLC cells acquired from Q-FISH: (a) View from a distance. The scale bar represents 5 um. (b) Normal signals of both cytobands, 2 per each cell. (c), (d), and (e) Copy number gains of both cytobands, 5 of 17q25.3 and 6 of 17p11.2 (c), 6 of 17q25.3 and 5 of 17p11.2 (d), 4 of 17q25.3 and 5 of 17p11.2, with 4 pairs of signals demonstrating co-localization of 17q25.3 and 17p11.2 in yellow (e). (f) Amplification of cytoband 17q25.3 (7 red signals) with normal 17p11.2 (2 green signals) (63X, Objective) (Sunpaweravong et al., 2016).

Table 11 summarizes the results of copy numbers for cytobands 17q25.3 and 17p11.2, showing that the copy numbers of cytobands 17q25.3 and 17p11.2 obtained from Q-FISH correlate well with corresponding CGH and/or SNP array data for the same regions.

Table 11. Quantitative analyses of copy numbers for cytobands 17q25.3 and 17p11.2

Case	Average 17q25.3	Average 17p11.2	Average Ratio	% of nuclei with ratio ≥ 1.5	Status of 17q25.3	CGH/SNP data for 17q25.3	CGH/SNP data for 17p11.2
1	4.56	4.57	1.00	1	gain of chr17	gain	gain
2	3.38	3.24	1.04	17	clonal gain of 17q25.3/ gain of chr17	normal	normal
3	3.78	4.26	0.89	12	clonal of 17q25.3/ gain of chr17	normal	normal
4	4.79	3.95	1.21	32	clonal gain of 17q25.3/ gain of chr17	normal	loss
5	2.65	3.17	0.84	3	no gain	gain	normal
6	2.91	3.40	0.86	9	no gain	gain	gain
7	3.27	3.52	0.93	18	clonal gain of 17q25.3/ gain of chr17	normal	normal
8	2.76	2.95	0.94	13	clonal gain of 17q25.3	loss	loss
9	3.00	2.64	1.14	26	clonal gain of 17q25.3	gain	normal
10	2.94	3.28	0.90	9	no gain	normal	normal
11	2.15	2.50	0.86	11	clonal gain of 17q25.3	normal	normal
12	2.61	2.57	1.02	22	clonal gain of 17q25.3	gain	gain
13	2.30	2.44	0.94	14	clonal gain of 17q25.3	normal	loss
14	2.40	2.93	0.82	3	no gain	loss	loss

15	2.96	3.79	0.78	5	no gain	gain	loss
16	3.01	3.13	0.96	13	clonal gain of 17q25.3/ gain of chr17	normal	normal
17	3.67	4.04	0.91	5	gain of chr17	gain	normal
18	2.41	2.62	0.92	15	clonal gain of 17q25.3	normal	normal

Table 11. Quantitative analyses of copy numbers for cytoband 17q25.3, with cytoband 17p11.2 as a control. Data of the loci of interest from CGH and/or SNP arrays were correlated with the results from Q-FISH. CGH, comparative genomic hybridization; SNP, single nucleotide polymorphism; chr, chromosome (Sunpaweravong et al., 2016).

A representative image shown in Fig. 23 illustrates 17q25.3 copy number compared to the reference cytoband (17p11.2) on chromosome 17. Clonal gains of cytoband 17q25.3, defined as ≥ 10% of the analyzed nuclei demonstrating a ratio between the cytoband 17q25.3 and the reference 17p11.2 probe ≥ 1.5, were observed in 11 of the 18 (61%) NSCLC patient samples. Seven of the 18 (38.9 %) showed copy gains of both cytobands 17q25.3 and 17p11.2 (reference region) suggestive of entire chromosome 17 gains, as shown in Table 11 and Fig. 23 C - E. This suggests that molecular heterogeneity in 17q25.3 copy numbers exists within individual NSCLC tumours. However, no clinical correlations with different copy numbers of 17q25.3 or gains of chromosome 17 were found.

Association of 3D telomere organization with NSCLC clinical features

To investigate the 3D nuclear telomeric architecture in 18 NSCLC tumours, Q-FISH with the telomere PNA probe was performed and TeloView^{TM} software was applied for the analyses (Fig. 24).

Figure 24.

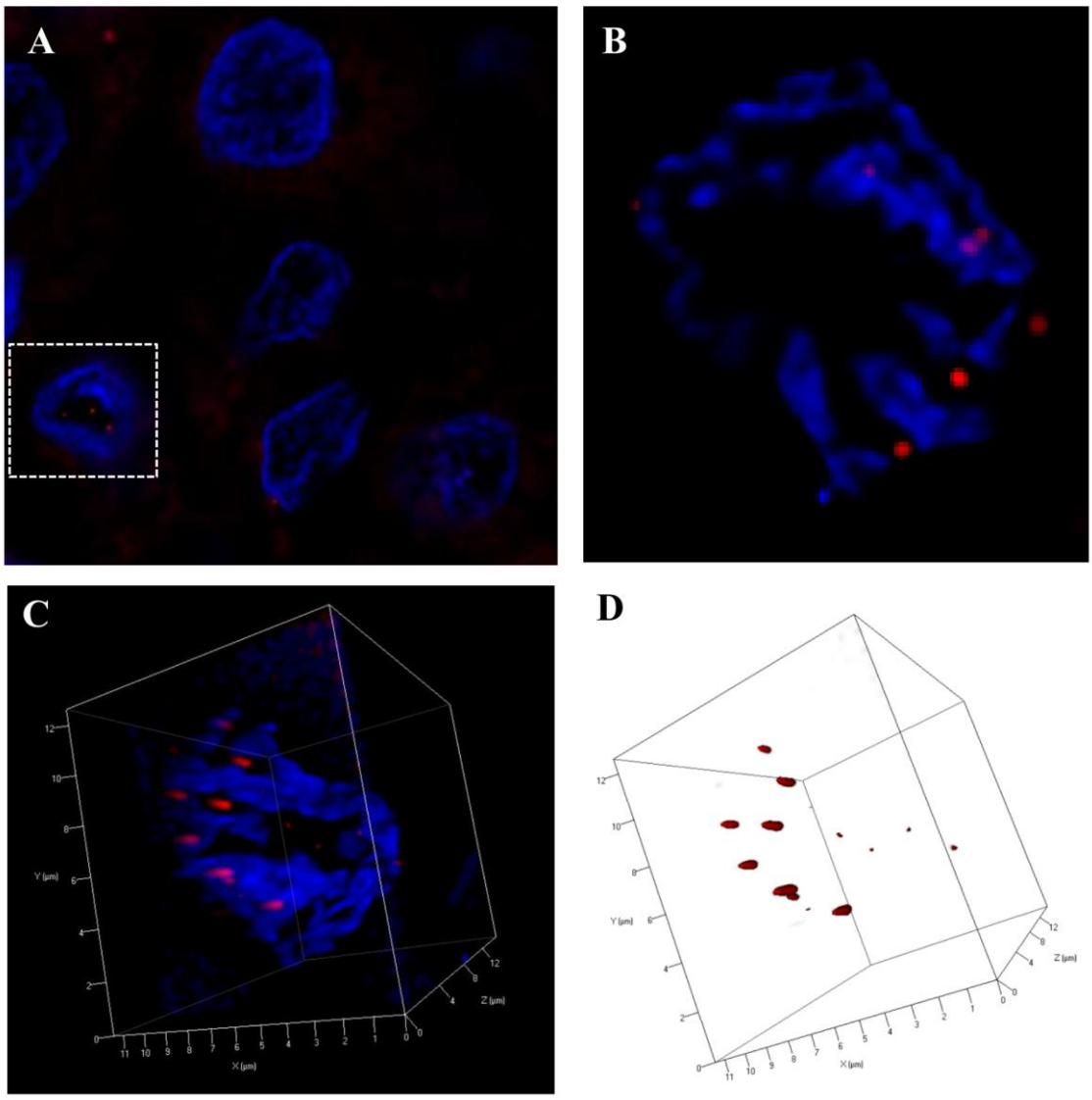

Figure 24. NSCLC cells after undergoing Q-FISH for PNA probe depicting: (a) Telomeres (red signals). A representative nucleus is outlined in white and enlarged in (b) – (d). (c) and (d) Telomeres in 3D view (63X, Objective) (Sunpaweravong et al., 2016).

Smokers, EGFR mutation-negative, or squamous cell carcinoma patients had a tendency towards higher telomere numbers and greater numbers of telomere aggregates per cell than non-smokers, EGFR mutation-positive, and adenocarcinoma patients, however the differences were not statistically significant (Table 12). Graphical analyses of 3D telomeric profiling also demonstrated

a tendency towards more lower-intensity telomeres, indicative of shorter telomeres, in the smoker, EGFR-negative, and squamous cell carcinoma patients (Fig. 25).

Table 12. Three-dimensional telomere parameters of specimens from non-small cell lung cancer patients

Specimens		Average number of telomere per cell	*P*	Average number of aggregates per cell	*P*	Average nuclear volume (μm3)	*P*	a/c ratio	*P*
EGFR mutation	Pos (n = 5)	19.23	0.37	1.95	0.48	206.63	0.30	2.24	0.55
	Neg (n = 6)	23.58		2.44		163.04		2.44	
	NA (n = 7)	23.29		2.43		191.98		2.33	
Histology	AC (n = 14)	20.69	0.11	2.08	0.13	180.61	0.51	2.30	0.59
	SQ (n = 4)	27.72		3.05		207.05		2.48	
Smoking	Yes (n = 8)	23.37	0.61	2.42	0.70	167.30	0.27	2.24	0.48
	No (n = 10)	21.36		2.20		201.83		2.43	

Table 12. Three-dimensional telomere parameters of non-small cell lung cancer patients with different EGFR mutations, histology, and smoking status. Pos, positive; Neg, negative; NA, not available; AC, adenocarcinoma; SQ, squamous cell carcinoma (Sunpaweravong et al., 2016)

Figure 25.

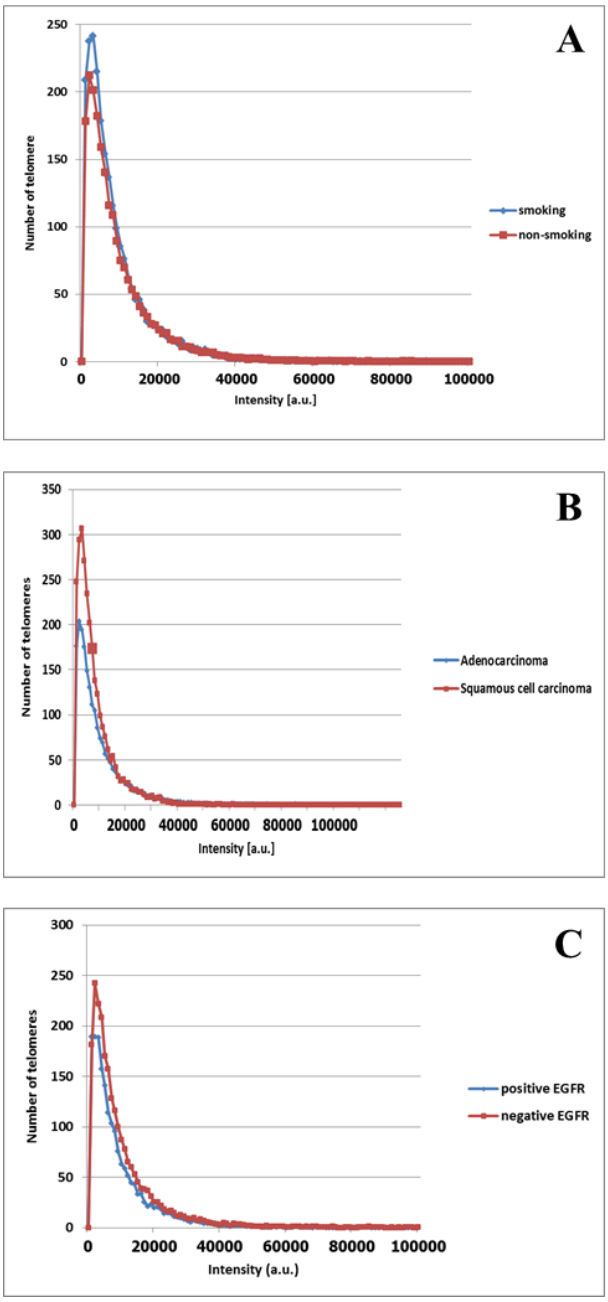

Figure 25. Telomere numbers plotted against telomere intensities for: (a) Non-smoking and smoking; (b) Histology; (c) EGFR mutation subgroups of the NSCLC patients (Sunpaweravong et al., 2016).

Survival analyses of NSCLC patients

Kaplan-Meier survival analyses were conducted to demonstrate and compare survival outcomes in subgroups of NSCLC patients based on smoking history, EGFR mutation status, and histological type. Although there was no statistical significance observed, the mean survival time tended to be shorter in patients having greater average telomere numbers per cell (50.1 months for those who had more than 20 average telomeres vs. 71.1 months for those who had 20 or less average telomeres, $P = 0.29$). EGFR-mutation positive patients tended to have a longer mean survival time than the EGFR-mutation negative group (61.0 months for the EGFR-mutation positive patients vs. 49.7 months for the EGFR-mutation negative patients, $P = 0.65$). Considering the status of cytoband 17q25.3, patients who had clonal gains, demonstrated a trend towards shorter mean survival times than those who had either gains of chromosome 17 only or no gain (57.2 months for patients who had clonal gains vs.64.1 months for those who had either gains of chromosome 17 only or no gain, $P = 0.57$).

Summary of Results

- Upon c-Myc upregulation, mouse PreB *v-abl/myc* cells demonstrated a repositioning of chromosome11 within the first hour, significantly different from the control cells.
- Statistically significant decreases of TRF2 intensities in parallel with increased numbers of lower intensity telomeres, representing telomeres shorter in length were observed within the first hour after c-Myc induction.
- Quantification of TRF2 signal intensity and TRF2 aggregates per cell demonstrated marked alterations of TRF2 numbers and TRF2 aggregates after c-Myc induction.
- Marked decreases in fluorescence intensities, reflecting the expression levels, of TRF2 and lamin A/C were observed as early as 20 minutes after c-Myc induction.

- Quantification of lamin A/C intensity per single signal of TRF2 in PreB *v-abl-myc* cells undergoing nuclear matrix preparation revealed a statistical significance of reduction in lamin A/C intensities surrounding single TRF2 signals.

- Eleven of the 18 (61%) NSCLC patients had clonal gains of cytoband 17q25.3. Seven of the 18 (38.9 %) had copy gains of both cytobands 17q25.3 and 17p11.2, reflecting an entire chromosome 17 gains.

- Smokers, *EGFR* mutation-negative, or squamous cell carcinoma patients had a tendency towards higher telomere numbers and greater numbers of telomere aggregates per cell than non-smokers, *EGFR* mutation-positive, and adenocarcinoma patients. However the differences were not statistically significant.

Chapter V : Discussion

c-Myc deregulation leads to genomic instability and mouse chromosome 11 repositioning

Genomic instability is a status of genomic changes or an increased propensity for genomic alterations which can potentially facilitate tumor initiation and progression. Genomic instability in cancer cells has also been characterized into structural and numerical instability (Bayani et al., 2007). Alterations of the genome can occur when a structural genetic aberration takes place, including mutations, amplifications, or deletions on specific genes, or a rearrangement or translocation of chromosome segments. In addition, numerical aberrations of the entire chromosomes, either gains or losses, can result in aneuploidy and lead to genomic instability (Shen Z, 2011). c-Myc has been shown to trigger a complex network of genomic instability, either at the level of single genes (Mai, 1994; Mai et al., 1996b; Kuschak et al., 2002; Mai and Mushinski, 2003) or the whole chromosome (Mai et al., 1996a; Felsher and Bishop, 1999; Rockwood et al., 2002; Mai and Mushinski, 2003). c-Myc is also responsible for illegitimate replication initiation resulting in more than one replication firing origin per cell (Kuschak et al., 2002), which induces chromosomal rearrangements and DNA breakage (Rockwood et al., 2002; Louis et al., 2005), influences alterations of DNA repair (Vafa et al., 2002; Hironaka et al., 2003; Karlsson et al., 2003), and is related to point mutations of several genes (Chiang et al., 2003; Mac Partlin et al., 2003).

In *v-abl/myc* induced fast-onset PCTs in mice, trisomy of chromosome 11 and duplication of chromosome 11 cytoband E2 was observed (Wiener et al., 2010). Wiener and colleagues reported that trisomy of chromosome 11 was present in 100% of the rapidly developing PCTs and the 11E2 subcytoband was always duplicated in the *v-abl/myc*- induced PCTs (Wiener et al., 2010). By using classic and molecular cytogenetics, they ascertained that the 11E2 region was the critical segment on chromosome 11. Since mouse 11E2 subcytoband is syntenic with the rat 10q32 region and the

chromosomal region 17q25 in humans (Koelsch et al., 2005), further exploration of human 17q25 cytoband is relevant to investigate its potential role in tumorigenesis. The rat 10q32 region (Koelsch et al., 2005) has been shown to be involved in schwannomas (Koelsch et al., 2005). Amplifications of 17q25 copy numbers has been demonstrated in various human cancers including breast, ovarian, and thyroid cancers, neuroblastomas, and osteosarcoma (Russell et al., 2000; Burrows et al., 2003; Montagna et al., 2003; Langan et al., 2004; Lastowska et al., 2004; Atiye et al., 2005; Hwang et al., 2008; Thomassen et al., 2009).

Kuzyk and Mai reported an association of *v-abl/myc*-induced accelerated mouse PCT development with selected telomere length changes and aberrant 3D nuclear telomere organization (Kuzyk and Mai, 2012). They found that fast-onset PCTs had a significantly different 3D telomere profile and that the translocation chromosome T(X;11) carrying 11E2 was the only chromosome with telomere lengthening, compared with primary B cells of wild-type littermates with and without rcpT(X;11). The finding supports the concept of individual telomere lengthening for maintenance of chromosomes that are functionally important for the tumorigenic process (Kuzyk and Mai, 2012).

Mouse subcytoband 11E2, syntenic with human chromosome 17q25, harbours commonly amplified genes in PCT, a B-cell lineage hematologic malignancy resulting from c-Myc–activating chromosomal translocation. The candidate genes on mouse subcytoband 11E2 include *ASPSCR1* (ASPSCR1 (database online), 2016), *TBCD* (Grynberg et al., 2003), *FoxK2* (Katoh and Katoh, 2004), *Kcnj2* (Hattersley and Pearson, 2006; Varadi et al., 2006; Xiong et al., 2006), *Ict1* (van Belzen et al., 1995), and *Sec14l1* (Kostenko et al., 2005; Mousley et al., 2007). In human, allelic aberrations, either gains or losses, on chromosome region 17q25 have been reported in various types of cancers, suggesting that oncogenes or tumor suppressor genes, respectively, are located there (Islam et al., 2000; Morris et al., 2000; Ladanyi et al., 2001; Risk et al., 2002; Uppal et al., 2003; Langan et al.,

2004; Presneau et al., 2005; McRonald et al., 2006; Bermudo et al., 2008; Gulten et al., 2009; Yu et al., 2009; Bermudo et al., 2010; Wojnarowicz et al., 2012). The changes of human chromosome region 17q25 support the importance of this region in tumorigenesis. Based on the synteny of mouse subcytoband 11E2 and human chromosome 17q25, the frequent aberrations of cytoband 17q25 in humans, and the alteration of subcytoband 11E2 in *v-abl/myc*-induced accelerated mouse PCT development, the study of this region to better understand its roles in tumour development and progression is rational.

This study examined whether c-Myc upregulation affected the 3D positioning of mouse chromosome 11 in the interphase nuclei of Pre B *v-abl/myc* cells. To this end, the effect of conditional c-Myc expression in immortalized mouse Pre B *v-abl/myc* cells, stably transfected with MycER^{TM} (Littlewood et al., 1995; Mai et al., 1999) was analyzed. Evaluation of the 3D positioning of mouse chromosome 11 in nuclei of non-MycER^{TM}-activated cells was conducted as a control, as was an evaluation of the positioning of chromosome 10 (negative control), and chromosomes 5 and 7 (positive controls). The RRD of a chromosome is defined by the distance away from the nuclear centre of each interested chromosome volume represented by the centre of the chromosome bulk from the centre of the nucleus, thus, in close representative of the precise 3D position of the respective chromosome in the interphase nucleus.

After MycER^{TM} activation with 4HT, nuclear c-Myc signals were increased in Pre B *v-abl/myc* cells, compared to the non-4HT treated control cells. This finding concurred with a previous publication by Littlewood et al. (1995). Upon c-Myc activation, the RRD of chromosome 11 changed significantly as early as hour 6 after c-Myc was upregulated. For mouse chromosome 11, analyses of the 3D chromosome positioning by using RRDs revealed that c-Myc deregulation induced chromosome repositioning at a higher statistical significance, when compared to the non-MycER^{TM}-

activated control cells and the negative control chromosome 10. The RRDs from the pair of mouse chromosomes 5 and 7, which were aimed to serve as positive controls (Louis et al., 2005), exhibited the pattern of chromosome repositioning. However, in this study, for uncertain reasons, the repositioning of chromosome 5 was more clearly observed than that of chromosome 7. The repositioning of chromosome 5 was observed as early as at hour 6 whereas the repositioning of chromosome 7 occurred as early as at hour 12. Subsequent experiments were performed to look more closely within the first 6 hours after c-Myc deregulation to reveal the earliest time point of c-Myc dependent chromosome 11 respositioning, with hour 1 found to be the earliest timepoint chromosome 11 repositioning was observed. Following experiments to investigate the potential mechanism underlying the c-Myc driven chromosome 11 repositioning were then carried out focusing on the first hour after c-Myc activation.

This study revealed a novel mechanism potentially underlying c-Myc-dependent genomic instability in which the repositioning of mouse chromosome 11 was observed. Upon c-Myc upregulation, mouse PreB *v-abl/myc* cells demonstrated a repositioning of chromosome 11 within the first hour, significantly different from the control cells. This observation supports the important role of c-Myc in chromosome organization and confirms the potential significance of mouse chromosome 11's involvement in PCT tumorigenesis. Mehta and colleagues reported that, upon a serum removal from the culture medium resulting in cellular quiescence, chromosomes of primary human fibroblasts altered their positions within 15 minutes (Mehta et al., 2010). The authors proposed that the chromosome repositioning was probably dependent on nuclear myosin 1β (Mehta et al., 2010). The phenomenon of chromosome repositioning has also been demonstrated during the differentiation of human T-cells (Kim et al., 2004a), adipocytes (Kuroda et al., 2004), and keratinocytes (Marella et al., 2009).

Telomere dysfunction can result in genomic instability, which could be from telomere shortening, or telomere aggregation (Chuang et al., 2004; Mai and Garini, 2005; Mai and Garini, 2006). The BBF cycle is a classical mechanism of telomere-contributed genomic instability, in which end-to-end fusion of chromosomes occurs from dysfunctional telomeres and creates dicentric chromosomes, then eventually breaks during the anaphase, resulting in terminal deletions and nonreciprocal translocations with one chromosome or chromatid being left with a piece from another chromosome or chromatid. The telomere-free ends resulting from this event then continue to have fusions with other chromosomes and initiate new BBF cycles until no more telomere-free chromosomal ends persist (Mueller, 1938; McClintock, 1941). BBF cycles are associated with tumorigenesis because they lead to deletions, gene amplification, nonreciprocal translocation, and overall genetic changes (Smith et al., 1992; Hande et al., 1999; Artandi et al., 2000; Gisselsson et al., 2001; Artandi, 2002; Ciullo et al., 2002; DePinho and Polyak, 2004; Murnane and Sabatier, 2004).

c-Myc-deregulation not only can trigger telomeric aggregates resulting in BBF cycles, but can also change nuclear architecture organization and lead to closer proximity of telomeres which results in chromosomal rearrangements (Louis et al., 2005). Although overlapping of mouse chromosomes 5, 7, and 10 has been observed in Myc-activated Pre B *v-abl/myc* nuclei previously (Louis et al., 2005), the repositioning of mouse chromosome 11 in conditional c-Myc expressing Pre B *v-abl/myc* cells, revealed from this study, is a new finding. Louis and colleagues have previously reported evidence of chromosomal rearrangements involving mouse chromosomes 7, 13, and 17 at a significant level in c-Myc-activated PreB *v-abl/myc* cells (Louis et al., 2005). By using chromosome paints, after c-Myc upregulation in PreB *v-abl/myc*, they observed a change in overlaps of several pairs of mouse chromosomes, especially between chromosomes 5 and 13 over the time course. The two chromosomes were found in closer proximity as the cells entered into the first telomere aggregation

cycle. Other chromosome overlapping events were also observed between mouse chromosomes 10 and 7, and chromosomes 7 and 17 (Louis et al., 2005).

In addition to the investigation of chromosome 11 positioning in PreB *v-abl/myc* cells as in this study, other orientation patterns of mouse chromosome 11 have been reported (Schmälter et al., 2014; Schmälter et al., 2015). Schmälter and colleagues studied in pristane and *v-abl/myc*-induced fast-onset mouse PCT in [T38HxBALB/c]N congenic mice with a reciprocal translocation between chromosomes X and 11 (rcpT(X;11). These mice exhibited a long chromosome T(11;X) and a short chromosome T(X;11). The short chromosome T(X;11) contained cytoband 11E2 and parts of cytoband E1. After the *v-abl/myc*– induced PCT, these unique mouse models exhibited a non-random duplication of chromosome 11, cytoband 11E2, associated with the overexpression of genes within 11E2 (Wiener et al., 2010). To study chromosome orientation, the authors compared the fast-onset PCT cells with control B lymphocytes of [T38HxBALB/c]N mice with rcpT(X;11) translocation (T38HT(X;11)) using multi-colour Banding (mBANDing) FISH probes to detect intrachromosomal changes in the metaphases. Chromosome 11 was labelled by different overlapping fluorochromes to analyse whether the centromeric or the telomeric end was orientated towards the nuclear centre or periphery. The most frequently observed orientation pattern of chromosome 11 in T38HT(X;11) was with both chromosomes located in parallel to the nuclear border ("PP") (35.0%) whereas in all PCTs "PP" was only observed in 10.7%. The orientation pattern "CP" with one homolog pointing with its centromeric end towards the nuclear periphery and the other homolog being in parallel was found most frequently in PCTs (13.4% of all PCTs) and in 23.7% of T38HT(X;11). Both chromosomes pointing with their centromeric ends towards the periphery ("CC") was observed in 18.7% of T38HT(X;11) and in 8.5% of all PCTs. The third most common orientation pattern in PCTs was "PT" with one homolog in parallel, the other pointing with its telomeric end to the periphery (8.5%)

whereas in T38HT(X;11) this orientation pattern was found in 13.6% (Schmälter et al., 2015). Chromosome orientation may reflect the dynamic rotation of chromosomes over time or upon specific cellular conditions. Although the mechanisms underlying a possible rotation are still unknown, one hypothesis suggests that the chromosomes might rotate in order to create easier access to transcription factories. The authors also proposed that transcription of genes within the telomeric end of subcytoband 11E2 might be enhanced due to telomeric orientation towards the nuclear centre (Schmälter et al., 2015).

Deregulation of c-Myc promotes the formation of telomeric aggregates and the accelerated PCTs development is usually associated with duplication of cytoband 11E2, telomere length changes in translocation chromosomes carrying 11E2, and aberrant 3D nuclear telomere organization. These findings upport the concept of individual telomere lengthening and organization of chromosomes that are functional prerequisites for tumorigenesis. Determining whether c-Myc driven chromosome 11 nuclear repositioning occurs in mouse PCT therefore is important in confirming the potential role of c-Myc involving chromosome organization which may be involved in mouse PCT development. The study conducted various procedures to prove such hypotheses. In PreB *v-abl/myc* cells, repositioning of chromosome 11 was demonstrated within 1 hour after c-Myc induction and the mechanism which potentially underlies this observation involves TRF2, telomere, and lamin A/C interaction. Further experiments revealed an alteration in TRF2, telomere, and lamin A/C interaction in c-Myc-upregulated Pre B *v-abl/myc* cells supporting a role of this mechanism potentially underlying c-Myc-driven chromosome 11 repositioning in mouse PCT. However, further *in vivo* experiments are needed to confirm the role of this molecular pathway for PCT tumorigenesis.

TRF2: The essential shelterin protein responsible for telomere protection

In this study, upon c-Myc upregulation in PreB *v-abl/myc* cells, TRF2 levels decreased which might have facilitated a certain mechanism leading to telomere shortening. Evidence from TRF2-manipulated experiments has revealed that TRF2 depletion results in chromosome end-to-end fusions and telomere dysfunction (van Steensel et al., 1998; Smogorzewska and de Lange 2002a, Celli and de Lange, 2005; Denchi and de Lange, 2007). de Lange and colleagues conducted experiments in which TRF2 was removed from telomeres which then caused chromosome end-to-end fusions, frequently preserving long tracts of telomeric repeats on either side of the fusion junction (van Steensel et al., 1998; Smogorzewska and de Lange, 2002a; Celli and de Lange, 2005). An absence or reduction of TRF2 proteins has also been shown to affect telomere homoeostasis and result in telomere-led genomic instability by promoting nonhomologous end joining (NHEJ) of telomeres with formation of giant chromosomes (Denchi and de Lange, 2007; Guffei et al., 2010).

Alteration of normal TRF2 levels can influence genomic instability. Elevated levels of TRF2 have been shown to affect telomere length maintenance (Nera et al., 2015). Nera and colleagues investigated whether an elevation of TRF2 level facilitates the signaling leading to the occurrence of short telomeres. They found that, in human cells upon TRF2 overexpression, replication at telomeric sequences was interrupted and the formation of telomeric ultra-fine bridges (UFB), the thin threads of bridges arising during segregation of anaphase chromosomes, was induced (Nera et al., 2015). The occurrence of these UFBs precedes stochastic loss of large segments of telomeric sequences, with a subsequent increase in chromosome fusions, providing more insight of how TRF2 might be involved with genomic instability. The authors examined the length of individual telomeres in cells overexpressing TRF2 and demonstrated a subpopulation of chromosome ends that had undergone loss of almost the entire telomeric tract, frequently accompanied by end-to-end fusions. They also

demonstrated that TRF2 overexpression induced persistent replication stalling and resulted in the formation of UFBs during the subsequent anaphase. The authors discussed a model describing events resulting from TRF2 overexpression, proposing that the primary defect might be affecting the inhibition of duplex telomeric DNA replication and leading to UFBs formation, possibly in turn resulting in stochastic loss of large segments of telomeric sequences (Nera et al., 2015).

In this study, a mechanistic insight into the molecular basis of chromosome 11 repositioning in mouse Pre-B MycER cells undergoing c-Myc upregulation is provided. Investigations into possible interactions between TRF2, telomeres, and lamin A/C were conducted. As early as 20 minutes after c-Myc induction, an increased level of short telomeres, in parallel to a significantly decreased level of the TRF2 shelterin protein, was observed in PreB *v-abl/myc* cells, indicating a possible effect of TRF2 depletion contributing to the promotion of telomere shortening. Alternatively, since an increase in the total number of telomeric signals in PreB *v-abl/myc* cells at minute 20 after c-Myc induction was also observed (Figs. 14 and 15), this finding may indicate the unfolding of the t-loops and the dissociation of sister chromatids. A concurrent decrease in the aggregation of TRF2 ,analysed by TeloviewTM and the expression of lamin A/C was also demonstrated. TRF2 aggregates are defined, with the same criteria of telomeric aggregates, as clusters of TRF2 that are found in close association and cannot be further resolved as separate signals at the optical resolution limit of 200 nm (Mai and Garini, 2006). The observation of decreasing TRF2 expression in paralell to telomere shortening, from this study, was different from a previous report in which TRF2 overexpression lead to telomere shortening (Nera et al., 2015). Nera and colleagues observed the pattern of telomere shortening, in which the distribution of bulk telomeres changed from a tight cluster of 6-10 kb to a smear that extended from ~10 kb to below 2 kb, in cells overexpressing TRF2 (Nera et al., 2015). However, an absence or reduction of TRF2 proteins has also been shown to result in chromosome end-to-end fusions and

telomere-led genomic instability (van Steensel et al., 1998; Smogorzewska and de Lange 2002a, Celli and de Lange, 2005; Denchi and de Lange, 2007). Therefore the effects of the level of TRF2 expression on telomere homoeostasis might be heterogeneous context- and time- dependent, depending on various cell types and concurrent cellular conditions.

ImmunoFISH for TRF2 and telomeres revealed a disappearance of some TRF2-associated telomere spots which have been previously discussed (Lacoste et al., 2010; Lajoie et al., 2015). This area is possibly the formation of non-telomere-binding or free TRF2 in certain cells. In addition to the colocalization of TRF2 and telomeres, TRF2 proteins have also been found to distribute diffusely in nuclei (Lajoie et al., 2015). The diffuse distribution of nuclear TRF2 in the area where telomeres are not present was also confirmed in this study. Since TRF2 is the major shelterin subunit responsible for the process of DNA damage repair, the appearance of non-telomere-binding or free TRF2 might reflect the areas where TRF2 is recruited to function as part of the DNA repair mechanism, which might be activated upon c-Myc upregulation. TRF2 has been demonstrated to be involved in recognition of an initial double-strand break (DSB), before the activation of ATM and ATM-dependent response network (Bradshaw et al., 2005). Bradshaw and colleagues studied photo-induced DSBs in nontelomeric DNA of human fibroblasts and found that TRF2 forms transient foci, colocalizing closely with DSBs. In addition, TRF2 overexpression inhibits DSB-induced phosphorylation of ATM signaling pathway (Bradshaw et al., 2005).

Significantly elevated levels of TRF2 have been demonstrated in a subset of human tumour samples and cancer cell lines including breast cancer and melanoma, compared with primary cancer cells (Matsutani et al., 2001; Nera et al., 2015). Nera and colleagues overexpressed full-length, untagged wild-type TRF2 in human fibrosarcoma cells which had active telomerase that maintains telomeres at a stable intermediate-length range and whose endogenous TRF2 level was comparable to

that of primary non-malignant cells. By using a lentiviral expression system, they observed how elevated TRF2 levels might affect telomere maintenance and found, in cells overexpressing TRF2, that the distribution of bulk telomeres changed from a tight cluster (6-10 kb) to a smaller smear (~10 kb to below 2 kb) (Nera et al., 2015). FISH analysis with a telomeric repeat probe on metaphase chromosomes of HeLa1.2.11 cells overexpressing TRF2 demonstrated a statistically significant increase in signal-free chromosome ends and chromosome end-to-end fusions. Interestingly, they also found that the majority of TRF2-driven chromosome fusions lacked detectable telomeric signals at the fusion junctions, supporting the hypothesis that the events of chromosome fusion follow the loss of telomeric sequences (Nera et al., 2015). This observation might also explain the appearance of non-telomere-binding TRF2 demonstrated in this study.

Lamin A/C: a nuclear matrix protein responsible for chromatin organization

The nuclear matrix, analogous to the cellular cytoskeleton, is defined as the network of fibres found throughout the inside of a cell nucleus and extending throughout the nucleoplasm (Razin et al., 2014). Unlike the cytoskeleton, the nuclear matrix possesses a highly dynamic structure mimicking an interchangable sponge with open space for free diffusion of nuclear molecules (Pederson, 2000). The structure of the nuclear matrix was first recognised by Zbarskii and Debov (Zbarskii and Debov, 1951). To date, several proteins associated with the nuclear matrix have been discovered including the scaffold, or matrix, associated proteins (SAR or MAR) which are identified as being responsible for chromatin organization. Also, the nuclear matrix is involved in regulation of gene expression (Tetko et al., 2006).

Lamin A/C is a component of the nuclear lamina which forms the cellular nucleoskeleton or nuclear matrix. The nuclear matrix or nuclear lamina is a type V intermediate filamentous network of

proteins, DNA, and RNA that is refractory to high salt extraction and serves as an architectural skeleton to the nucleus (Razin et al., 2014). The nuclear lamina underlies the inner membrane of the nucleus and is distributed throughout the nucleoplasm. It provides support for chromatin organization and various nuclear functions including DNA replication, transcription and DNA repair (Smith et al., 2005; Dechat et al., 2008). There are 2 classes of nuclear lamina, the A-type lamins (lamin A and C, encoded by the gene LMNA) and the B-type lamins (lamin B1 and B2, encoded by the genes LMNB1 and LMNB2). Each class of lamins forms its own nuclear network and has a distinct role in gene regulation and chromatin organization (Shimi et al., 2008). In Hutchinson Gilford Progeria Syndrome (HGPS), a premature aging disorder, and other progeroid syndromes, LMNA, the gene encoding lamin A/C, is mutated and results in expression of progerin, a permanently farnesylated therefore truncated form of the lamin A/C protein which leads to premature aging (Cau et al., 2014).

Lamin A/C also plays a role in the DNA damage response pathway (Liu et al., 2005; Manju et al., 2006; Gonzalez-Suarez et al., 2009; Saha et al., 2013). The expression of progerin from mutated LMNA results in DNA damage at the telomeres by triggering loss of the heterochromatic marker H3K27me3 and premature senescence (Chojnowski et al., 2015). This defective process can be rescued by an expression of human telomerase reverse transcriptase (hTERT), a telomerase subunit, along with the rescue of cell proliferation defects (Kudlow et al., 2008; Benson et al., 2010). Therefore disrupted lamin A/C may lead to telomere instability and result in the decreased capacity of cells to replicate.

Mammalian telomeres have been shown to be associated with the nuclear matrix (de Lange, 1992). The 3D telomere organization has been demonstrated to be altered in tumour cells (Chuang et al., 2004; Mai and Garini, 2006) and in senescent cells harbouring defects in nuclear lamina (Raz et al., 2008). Gonzalez-Suarez and colleagues demonstrated that A-type lamins maintain telomere structure,

length, and function, as well as stabilizing the DNA damage response. They also found that loss of A-type lamins caused changes in the nuclear telomere distribution and defects in telomeric heterochromatin, inducing telomere shortening and increasing genomic instability (Gonzalez-Suarez et al., 2009). The authors compared the nuclear distribution of telomeres between wild-type mouse embryonic fibroblasts (MEFs) and MEFs devoid of A-type lamins to determine the role of A-type lamins in regulating nuclear telomere organization using the TeloView^{TM} program (Gonzalez-Suarez et al., 2009). Upon loss of A-type lamins, a shift in the localization of telomeres towards the nuclear periphery was observed and the changes in telomere distribution were not due to differences in cell-cycle profiles. By applying chromatin immunoprecipitation (ChIP) assays performed using lamin A/C antibodies, they demonstrated the binding of lamins to telomeres, suggesting a possible regulatory role of the tethering lamins scaffold to telomeres on their nuclear distribution. The authors also investigated alterations in the telomere-bound levels of TRF1 and TRF2 by ChIP analysis and the level of telomerase activity, upon the loss of A-type lamins, and found no significant changes in these parameters. Therefore they concluded that the binding of these known regulators of telomere length homoeostasis is not affected by the loss of A-type lamins (Gonzalez-Suarez et al., 2009).

In addition, alterations of A-type lamins may affect the epigenetic status of constitutive heterochromatin (Shumaker et al., 2006) and contribute to the repositioning of chromosome 11. Gonzalez-Suarez and colleagues investigated whether loss of A-type lamins affects the assembly of telomeric heterochromatin. They performed ChIP assays using antibodies recognizing well-established heterochromatic marks H3K9me3 and H4K20me3 and observed no changes in H3K9me3 levels, but a significant decrease in telomeric H4K20me3 levels in MEFs with a loss of A-type lamins, suggesting a role of A-type lamins in the maintenance of histone marks characteristic of telomeric heterochromatin (Gonzalez-Suarez et al., 2009). The authors also demonstrated that the loss of A-type

lamins has an impact on telomere function and genomic stability by determining the loss of telomeric signals (signal-free ends), the frequency of chromosome/ chromatid breaks and end-to-end fusions, and the presence of aneuploidy in pre-senescent wild-type lamin MEFs and MEFs with loss of A-type lamins. They found a threefold increase in the number of signal-free ends and a twofold increase in breaks in lamin-depleted MEFs, indicating increased genomic instability (Gonzalez-Suarez et al., 2009).

Lamin A has been speculated to form chromosomal inter-chain interactions throughout the nucleus and the loss of lamin A has recently been demonstrated to increase dynamics of nuclear interior chromatin organization (Bronshtein et al., 2015). Bronshtein and colleagues studied the dynamics of different genomic regions in the nucleus of live cells. Loss of lamin A function induced a striking transition from slow anomalous diffusion to fast and normal diffusion of chromatin organization, whereas no such effect was observed with the depletion of LAP2a, a protein interacting with lamin A and chromatin. Furthermore, in lamin A- depleted cells, rescuing lamin A results in full recovery of the slow dynamics to normal status, whereas the mutated lamin A only partially recovers the slow dynamics. The authors suggest that lamin A regulates chromatin diffusion in the nuclear interior and the function of lamin A is important in maintaining genome organization (Bronshtein et al., 2015).

In this study, upon c-Myc upregulation, decreases in the aggregation of TRF2 analysed by Teloview^{TM} and the expression of lamin A/C were exhibited along with a decrease in TRF2 expression and an increase in the frequency of shorter telomeres. Therefore, it is possible that disruption of the interaction between telomeres, telomeric shelterin proteins especially TRF2, and the nuclear matrix protein lamin A/C might relax the telomeric chromatin and create a change in telomere organization or nuclear distribution, which leads to chromosome 11 repositioning in PreB *v-abl/myc* cells.

Interaction between TRF2, telomere, and lamin A/C is potentially responsible for c-Myc-driven chromosome 11 repositioning.

Telomeres consist of a repetitive DNA sequence $(TTAGGG)_n$ located at the end of each chromosome to pretect it from fusion, degradation, the DNA damage repair mechanism, and recombination. The telomeric shelterin protein complex protects telomeres by preventing the activation of DNA damage response pathways through DNA damage machinery (de Lange, 2005). Human telomeres are found to attach to the nuclear matrix and the telomeric position of the $(TTAGGG)_n$ repeats is required for their interaction with the nuclear matrix (de Lange, 1992). Therefore, this study to identify whether a detachment of telomeric shelterin proteins from the nuclear matrix occurs in PreB cells after c-Myc deregulation is a potential approach to reveal the cause and consequence-relationship between chromosome 11 repositioning and fast-onset PCT development. Following a well-established method with which chromatin and the nuclear matrix could be separated (Nickerson et al., 1997), this was an ideal model to study the relationship between these structures. TRF2 was used in this study as a candidate telomeric shelterin protein due to its direct binding to telomeres (de Lange, 2005) and its essential role in telomere protection.

This study investigated the 3D positioning of mouse chromosome 11 in c-Myc activated PreB *v-abl/myc* cells. Exploration of the potential mechanism responsible for the repositioning of chromosome 11 after c-Myc upregulation was conducted to further investigate whether this manifestation was due to a change in one of the components of the telomeric shelterin protein complex, in particular a detachment of TRF2, a major shelterin subunit known to interact with the nuclear matrix protein lamin A/C (Wood et al., 2014). The manifestation of c-Myc-induced 3D positional change of mouse chromosome 11 in interphase nuclei of conditionally Myc expressing

PreB *v-abl/myc* cells was observed at a significantly higher frequency than in the control cells. When explored more deeply to understand the potential mechanism underlying this observation, significant alterations in signal intensities of TRF2, telomeres, and lamin A/C were demonstrated in c-Myc activated nuclei within the first hour that the repositioning of chromosome 11 took place, suggesting the changing interaction between these molecules as a possible mechanism behind this event.

The phenomenon of c-Myc induced chromosome 11 repositioning in Pre B *v-abl/myc* nuclei was first observed within the first hour after c-Myc activation. Following experiments were therefore conducted to explore the potential mechanism causing this observation after c-Myc upregulation within this period. This study examined the possible interaction between TRF2, a telomeric shelterin protein subunit, and the nuclear lamin A/C, underlying the chromosome 11 repositioning. These 2 proteins have been demonstrated to interact with each other and play a major role in regulating telomere structures, as well as BBF cycles. Louis and colleagues reported that c-Myc induced BBF in MycER^{TM}-activated Pre B *v-abl/myc* cells (Louis et al., 2005). At first, in Pre B *v-abl/myc* cells, they found telomere aggregations after c-Myc was activated. The metaphase chromosomes were then examined both by spectral karyotyping and telomeric FISH, at different times for a 120-hour period. Whereas the control cells revealed normal karyotypes, a significant level of dicentric chromosomes in the Pre B *v-abl/myc* cells was observed, reflecting chromosome fusions. Analyses of telomeric FISH also confirmed telomeric fusions involving both ends of chromosomes as well as sister chromatids (Louis et al., 2005).

The dynamics of 3D nuclear organization of TRF2 and telomeres and the signal intensity of lamin A/C during c-Myc driven chromosome 11 repositioning in PreB *v-abl/myc* cells were also investigated. In this study, the interactions between TRF2, telomeres, and lamin A/C in cells during the first hour after c-Myc activation, in which the repositioning of chromosome 11 was observed, were

explored. ImmunoFISH of TRF2 and telomeres, and coimmunofluorescence of TRF2 and lamin A/C in c-Myc-activated PreB *v-abl/myc* cells demonstrated a significant decrease of TRF2 and lamin A/C expression ($P < 0.0001$), in conjunction with evidence of telomere shortening. Observation of significantly decreased lamin A/C intensity surrounding a single area of TRF2, in Pre B *v-abl/myc* cells with nuclear matrix preparation, supports the possibility of a detachment of the telomere-TRF2 complex from the nuclear matrix where the telomeres have been reported to anchor to (de Lange, 1992).

This study also revealed, in Myc-activated Pre B *v-abl/myc* cells, an alteration in the length (reflected by intensity) of telomeres and the expression of TRF2. As early as 20 minutes after c-Myc activation, an increased frequency of shorter telomeres and a decrease in TRF2 intensity were identified. This reflects the possibility that c-Myc upregulation is influencing an alteration in telomere / TRF2 homeostasis. Comparisons of telomeric intensity distributions in which intensity correlates to telomere length revealed that at the 20-min timepoint after c-Myc activation, significantly more short telomeres were present than prior to c-Myc induction. TRF2 signal intensity decreased significantly after c-Myc activation compared to the control cells without c-Myc activation. In nuclear matrix preparations of PreB *v-abl/myc* cells in which DNAseI digestion was applied to better examine the correlation between telomeres, TRF2, and lamin A/C, a similar pattern of alterations in telomeres and TRF2 intensities was demonstrated. A significant decrease of lamin A/C surrounding a single signal of TRF2 was observed after c-Myc activation, potentially indicating detachment of telomeres and TRF2 from the nuclear matrix after c-Myc induction.

c-Myc has been reported to induce telomeric aggregates, fusions, and BBF cycles in Pre B *v-abl/myc* cells (Louis et al., 2005). Moreover, c-Myc enables an alteration in 3D nuclear organization and the organization of chromatin (Fischer et al., 1998a; Fischer et al., 1998b; Chadee et al., 1999).

Various c-Myc-dependent mechanisms potentially affecting nuclear remodeling and organization have been revealed. c-Myc involves in DNA repair regulation (Hironaka et al., 2003; Karlsson et al., 2003) and induces DNA breakage (Vafa et al., 2002). Alterations of the expression of TRF2 and lamin A/C, along with telomere shortening in c-Myc-induced Pre B *v-abl/myc* cells could underly the phenomenon of chromosome 11 repositioning concurrently occurring with the dissociation of telomeres and the telomeric shelterin subunit TRF2 from the nuclear matrix lamin A/C. c-Myc activation has been shown to initiate genomic instability in Pre B *v-abl/myc* cells through BBF cycles (Louis et al., 2005). Furthermore, c-Myc-induced mouse PCT exhibited duplication of subcytoband 11E2. This current study demonstrated the repositioning of mouse chromosome 11 within 1 hour, in Pre B *v-abl/myc* cells after c-Myc upregulation, a finding which confirms an important role for c-Myc in chromosome organization and nuclear remodeling. An alteration of the interaction between the telomeric shelterin protein complex and the nuclear matrix protein, proposedly a detachment of telomere-bound TRF2 from lamin A/C, in Pre B *v-abl/myc* cells is a characteristic of upregulated c-Myc expression, leading to the repositioning of mouse chromosome 11 in this study, and subsequently potential to genomic instability. This thesis therefore has demonstrated a novel pathway of c-Myc-dependent genomic instability that involves an alteration of the TRF2, telomeres, and lamin A/C interactions.

Changes in local positioning of some chromosomes, as revealed in this study and from other authors (Ferguson and Ward, 1992; Vourc'h et al., 1993; Zink and Cremer, 1998; Bridger et al., 2000; Walter et al., 2003), along with detachment of the telomeric shelterin protein complex from the nuclear matrix, may facilitate recombinations and/or fusions of chromosomal ends and promote genomic instability. The repositioning of mouse chromosome 11 observed after c-Myc upregulation in this study supports a major role of c-Myc in nuclear remodeling and organization of chromosomes.

In rapidly dividing cells, telomere lengthening is a cellular mechanism to prevent genomic instability (Collins and Mitchell, 2002). Lengthening of telomeres can occur due to the function of enzyme telomerase (Greider and Blackburn, 1985) or from the cycles of homologous recombination during the process of alternative telomere lengthening (ALT) (Cesare and Reddel, 2010). Kuzyk and Mai demonstrated in fast-onset PCTs that the telomere length is significantly increased for the translocation chromosome T(X;11) carrying 11E2 (Kuzyk and Mai, 2012). However, contrarily to the chromosome-specific telomere lengthening observed previously, this thesis examined telomeres of PreB *v-abl/myc* cells in overall chromosomes. As early as 20 minutes after c-Myc upregulation, a higher frequency of shorter telomeres was observed in PreB *v-abl/myc* cells, compared to the control cells. This phenomenon of telomere shortening might in part contribute to the repositioning of chromosome 11 and result in a c-Myc-driven genomic instability pathway. At the same time, there was an anteration in TRF2 and lamin A/C expression which also might play a key role as a major facilitator in the process of c-Myc-induced genomic instability.

Telomeres protect chromosome ends, and the shortening of telomeres is associated with tumorigenesis. Natural protection mechanisms for telomeres includes the t-loop formation which is the invasion of the 3' overhang into telomeric DNA, a process which is facilitated by TRF2. Wood and colleagues described the area at internal genomic sites, mostly at the $(TTAGGG)_n$ repeat sequences and referred to them as interstitial telomeric sequences (ITSs), at which the TRF2 usually binds to (Simonet et al., 2011; Yang et al., 2011). The authors introduced a novel chromosome-end structure where the ITSs interacted with DNA located outside of the telomere and formed a long-range chromosome loop encompassing several megabases of chromatin (Wood et al., 2014). This novel chromosome-end structure is termed interstitial telomere loops (ITLs). ITLs have been found to be associated with telomere stability and, as a t-loop within the telomere itself, is TRF2 dependent.

However, the ITLs, although evident in mitotic nuclei from various cell types of humans and mice as well as in human interphase chromosomes, have been visualized only in approximately 30% of all cells, suggesting other mechanisms are involved in the formation of this chromosome-end structure. ITL formation might play an important role in organismal aging, telomere and genome stability, regulation of gene expression, and chromosome condensation (Wood et al., 2014). Furthermore the authors proposed that ITLs are formed in a TRF2- and lamin A/C- dependent manner. They found that lamin A/C interacts with TRF2 to facilitate the functional organization of telomeres. A reduction in levels of lamin A/C leads to reduced ITL formation and the loss of telomeres, therefore changes in the interaction between TRF2 and lamin A/C may potentially lead to alterations in chromosome end structure (Wood et al., 2014).

Robin and colleagues reported interactions between subtelomeric regions and intrachromosomal DNA several megabases away, suggestive of long range, chromosome-end looping similar to what Wood and colleagues have proposed as ITLs (Robin et al., 2014). Wood and colleagues also showed a loss of looping upon replication-induced telomere shortening that was accompanied by changes in gene expression, further suggesting that beyond telomere stability, chromosome-end structure may play a critical role in regulation of gene expression (Wood et al., 2014). Robin and colleagues identified a minimum of 144 genes within 10 Mb of telomeres that showed the phenomenon of a telomere positive effect over a long distance, though it is not clear how many of these genes participated in telomere looping themselves and which experienced regulation from downstream effects. Although it is still unclear mechanistically how long-range telomere looping affects gene expression, TRF2, however, is found at promoters of these genes and a loss of TRF2 association was observed in cells with shortened telomeres (Robin et al., 2014). This thesis also demonstrated a decrease in TRF2 in parallel with a higher frequency of shorten telomeres in preB *v-abl/myc* cells

upon c-Myc upregulation, which correlates with their observation.The results from Robin and colleagues also parallel Wood and colleagues' work, which demonstrated that TRF2 is necessary to facilitate long-range telomere looping. Further analysis is necessary to determine whether TRF2 has a direct role in the regulation of gene expression at these promoters or if its role is indirect through the regulation of telomere looping. If ITLs can effect gene expression, this raises new possibilities for transcriptional regulation. There are many ITSs found throughout the genome and TRF2 association with these sites seems to be cell-type specific and cannot be predicted based on sequence alone. (Simonet et al., 2011; Yang et al., 2011). This implies that ITL formation is cell-type specific, and could therefore serve as a mechanism for cell-type specific regulation of gene expression. Furthermore, changes in ITL formation during cellular aging may have a role beyond telomere protection in that reduced ITL formation may alter gene expression patterns that influence cell fitness and replicative capacity.

Lamin A/C interacts with the major telomeric shelterin protein TRF2 and the interaction is necessary for the association of TRF2 with ITSs (Wood et al., 2014). When LMNA is mutated and expresses progerin, a permanently farnesylated form of the lamin A/C protein, the interaction between TRF2 and lamin A/C is disrupted and results in a decreased ITL formation. This phenomenon of dramatic telomere instability correlates with the observation in either after the knockdown of lamin A/C or in HGPS patient cells (Wood et al., 2014). Taken all together, reduction in levels of TRF2 and lamin A/C, represented by the quantification of fluorescence intensity per cell for TRF2 and lamin A/C,,as observed in this study after c-Myc activation, potentially facilitates changes in telomere organization. Upon c-Myc upregulation in PreB *v-abl/myc* cells, the TRF2 level was found to be decreased, which might have facilitated a certain mechanism leading to telomere shortening. In parallel, the decrease of TRF2 and lamin A/C might also affect the interaction between TRF2 and

lamin A/C homoeostasis. Regulatory mechanism of lamin A/C is still yet to be identified. However, the anchoring of TRF2 protein to the nuclear matrix may stabilize the lamin A/C protein, a decrease in TRF2 protein may therefore result in a decrease in lamin A/C protein level. The events of critically shortened telomeres and alterations in TRF2- lamin A/C interaction might then result in a detachment of telomere/TRF2 anchoring from the nuclear matrix, ultimately ending up with a repositioning of certain chromosomes including chromosome 11 (Fig. 26). Therefore this thesis proposes that, upon c-Myc upregulation, reduction in TRF2 expression and aggregation occurs and potentially interacts with an alteration in lamin A/C expression. This may affect telomere configuration resulting in telomere shortening and a detachment of telomeres and TRF2 from the nuclear matrix, which ultimately leads to chromosome 11 repositioning (Fig. 26). The molecular mechanism underlying this process, either directly or indirectly through its shelterin subunit members and telomerase activity, deserves further investigation. To date, the definite role of TRF2 shelterin subunit in telomere length homoeostasis has not been clearly established, therefore future experiments attempting to look more deeply into this process, focusing on the interactions between TRF2, telomerase, and the other shelterin components affecting the regulation of telomere length, are warranted.

Figure 26.

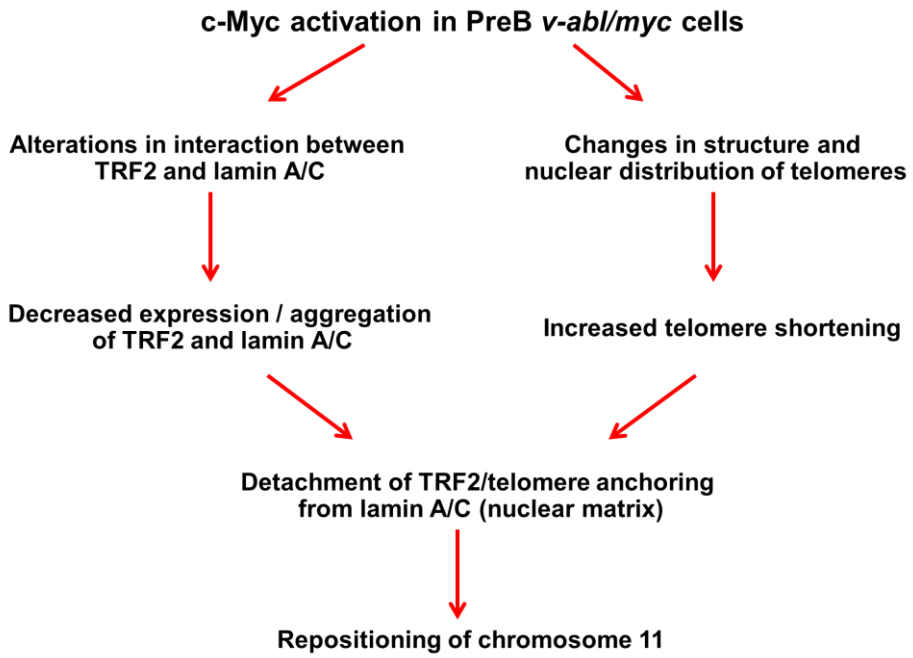

Figure 26. Proposed schema describing the mechanism of chromosome 11 repositioning after c-Myc activation in PreB *v-abl/myc* cells. c-Myc upregulation induces alterations in the TRF2 and lamin A/C interaction resulting in decreased protein expression and aggregation. At the same time, c-Myc also contributes to the changes in structure and distribution of telomeres, leading to increased telomere shortening. These manifestations result in a detachment of TRF2/telomere anchoring from lamin A/C or the nuclear matrix and lead to the repositioning of mouse chromosome 11.

Lung cancer: Urgent need for novel diagnostic and therapeutic principle

Lung cancer is the leading cause of cancer-related death worldwide, and urgently requires new diagnostic, therapeutic, and monitoring advances. NSCLC represents the most common lung cancer histology. Similar to other cancer types, NSCLC is characterized by both clinical and molecular heterogeneity. Personalized therapeutic approaches based on molecular genetic characterization to improve response and prolong survival have been implemented into NSCLC treatment.

Advanced-stage NSCLC patients who harbour the *EGFR* mutation or echinoderm microtubule-associated protein-like 4 (*EML4*)–anaplastic lymphoma kinase (*ALK*) rearrangement achieve greater survival benefits when treated with tyrosine kinase inhibitors (TKI) specific for EGFR or ALK compared with conventional standard chemotherapy (Kaneda et al., 2013), although acquired resistance to these therapies is a clinical issue. Patients with advanced-stage NSCLC who are negative for *EGFR* mutation or *EML4-ALK* rearrangement, patients who harbour *KRAS* mutations, or patients whose tumours do not harbour any known targetable molecular alterations, suffer from a lack of effective treatments and are often resistant to the most intensive multi-modal therapies, emphasizing the need to develop novel diagnostic and therapeutic approaches. Therefore, novel molecular, genetic, and cytogenetic discoveries are needed to better understand the disease and ultimately lead to the development of more effective therapeutic approaches. In this study, NSCLC which represents the most common histology of lung cancers as a clinical model, was explored.

Clinical factors used to determine prognosis and patient management for NSCLC include disease stage, *EGFR* mutation status, and *EML4-ALK* rearrangement. Existing clinical stage and biological markers such as gene expression signatures still yield inconsistent results, therefore more reliable prognostic biomarkers are needed to guide NSCLC treatment. Major improvements in NSCLC patient survival have recently resulted from the implementation of molecularly targeted therapies including anti-EGFR inhibitors. EGFR is a transmembrane tyrosine kinase receptor with a key role in mediating signal transduction pathways that promote cancer development, proliferation, and metastasis. EGFR inhibitors have shown great benefits in treating NSCLC patients whose tumours harbour *EGFR* mutations and/or amplifications (Mok et al., 2009). *EGFR* mutational status has been well established as a biological marker to predict the response to anti-EGFR targeted therapy in advanced NSCLC patients. Survival analyses have revealed a tendency of longer mean survival times in *EGFR* mutation-

positive patients compared with *EGFR* mutation-negative patients, confirming the significance of the *EGFR* mutation for a favourable prognosis. However, the difference in survival duration of these two groups was not statistically significant, likely due to the limited number of patients harbouring the *EGFR* mutation included in the study.

Since c-Myc deregulation and the *EGFR* mutation are prevalent in NSCLC patients (Chou et al., 2010; Graziano et al., 2011; Tran et al., 2011), further investigations examining their correlation and clinical significance are warranted to explore their possible interactions as potential targets for NSCLC tumorigenesis and therapy. Future studies to investigate whether c-Myc-driven telomeric aberration occurs in NSCLC patients are also warranted, to confirm the role of c-Myc in changes of telomere and chromosome organization in NSCLC tumorigenesis.

Clinical relevance of 17q25.3 copy number and 3D telomere profile in NSCLC patients

Chromosome region 17q25 in humans has been reported to be involved in a variety of human cancers including ovary (Presneau et al., 2005; Wojnarowicz et al., 2012), prostate (Bermudo et al., 2008; Bermudo et al., 2010), leukemia (Gulten et al., 2009), neuroblastoma (Islam et al., 2000; Yu et al., 2009), esophagus (Risk et al., 2002; Langan et al., 2004; McRonald et al., 2006), sarcoma (Ladanyi et al., 2001; Uppal et al., 2003), and breast (Morris et al., 2000). The frequent observations of genomic instability in this chromosomal region in corresponding cancers suggest that candidate genes involving tumorigenesis are located there.

This study examined the 17q25.3 region to evaluate its disruption status and prognostic value in order to determine its significance as a potential molecular target for therapy based on pre-clinical and clinical evidence of this region's association with tumorigenesis. Cytoband 11E2 of mouse chromosome 11 is syntenic with chromosome 17q25 in humans. Since *v-abl/myc* induced accelerated

mouse PCT development associated with alteration of chromosome 11 and of cytoband 11E2, it is interesting to study this particular region, 17q25, in humans to explore its role in tumorigenesis and potentially targeted therapy. This region is conserved in mice and humans, therefore, information on subcytoband 11E2 aberration in the fast-growing mouse PCT caused by c-Myc deregulation is potentially applicable to further exploration in the tumorigenesis mechanism and specification of therapeutic targets in various human cancers.

Studies in animal models have revealed that regions syntenic to 17q25.3 in mouse (11E2) and rat (10q32) are gained and associated with accelerated tumor development (Helou et al., 2001; Wiener et al., 2010). In mice with fast-onset PCTs, duplication of the 11E2 region is the major molecular aberration observed. The phenomenon does not occur in mice developing PCTs in a slow-onset (i.e. non-aggressive) pattern (Wiener et al., 2010). In rat endometrial adenocarcinomas of various genetic backgrounds, a gain of 10q32 is observed (Helou et al., 2001). Thus, a cross-species association of this oncogenic region with tumour aggressiveness seems apparent. Therefore, a hypothesis of this thesis was that 17q25.3 copy gains may also be an indicator of tumor progession and agressiveness in NSCLC patients. An investigation into this oncogenic cytoband/region to delineate its prognostic relevance in NSCLC was then conducted.

Array CGH performed in human NSCLC identified alterations on chromosome 17q25 which includes gains of *MAFG* (17q25.3) (Choi et al., 2006) and losses of *DMC1* (17q25.1) (Harada et al., 2001). Gains of oncogenes (Goeze et al., 2002; Sy et al., 2003) and down regulation of tumor suppressor gene *hRAB37* (Wu et al., 2009) on chromosome 17q25 are associated with aggressive phenotypes of human NSCLC, which renders this region a target of interest to study candidate genes in cancer development, progression, and treatment. Based on the synteny of mouse subcytoband 11E2 and human chromosome 17q25 and the available data concerning its potential role in NSCLC

tumorigenesis, cytoband 17q25.3, considering the pre-clinical and clinical evidence of this region in tumorigenesis, was selected to study its significance as a potential molecular target for therapy.

NSCLCs display molecular heterogeneity and this study revealed that a majority (61%) of NSCLC patients harboured clonal gains of cytoband 17q25.3. The gain of 17q25.3 in conjunction with the increase of the control region 17p11.2, reflecting a gain of chromosome 17, was also observed in approximately one third (38.9%) of the patients. Therefore the gain of whole chromosome 17 is proposed to represent a frequent phenomenon in NSCLC.

The copy number of 17q25.3 obtained by Q-FISH was well correlated with the CGH/SNP array data (Table 11), and showed a consistent and reliable method for measuring and interpreting 17q25.3 copy numbers in archival tumour tissue specimens. The criteria being used to define 17q25.3 gains account for intratumor heterogeneity, and the 3D approaches of Q-FISH and imaging avoid analyses of incomplete nuclei due to tissue sectioning. The patients whose specimens harboured a clonal gain of cytoband 17q25.3 also had a tendency towards poorer overall survival than the other patients.

In this study, molecular markers including *EGFR* mutational status and amplification of cytoband 17q25.3 in different subgroups of NSCLC patients, including smoking status as well as histology subtypes, were examined and provided a better understanding of NSCLC behavior, and our findings should contribute to the development of new therapeutic strategies to improve patient outcomes further on. However, future investigations to increase molecular and clinical information in this area should be conducted, including studies to identify possible correlations between c-Myc and *EGFR* expression, and the amplification of the 17q25.3 region. The ultimate goal is to identify these molecular markers as a potential therapeutic target for therapy in NSCLC and other cancer types further on, which will lead to improved patient outcomes.

The clinically translational aspects of this study involve the clinical significance of novel molecular therapeutic targets for therapy, including 3D nuclear telomere organization, in determining patient subpopulations according to predictive and/or prognostic significance. 3D nuclear imaging technology reveals a comprehensive and quantitative analysis of nuclei and their morphology and all the signals of specific regions of interest. 3D nuclear telomere organization profiling has been investigated and shown to be a potential molecular biomarker useful for categorizing patients according to various clinical features in different types of cancers, including Hodgkin lymphoma, multiple myeloma, acute myeloid leukemia, glioblastoma, and prostate cancer (Gadji et al., 2010; Gadji et al., 2012; Knecht et al., 2012; Adebayo Awe et al., 2013; Klewes et al., 2013). The evidence from these and other studies strengthens the rationale of investigating 3D telomere organization in NSCLC patients in this study.

To validate the significance of different telomeric organizations in early-staged NSCLC patients undergoing surgery as a primary therapy, a cohort of 18 paraffin-embedded tissue samples collected from NSCLC patients from the University of British Columbia in Canada, whose *EGFR* mutational and smoking statuses were known, was conducted. 3D telomeric profiling revealed that NSCLC patients who were smokers, *EGFR*-negative, or had squamous cell carcinoma histology had shorter telomeres and a higher incidence of telomeric aggregation than non-smokers, *EGFR*-positive patients, or adenocarcinomas patients, respectively.

Telomere length has been reported to be a potential biomarker of increased risk of lung cancer in diverse populations and different histologic subtypes (Shen M. et al., 2011; Lan et al., 2013; Machiela et al., 2015; Sanchez-Espiridion et al., 2014; Seow et al., 2014). A meta-analysis revealed an association of higher lung cancer risks and longer telomere length of peripheral leukocytes DNA, especially in female adenocarcinomas (Seow et al., 2014). A case-control study reported the association of long telomeres and the increased risk of adenocarcinomas, especially in females,

younger adults, and individuals with light smoking histories. In contrast, long telomeres were protective against squamous cell carcinomas, particularly in male patients (Sanchez-Espiridion et al., 2014).

Telomere crisis, implied by patterns of telomere shortening, genomic instability, and telomerase expression, has been recognized as a common and crucial event in tumorigenesis (Prescott et al., 2012). In early-stage NSCLC patients, long relative telomere length (RTL) of peripheral leukocytes has been reported to be associated with recurrence after curative resection, especially in female adenocarcinomas (Kim et al., 2015). When measured in tumor tissues from early-stage NSCLC patients undergoing surgical resection, shorter RTLs were associated with poorer overall and disease-free survival (Jeon et al., 2014). This finding is similar to the results of this thesis in which NSCLC patients who smoked, harboured *EGFR*-negative status, or had squamous cell carcinoma histology had a tendency to have shorter telomeres and shorter overall survival. The authors also found that an association between RTL and survival outcome was more pronounced in squamous cell carcinomas than adenocarcinomas (Jeon et al., 2014), but our sample size was too small to assess subtype specific differences.

In this study, patients with higher average numbers of telomeres per cell tended to have a shorter mean survival time, suggesting 3D telomere organization profiling is a potential molecular biomarker to estimate prognosis in NSCLC patients. Further studies into 3D telomere organization in a larger NSCLC cohort are therefore warranted, with the intention of validating whether this molecular biomarker is useful for diagnostic and therapeutic purposes in the management of patients with this devastating disease. This study suggests that 3D telomeric organization parameters, *EGFR*-mutation status, and 17q25.3 copy numbers are strong correlative biomarkers indicative of aggressive NSCLCs. Thus, 3D telomere profiling could present a novel molecular biomarker that could be clinically

implemented to identify NSCLC patients with unfavorable prognoses, and thus further study in a larger cohort is warranted.

Shortening of telomeres leads to genomic instability and tumorigenesis by activation of telomerase (Jeon et al., 2014). Therefore, targeting telomeres and/or telomerase is considered a rational therapeutic approach currently under investigation. Recently, a randomized phase II clinical trial evaluating the efficacy of a telomerase inhibitor called imetelstat as switch maintenance therapy in advanced NSCLC patients responding to first-line therapy was reported (Chiappori et al., 2015). The primary endpoint of the study was progression-free survival and the study included an exploratory analysis of telomere length as a novel biomarker for NSCLC prognosis/treatment response. Quantitative polymerase chain reaction and TeloFISH in tumor tissue of patients receiving imetelstat werd performed and correlated with patient response. Although the maintenance imetelstat failed to improve progression-free survival in advanced NSCLC patients, trends toward longer median PFS and overall survival in imetelstat-treated patients with short telomere length were evident, further suggesting telomeres could be useful molecular biomarkers and potential therapeutic targets in NSCLC (Chiappori et al., 2015).

Chapter VI : Conclusions

Upregulation of c-Myc leads to multiple changes in nuclear organization and selective chromosome repositioning which may promote neoplastic transformation including in mouse PCT. In a *v-abl/myc* -induced fast-growing mouse PCT model, accelerated tumor development was associated with duplication of subcytoband 11E2 of mouse chromosome 11. This research aimed to investigate whether c-Myc drives chromosome 11 nuclear repositioning in mouse PCTs and if so, whether a potential mechanism could be the interaction between TRF2, telomeres, and the nuclear matrix protein lamin A/C. Also this study examined the clinical significance of c-Myc, cytoband 17q25.3 (syntenic to mouse chromosome 11, cytoband E2), and nuclear telomere organization in NSCLC, to obtain a better understanding of NSCLC genetic profiles, which could lead to the development of new therapeutic strategies to improve patient outcome. Repositioning of mouse chromosome 11 was demonstrated within 1 hour after c-Myc upregulation in PreB *v-abl/myc* cells. Alterations in the interaction between TRF2, telomeres, and lamin A/C was proposed to be a potential mechanism for the repositioning of mouse chromosome 11 in PreB *v-abl/myc* cells after c-Myc activation. Upon c-Myc upregulation in PreB *v-abl/myc* cells, this thesis proposes that TRF2 levels decrease which facilitates a certain mechanism leading to telomere shortening. In parallel, decreased TRF2 might also affect the interaction between TRF2 and lamin A/C homeostasis. Critically shortened telomeres and the alterations in TRF2- lamin A/C interaction might then result in a detachment of telomere/TRF2 anchoring from the nuclear matrix, ultimately ending up with the repositioning of active chromosomes including chromosome 11. Moreover, highly frequent clonal gains of cytoband 17q25.3 were also confirmed, suggesting this specific region could harbour oncogenes with significant importance in NSCLC tumorigenesis. In addition, this study provides a better understanding of 3D nuclear telomere organization in NSCLC patients with different smoking backgrounds, *EGFR* mutational status, and

histology, providing a strong rationale for further exploration of this molecular profile in a larger cohort of NSCLC patients. The findings provide a better understanding of therapeutic targets leading to improvements in patient treatment and outcome.

In conclusion, this thesis proposes that an alteration of interactions between TRF2, telomeres, and lamin A/C, in particular, a detachment of telomeric shelterin protein complex from the nuclear lamin, contributes to repositioning of mouse chromosome 11. The phenomenon is induced by conditional c-Myc upregulation and leads to the onset of genomic instability, demonstrated by the chromosomal repositioning and rearrangements as revealed in this thesis and previous publications. Next, this thesis investigated whether the mouse subcytoband 11E2 (syntenic to human chromosomal region 17q25.3) appeared to be a candidate region in NSCLC tumorigenesis. Copy gains of 17q25.3 were demonstrated in a majority of NSCLC patients undergoing primary surgery, potentially supporting a hypothesis of one or more 'key' genes being responsible for NSCLC tumorigenesis being harboured by this region. In addition, 3D telomere organization profiling confirmed its efficiency for application in a clinical setting as a diagnostic tool to categorize NSCLC patients according to different clinical and pathological subgroups, adding this tumour into a preexisting list of 3D telomere organization use.

Chapter VII : Future Direction

Future *in vivo* experiments to determine whether c-Myc is a driving force promoting chromosome 11 repositioning during fast onset PCT development have been planned. The mouse model with *v-abl/myc*-induced PCT development will be used. In the study, T38HxBALB/c mice, with and without rcpT(X;11) will be infected with the *v-abl/myc* virus. Analysis of the cells will be done by peritoneal washes, allowing the same mouse to be observed over time. B cells will be isolated prior to infection, and again at 7, 14, 28 and 45 days post infection. Using B220, all B cells will be stained. And by using anti-surface IgM and CD138, only PCT cells will be stained. The infected B cells will stain positive for the *v-abl/myc* virus in FISH experiments, while non-infected B cells constitute negative controls for viral infection and for chromosome 11 positions. Pristane-only-induced mice will serve as internal controls. Chromosomes 5 and 7 will be included as positive controls and chromosome 10 as a negative control. Analyses of chromosome positioning will be performed using the same method as described in this thesis. The proposed time frame of B cell harvests will establish whether the repositioning of chromosome 11 precedes tumor formation or is its consequence.

Whether the c-myc-driven chromosome 11 repositioning occurs *in vivo* setting deserves further investigations in mouse model of fast-onset PCTs. Future experiments determining the correlation of c-Myc and cytoband 17q25.3 in NSCLC are also warranted to identify novel molecular targets for therapy in NSCLC. In agreement with previously published results in other tumour types, our study again found that 3D nuclear telomeric organization in NSCLC has a significant role in categorizing patient subgroups with different pathological and clinical statuses, and further exploration of its role in this disease is warranted.

References

Adams JM, Gerondakis S, Webb E, Corcoran LM, Cory S. Cellular myc oncogene is altered by chromosome translocation to an immunoglobulin locus in murine plasmacytomas and is rearranged similarly in human Burkitt lymphomas. Proc Natl Acad Sci USA 1983; 80(7): 1982-6.

Adams JM, Harris AW, Pinkert CA, Corcoran LM, Alexander WS, Cory S, et al. The c-myc oncogene driven by immunoglobulin enhancers induces lymphoid malignancy in transgenic mice. Nature 1985; 318(6046): 533-8.

Adebayo Awe J, Xu MC, Wechsler J, Benali-Furet N, Cayre YE, Saranchuk J, et al. Three-Dimensional Telomeric Analysis of Isolated Circulating Tumor Cells (CTCs) Defines CTC Subpopulations. Transl Oncol 2013; 6(1): 51-65.

Alexander WS, Adams JM, Cory S. Oncogene cooperation in lymphocyte transformation: malignant conversion of E mu-myc transgenic pre-B cells in vitro is enhanced by v-H-ras or v-raf but not v-abl. Mol Cell Biol 1989; 9(1): 67-73.

Amiard S, Doudeau M, Pinte S, Poulet A, Lenain C, Faivre-Moskalenko C, et al. A topological mechanism for TRF2-enhanced strand invasion. Nat Struct Mol Biol 2007; 14: 147-54.

Artandi SE, Chang S, Lee SL, Alson S, Gottlieb GJ, Chin L, et al. Telomere dysfunction promotes non-reciprocal translocations and epithelial cancers in mice. Nature 2000; 406: 641-5.

Artandi SE. Telomere shortening and cell fates in mouse models of neoplasia. Trends Mol Med 2002; 8(1): 44-7.

ASPSCR1 alveolar soft part sarcoma chromosome region, candidate 1 [Homo sapiens (human)] [database online]. Available at: http://www.ncbi.nlm.nih.gov/gene/79058 Accessed March 11, 2016.

Atiye J, Wolf M, Kaur S, Monni O, Böhling T, Kivioja A, et al. Gene amplifications in osteosarcoma-CGH microarray analysis. Genes Chromosomes Cancer 2005; 42(2): 158-63.

Aukema SM, Kreuz M, Kohler CW, Rosolowski M, Hasenclever D, Hummel M, et al. Biological characterization of adult Myc-translocation-positive mature B-cell lymphomas other than molecular Burkitt lymphoma. Haematologica 2014; 99(4): 726-35.

Barlow JH, Faryabi RB, Callén E, Wong N, Malhowski A, Chen HT, et al. Identification of early replicating fragile sites that contribute to genome instability. Cell 2013; 152(3): 620-32.

Baumann P, Cech TR. Pot1, the putative telomere end-binding protein in fission yeast and humans. Science 2001; 292: 1171-5.

Bayani J, Selvarajah S, Maire G, Vukovic B, Al-Romaih K, Zielenska M, et al. Genomic mechanisms and measurement of structural and numerical instability in cancer cells. Semin Cancer Biol 2007; 17: 5-18.

Beer S, Komatsubara K, Bellovin DI, Kurobe M, Sylvester K, Felsher DW. Hepatotoxin-induced changes in the adult murine liver promote MYC-induced tumorigenesis. PLoS One 2008; 3(6): e2493.

Benedek K, Chudoba I, Klein G, Wiener F, Mai S. Rearrangements of the telomeric region of mouse chromosome 11 in Pre-B ABL/MYC cells revealed by mBANDing, spectral karyotyping, and fluorescence in-situ hybridization with a subtelomeric probe. Chromosome Res 2004; 12(8): 777-85.

Benson E, Lee S, Aaronson S. Role of progerin-induced telomere dysfunction in HGPS premature cellular senescence. J Cell Sci 2010; 123: 2605-12.

Bermudo R, Abia D, Ferrer B, Nayach I, Benguria A, Zaballos A, et al. Co-regulation analysis of closely linked genes identifies a highly recurrent gain on chromosome 17q25.3 in prostate cancer. BMC Cancer 2008; 8: 315-26.

Bermudo R, Abia D, Benitez D, Carrió A, Vilella R, Ortiz AR, Thomson TM, Fernández PL. Discovery of genomic alterations through coregulation analysis of closely linked genes: a frequent gain in 17q25.3 in prostate cancer. Ann NY Acad Sci 2010; 1210: 17-24.

Bianchi A, Smith S, Chong L, Elias P, de Lange T. TRF1 is a dimer and bends telomeric DNA. EMBO J 1997; 16: 1785-94.

Bianchi A, Stansel RM, Fairall L, Griffith JD, Rhodes D, de Lange T. TRF1 binds a bipartite telomeric site with extreme spatial flexibility. EMBO J 1999; 18: 5735–44.

Bilaud T, Brun C, Ancelin K, Koering CE, Laroche T, Gilson E. Telomeric localization of TRF2, a novel human telobox protein. Nat Genet 1997; 17: 236-9.

Bradshaw PS, Stavropoulos DJ, Meyn MS. Human telomeric protein TRF2 associates with genomic double-strand breaks as an early response to DNA damage. Nat Genet 2005; 37(2): 193-7.

Branco MR, Pombo A. Chromosome organization: new facts, new models. TRENDS in Cell Biology 2006; 17(3): 127-34.

Bridger JM, Boyle S, Kill IR, Bickmore WA. Re-modelling of nuclear architecture in quiescent and senescent human fibroblasts. Curr Biol 2000; 10(3): 149-52.

Broccoli D, Smogorzewska A, Chong L, de Lange T. Human telomeres contain two distinct Myb-related proteins, TRF1 and TRF2. Nat Genet 1997; 17: 231-5.

Bronshtein I, Kepten E, Kanter I, Berezin S, Lindner M, Redwood AB, et al. Loss of lamin A function increases chromatin dynamics in the nuclear interior. Nat Commun 2015; 6: 8044. doi: 10.1038/ncomms9044.

Burrows JF, Chanduloy S, McIlhatton MA, Nagar H, Yeates K, Donaghy P, et al. Altered expression of the septin gene, SEPT9, in ovarian neoplasia. J Pathol 2003; 201(4): 581-8.

Burton RA, Mattila S, Taparowsky EJ, Post CB. B-myc: N-terminal recognition of myc binding proteins. Biochemistry 2006; 45(32): 9857-65.

Campaner S, Amati B. Two sides of the Myc-induced DNA damage response: from tumor suppression to tumor maintenance. Cell division 2012; 7(1): 6.

Campbell KJ and White RJ. Myc regulation of cell growth through control of transcription by RNA polymerases I and III (Book Chapter). Cold Spring Harb Perspect Med 2014; 4(5). pii: a018408.

Canadian Cancer Statistics 2015 [database online]. Toronto, ON: Canadian Cancer Society; 2015. Available at: http://www.cancer.ca/~/media/cancer.ca/CW/publications/Canadian%20Cancer%20Statistics/canadian-cancer-statistics-2013-EN.pdf. Accessed February 23, 2016.

Caporali A, Wark L, Vermolen BJ, Garini Y, Mai S. Telomeric aggregates and end-to-end chromosomal fusions require myc box II. Oncogene 2007; 26(10): 1398-406.

Cashman DJ, Buscaglia R, Freyer MW, Dettler J, Hurley LH, Lewis EA. Molecular modeling and bio-physical analysis of the c-Myc NHE-III1 silencer element. J Mol Model 2008; 14(2): 93-101.

Cau P, Navarro C, Harhouri K, Roll P, Sigaudy S, Kaspi E, et al. Nuclear matrix, nuclear envelope and premature aging syndromes in a translational research perspective. Semin Cell Dev Biol 2014; 29: 125-47.

Celli GB, de Lange T. DNA processing not required for ATM-mediated telomere damage response after TRF2 deletion. Nat Cell Biol 2005: 7: 712-8.

Cesare AJ, Reddel RR. Alternative lengthening of telomeres: models, mechanisms and implications. Nat Rev Genet 2010; 11: 319-30.

Chadee DN, Hendzel MJ, Tylipski CP, Allis CD, Bazett-Jones DP,Wright JA, et al. J Biol Chem 1999; 274: 24914-20.

Chen BJ, Wu YL, Tanaka Y, Zhang W. Small molecules targeting c-Myc oncogene: promising anti-cancer therapeutics. Int J Biol Sci 2014; 10(10): 1084-96.

Chen S, Xu Y, Chen Y, Li X, Mou W, et al. SOX2 gene regulates the transcriptional network of oncogenes and affects tumorigenesis of human lung cancer cells. PLoS ONE 2012; 7(5): e36326.

Chen Y, McGee J, Chen X, Doman T, Gong X, Zhang Y, et al. Identification of druggable cancer driver genes amplified across TCGA datasets. PLoS One 2014; 9(5): e98293.

Chiang YC, Teng SC, Su YN, Hsieh FJ, Wu KJ. c-Myc directly regulates the transcription of the NBS1 gene involved in DNA double-strand break repair. J Biol Chem 2003; 278(21): 19286-91.

Chiappori AA, Kolevska T, Spigel DR, Hager S, Rarick M, Gadgeel S, et al. A randomized phase II study of the telomerase inhibitor imetelstat as maintenance therapy for advanced non-small cell lung cancer. Ann Oncol 2015; 26(2): 354-62.

Choi JS, Zheng LT, Ha E, Lim YJ, Kim YH, Wang YP, et al. Comparative Genomic Hybridization Array Analysis and Real-Time PCR Reveals Genomic Copy Number Alteration for Lung Adenocarcinomas. Lung 2006; 184(6): 355–62.

Chojnowski A, Ong PF, Wong ES, Lim JS, Mutalif RA, Navasankari R, et al. Progerin reduces LAP2α-telomere association in Hutchinson-Gilford progeria. eLife 2015; 4: e07759.

Chong L, van Steensel B, Broccoli D, Erdjument-Bromage H, Hanish J, Tempst P, et al. A human telomeric protein. Science 1995; 270: 1663-7.

Chou YT, Lin HH, Lien YC, Wang YH, Hong CF, Kao YR, et al. EGFR promotes lung tumorigenesis by activating miR-7 through a Ras/ERK/Myc pathway that targets the Ets2 transcriptional repressor ERF. Cancer Res 2010; 70(21): 8822-31.

Chuang TC, Moshir S, Garini Y, Chuang AY, Young IT, Vermolen B, et al. The three-dimensional organization of telomeres in the nucleus of mammalian cells. BMC Biol 2004; 2: 12.

Ciullo M, Debily MA, Rozier L, Autiero M, Billault A, Mayau V, et al. Initiation of the breakage-fusion-bridge mechanism through common fragile site activation in human breast cancer cells: the model of PIP gene duplication from a break at FRA7I. Hum Mol Genet 2002; 11(23): 2887-94.

Collins K, Mitchell JR. Telomerase in the human organism. Oncogene 2002; 21: 564-79.

Conacci-Sorrell M, McFerrin L, Eisenman RN. An overview of Myc and its interactome (Book Chapter). Cold Spring Harb Perspect Med 2014; 4(1). pii: a014357.

Corcoran LM, Cory S, Adams JM. Transposition of the immunoglobulin heavy chain enhancer to the myc oncogene in a murine plasmacytoma. Cell 1985. 40: 71.

Cory S. Activation of cellular oncogenes in hemopoietic cells by chromosome translocation. Adv Cancer Res 1986; 47: 189-234.

Cotterman R, Jin V, Krig S, Lemen J, Wey A, Farnham P, et al. N-Myc regulates a widespread euchromatic program in the human genome partially independent of its role as a classical transcription factor. Cancer Res 2008; 68(23): 9654-62.

Court R, Chapman L, Fairall L, Rhodes D. How the human telomeric proteins TRF1 and TRF2 recognize telomeric DNA: A view from high-resolution crystal structures. EMBO Rep 2005; 6: 39–45.

Cowling VH, Cole MD. Mechanism of transcriptional activation by the Myc oncoproteins. Semin Cancer Biol 2006; 16(4): 242-52.

Cremer T, Cremer M. Chromosome territories. Cold Spring Harb Perspect Biol 2010; 2(3): a003889.

Cremer T, Cremer M, Hübner B, Strickfaden H, Smeets D, Popken J, et al. The 4D nucleome: Evidence for a dynamic nuclear landscape based on co-aligned active and inactive nuclear compartments. FEBS Lett 2015; 589(20 Pt A): 2931-43.

Dang CV, Lee WM. Identification of the human c-myc protein nuclear translocation signal. Mol Cell Biol 1988; 8(10): 4048-54.

Dang CV, Le A, Gao P. Myc-induced cancer cell energy metabolism and therapeutic opportunities. Clin Cancer Res 2009; 15(21): 6479-83.

D'Cruz CM, Gunther EJ, Boxer RB, Hartman JL, Sintasath L, Moody SE, et al. c-Myc induces mammary tumorigenesis by means of a preferred pathway involving spontaneous Kras2 mutations. Nat Med 2001; 7(2): 235-9.

Dechat T, Pfleghaar K, Sengupta K, Shimi T, Shumaker DK, Solimando L, et al. Nuclear lamins: major factors in the structural organization and function of the nucleus and chromatin. Genes Dev 2008; 22: 832-53.

de Lange T. Human telomeres are attached to the nuclear matrix. EMBO 1992; 11(2): 717-24.

de Lange T. Protection of mammalian telomeres. Oncogene 2002; 21: 532-40.

de Lange T. T-loops and the origin of telomeres. Nat Rev Mol Cell Biol 2004; 5: 323-9.

de Lange T. Shelterin: the protein complex that shapes and safeguards human telomeres. Genes Dev 2005; 19: 2100 -10.

de Lange T. How telomeres solve the end-protection problem. Science 2009; 326(5955): 948-52.

Delmore JE, Issa GC, Lemieux ME, Rahl PB, Shi J, Jacobs HM, et al. BET bromodomain inhibition as a therapeutic strategy to target c-Myc. Cell 2011; 146(6): 904-17.

Denchi EL, de Lange T. Protection of telomeres through independent control of ATM and ATR by TRF2 and POT1. Nature 2007; 448(7157): 1068-71.

DePinho RA, Polyak K. Cancer chromosomes in crisis. Nat Genet 2004; 36(9): 932-4.

Doksani Y, Wu JY, de Lange T, Zhuang X. Super-resolution fluorescence imaging of telomeres reveals TRF2-dependent T-loop formation. Cell 2013; 155: 345-56.

Eberhardy SR, Farnham PJ. Myc recruits P-TEFb to mediate the final step in the transcriptional activation of the cad promoter. J Biol Chem 2002; 277: 40156-62.

Eilers M, Eisenman RN. Myc's broad reach. Genes Dev 2008; 22: 2755-66.

El-Telbany A, Ma PC. Cancer genes in lung cancer: racial disparities: are there any?

Genes Cancer 2012; 3(7-8): 467 –80.

Felsher DW, Bishop JM. Transient excess of Myc activity can elicit genomic instability and tumorigenesis. Proc Natl Acad Sci USA 1999; 96(7): 3940-4.

Felsher DW, Zetterberg A, Zhu J, Tlsty T, Bishop JM. Overexpression of Myc causes p53-dependent G2 arrest of normal fibroblasts. Proc Natl Acad Sci USA 2000; 97(19): 10544-8.

Ferguson M, Ward DC. Cell cycle dependent chromosomal movement in pre-mitotic human T-lymphocyte nuclei. Chromosoma 1992; 101(9): 557-65.

Fernandez PC, Frank SR, Wang L, Schroeder M, Liu S, Greene J, et al. Genomic targets of the human c-Myc protein. Genes Dev 2003; 17(9): 1115-29.

Fischer AH, Bond JA, Taysavang P, Battles OE, Wynford-Thomas D. Am J Pathol 1998a; 153: 1443-50.

Fischer AH, Chadee DN, Wright JA, Gansler TS, Davie JR. J Cell Biochem 1998b; 70: 130-40.

Fouché N1, Cesare AJ, Willcox S, Ozgür S, Compton SA, Griffith JD. The basic domain of TRF2 directs binding to DNA junctions irrespective of the presence of TTAGGG repeats. J Biol Chem 2006; 281(49): 37486-95.

Fukasawa K, Wiener F, Vande Woude GF, Mai S. Genomic instability and apoptosis are frequent in p53 deficient young mice. Oncogene 1997; 15(11): 1295-302.

Fukuoka M, Wu YL, Thongprasert S, Sunpaweravong P, Leong SS, Sriuranpong V, et al. Biomarker analyses and final overall survival results from a phase III, randomized, open-label, first-line study of gefitinib versus carboplatin/paclitaxel in clinically selected patients with advanced non-small-cell lung cancer in Asia (IPASS). J Clin Oncol 2011; 29(21): 2866-74.

Gabay M, Li Y, Felsher DW. Myc activation is a hallmark of cancer initiation and maintenance. Cold Spring Harb Perspect Med 2014; 4(6), pii: a014241.

Gadji M, Fortin D, Tsanaclis AM, Garini Y, Katzir N, Wienburg Y, et al. Three-dimensional nuclear telomere architecture is associated with differential time to progression and overall survival in glioblastoma patients. Neoplasia 2010; 12(2): 183–91.

Gadji M, Vallente R, Klewes L, Righolt C, Wark L, Kongruttanachok N, et al. Nuclear remodeling as a mechanism for genomic instability in cancer. Adv Cancer Res 2011; 112:77-126.

Gadji M, Adebayo Awe J, Rodrigues P, Kumar R, Houston DS, Klewes L, et al. Profiling three-dimensional nuclear telomeric architecture of myelodysplastic syndromes and acute myeloid leukemia defines patient subgroups. Clin Cancer Res 2012; 18(12): 3293-304.

George RE, Kenyon RM, McGuckin AG, Malcolm AJ, Pearson AD, Lunec J. Investigation of co-amplification of the candidate genes ornithine decarboxylase, ribonucleotide reductase, syndecan-1 and a DEAD box gene, DDX1, with N-myc in neuroblastoma. United Kingdom Children's Cancer Study Group. Oncogene 1996; 12: 1583-87.

Gisselsson D, Jonson T, Petersen A, Strombeck B, Dal Cin P, Hoglund M, et al. Proc Natl Acad Sci USA 2001; 98: 12683-8.

Giuriato S, Ryeom S, Fan AC, Bachireddy P, Lynch RC, Rioth MJ, et al. Sustained regression of tumors upon Myc inactivation requires p53 or thrombospondin-1 to reverse the angiogenic switch. Proc Natl Acad Sci USA 2006; 103(44): 16266-71.

Goeze A, Schlüns K, Wolf G, Thäsler Z, Petersen S, Petersen I. Chromosomal imbalances of primary and metastatic lung adenocarcinomas. J Pathol 2002; 196 (1): 8-16.

Gonzalez-Suarez I, Redwood A, Perkins S, Vermolen B, Lichtensztejin D, Grotsky D, et al. Novel roles for A-type lamins in telomere biology and the DNA damage response pathway. EMBO J 2009; 28: 2414-27.

Graziano P, Cardillo G, Mancuso A, Paone G, Gasbarra R, De Marinis F, et al. Long-term disease-free survival of a patient with synchronous bilateral lung adenocarcinoma displaying different EGFR and C-MYC molecular characteristics. Chest 2011; 140(5): 1354-6.

Greider CW, Blackburn EH. Identification of a specific telomere terminal transferase activity in Tetrahymena extracts. Cell 1985; 43: 405-13.

Grenman S, Shapira A, Carey TE. In vitro response of cervical cancer cell lines CaSki, HeLa, and ME-180 to the antiestrogen tamoxifen. Gynecol Oncol 1988a; 30(2): 228-38.

Grenman SE, Roberts JA, England BG, Grönroos M, Carey TE. In vitro growth regulation of endometrial carcinoma cells by tamoxifen and medroxyprogesterone acetate. Gynecol Oncol 1988b; 30(2): 239-50.

Griffith J, Bianchi A, de Lange T. TRF1 promotes parallel pairing of telomeric tracts in vitro. J Mol Biol 1998; 278: 79–88.

Griffith JD, Comeau L, Rosenfield S, Stansel RM, Bianchi A, Moss H, et al. Mammalian telomeres end in a large duplex loop. Cell 1999; 97: 503-14.

Grynberg M, Jaroszewski L, Godzik A. Domain analysis of the tubulin cofactor system: a model for tubulin folding and dimerization. BMC Bioinformatics 2003; 4: 46

Guffei A, Sarkar R, Klewes L, Righolt C, Knecht H, Mai S. Dynamic chromosomal rearrangements in Hodgkin's lymphoma are due to ongoing three-dimensional nuclear remodeling and breakage-bridge-fusion cycles. Haematologica 2010; 95(12): 2038-46.

Gulten T, Yakut T, Karkucak M, Baytan B, Guneş AM. AML1 amplification and 17q25 deletion in a case of childhood acute lymphoblastic leukemia. J Clin Lab Anal 2009; 23(6): 368-71.

Hanaoka S, Nagadoi A, Nishimura Y. Comparison between TRF2 and TRF1 of their telomeric DNA-bound structures and DNA-binding activities. Protein Sci 2005; 14: 119-30.

Hande MP, Samper E, Lansdorp P, Blasco MA. Telomere length dynamics and chromosomal instability in cells derived from telomerase null mice. J Cell Biol 1999; 144: 589–601.

Harada H, Nagai H, Tsuneizumi M, Mikami I, Sugano S, Emi M. Identification of DMC1, a novel gene in the TOC region on 17q25.1 that shows loss of expression in multiple human cancers. J Hum Genet 2001; 46: 90–5.

Hattersley AT, Pearson ER. Minireview: pharmacogenetics and beyond: the interaction of therapeutic response, beta-cell physiology, and genetics in diabetes. Endocrinology 2006; 147(6): 2657-63.

He DC, Nickerson JA, Penman S. Core filaments of the nuclear matrix. J Cell Biol 1990; 110(3): 569-80.

Helou K, Walentinsson A, Levan G, Stahl F. Between rat and mouse zoo-FISH reveals 49 chromosomal segments that have been conserved in evolution. Mamm Genome 2001; 12(10): 765-71.

Hendriks CL, van Vliet LJ, Rieger B, van Ginkel M. DIPimage: a scientific image processing toolbox for MATLAB, 1999. Pattern recognition group, Department of Applied Physics, Delft University of Technology, Available at: http://www.ph.tn.tudelft.nl/DIPlib. Accessed February 23, 2016.

Hironaka K, Factor VM, Calvisi DF, Conner EA, Thorgeirsson SS. Dysregulation of DNA repair pathways in a transforming growth factor alpha/c-myc transgenic mouse model of accelerated hepatocarcinogenesis. Lab Invest 2003; 83(5): 643-54.

Hockemeyer D, Daniels JP, Takai H, de Lange T. Recent expansion of the telomeric complex in rodents: Two distinct POT1 proteins protect mouse telomeres. Cell 2006; 126(1): 63-77.

Houghtaling BR, Cuttonaro L, Chang W, Smith S. A dynamic molecular link between the telomere length regulator TRF1 and the chromosome end protector TRF2. Curr Biol 2004; 14: 1621–31.

Hübner B, Lomiento M, Mammoli F, Illner D, Markaki Y, Ferrari S, et al. Remodeling of nuclear landscapes during human myelopoietic cell differentiation maintains co-aligned active and inactive nuclear compartments. Epigenetics Chromatin 2015; 8: 47-67.

Hulf T, Bellosta P, Furrer M, Steiger D, Svensson D, Barbour A, et al. Whole- genome analysis reveals a strong positional bias of conserved dMyc-dependent E-boxes. Mol Cell Biol 2005; 25(9): 3401-10.

Huppi K, Volfovsky N, Runfola T, Jones TL, Mackiewicz M, Martin SE, et al. The identification of microRNAs in a genomically unstable region of human chromosome 8q24. Mol Cancer Res 2008; 6(2): 212-21.

Huppi K, Pitt J, Wahlberg B, Caplen NJ. Genomic instability and mouse microRNAs. Toxicol Mech Methods 2011; 21(4): 325-33.

Hwang KT, Han W, Cho J, Lee JW, Ko E, Kim EK, et al. Genomic copy number alterations as predictive markers of systemic recurrence in breast cancer. Int J Cancer 2008; 123(8): 1807-15.

Ikegaki N, Minna J, Kennett RH. The human L-myc gene is expressed as two forms of protein in small cell lung carcinoma cell lines: detection by monoclonal antibodies specific to two myc homology box sequences. EMBO 1989; 8 (6): 1793-9.

Islam A, Kageyama H, Hashizume K, Kaneko Y, Nakagawara A. Role of survivin, whose gene is mapped to 17q25, in human neuroblastoma and identification of a novel dominant-negative isoform, survivin-beta/2B. Med Pediatr Oncol 2000; 35(6): 550-3.

Islam MA, Thomas SD, Murty VV, Sedoris KJ, Miller DM. c-Myc quadruplex-forming sequence Pu-27 induces extensive damage in both telomeric and non-telomeric regions of DNA. J Biol Chem 2014; 289(12): 8521-31.

Jacobs JJ, de Lange T. Significant role for p16 (INK4a) in p53-independent telomere-directed senescence. Curr Biol 2004; 14: 2302-8.

Jeon HS, Choi YY, Choi JE, Lee WK, Lee E, Yoo SS, et al. Telomere length of tumor tissues and survival in patients with early stage non-small cell lung cancer. Mol Carcinog 2014; 53(4): 272-9.

Johansson B, Fioretos T, Mitelman F. Cytogenetic and molecular genetic evolution of chronic myeloid leukemia Acta haematologica 2002; 107: 76-94.

Kaneda H, Yoshida T, Okamoto I. Molecularly targeted approaches herald a new era of non-small-cell lung cancer treatment. Cancer Manage Res 2013; 5: 91–101.

Kapeli K, Hurlin PJ. Differential regulation of N-Myc and c-Myc synthesis, degradation, and transcriptional activity by the Ras/mitogen-activated protein kinase pathway. J Biol Chem 2011; 286(44): 38498-508.

Karlseder J, Broccoli D, Dai Y, Hardy S, de Lange, T. p53- and ATM-dependent apoptosis induced by telomeres lacking TRF2. Science 1999; 283: 1321-5.

Karlsson A, Deb-Basu D, Cherry A, Turner S, Ford J, Felsher DW. Defective double-strand DNA break repair and chromosomal translocations by MYC overexpression. Proc Natl Acad Sci USA 2003; 100(17): 9974-9.

Katoh M, Katoh M. Human FOX gene family (Review). Int J Oncol 2004; 25(5): 1495-500.

KC W, Satpathy AT, Rapaport AS, Briseño CG, Wu X, Albring JC, et al. L-Myc expression by dendritic cells is required for optimal T-cell priming. Nature 2014; 507: 243-7.

Kim SH, Kaminker P, Campisi J. TIN2, a new regulator of telomere length in human cells. Nat Genet 1999; 23: 405–12.

Kim SH, Han S, You YH, Chen DJ, Campisi J. The human telomere-associated protein TIN2 stimulates interactions between telomeric DNA tracts in vitro. EMBO Rep 2003; 4: 685-91.

Kim SH, McQueen PG, Lichtman MK, Shevach EM, Parada LA, Misteli T. Spatial genome organization during T-cell differentiation Cytogenetic and genome research 2004a; 105: 292-301.

Kim ES, Ye Y, Vaporciyan AA, Xing J, Huang M, Gu J, et al. Telomere length and recurrence risk after curative resection in patients with early-stage non–small-cell lung cancer: A prospective cohort study. J Thorac Oncol 2015; 10: 302-8.

Klein G. Specific chromosomal translocation and genesis of B-cell-derived tumors in mice and men. Cell 1983; 32: 311-6.

Klewes L, Vallente R, Dupas E, Brand C, Grün D, Guffei A, et al. Three-dimensional Nuclear Telomere Organization in Multiple Myeloma. Transl Oncol 2013; 6(6): 749-56.

Knecht H, Kongruttanachok N, Sawan B, Brossard J, Prevost S, Turcotte E, et al. Three-dimensional Telomere Signatures of Hodgkin- and Reed-Sternberg Cells at Diagnosis Identify Patients with Poor Response to Conventional Chemotherapy. Transl Oncol 2012; 5(4): 269-77.

Koelsch BU, Rajewsky MF, Kindler-Rohrborn A. A 6-Mb contig-based comparative gene and linkage map of the rat schwannoma tumor suppressor region at 10q32.3. Genomics 2005; 85(3): 322-9.

Kostenko EV, Mahon GM, Cheng L, Whitehead IP. The Sec14 homology domain regulates the cellular distribution and transforming activity of the Rho-specific guanine nucleotide exchange factor Dbs. J Biol Chem 2005; 280(4): 2807-17.

Kudlow B, Stanfel M, Burtner C, Johnston E, Kennedy B. Suppression of proliferative defects associated with processing-defective lamin A mutants by hTERT or inactivation of p53. Mol Biol Cell 2008; 19: 5238-48.

Kuroda M, Tanabe H, Yoshida K, Oikawa K, Saito A, Kiyuna T, et al. Alteration of chromosome positioning during adipocyte differentiation. J Cell Sci 2004; 117(Pt 24): 5897-903.

Kuschak TI, Taylor C, McMillan-Ward E, Israels S, Henderson DW, Mushinski JF, et al. The ribonucleotide reductase R2 gene is a non-transcribed target of c-Myc-induced genemic instability. Gene 1999; 238: 351-65.

Kuschak TI, Kuschak BC, Taylor CL, Wright JA, Wiener F, Mai S. c-Myc initiates illegitimate replication of the ribonucleotide reductase R2 gene. Oncogene 2002; 21(6): 909-20.

Kuttler F, Mai S. c-Myc, genomic instability and disease. 2006. In Genome dynamics. Vol 1: Genome and Disease. Ed: Volff, J-N. Karger Publishers, Würzburg, Germany. pp. 171-91.

Kuzyk A, Booth S, Righolt C, Mathur S, Gartner J, Mai S. MYCN overexpression is associated with unbalanced copy number gain, altered nuclear location, and overexpression of chromosome arm 17q genes in neuroblastoma tumors and cell lines. Genes Chromosomes Cancer 2015; 54(10): 616-28.

Kuzyk A, Mai S. Selected telomere length changes and aberrant three-dimensional nuclear telomere organization during fast-onset mouse plasmacytomas. Neoplasia 2012; 14(4): 344-51.

Kuzyk A, Mai S. c-Myc-induced genomic instability (Book Chapter). Cold Spring Harb Perspect Med 2014; 4(4). pii: a014373.

Lacoste S, Wiechec E, Dos Santos Silva AG, Guffei A, Williams G, Lowbeer M, et al. Chromosomal rearrangements after ex vivo Epstein-Barr virus (EBV) infection of human B cells. Oncogene 2010; 29(4): 503-15.

Ladanyi M, Lui MY, Antonescu CR, Krause-Boehm A, Meindl A, Argani P, et al. The der (17)t(X;17)(p11;q25) of human alveolar soft part sarcoma fuses the TFE3 transcription factor gene to ASPL, a novel gene at 17q25. Oncogene 2001; 20(1): 48-57.

Lajoie V, Lemieux B, Sawan B, Lichtensztejn D, Lichtensztejn Z, Wellinger R, et al. LMP1 mediates multinuclearity through downregulation of shelterin proteins and formation of telomeric aggregates. Blood 2015; 125(13): 2101-10.

Lan Q, Cawthon R, Gao Y, Hu W, Hosgood HD 3rd, Barone-Adesi F, et al. Longer telomere length in peripheral white blood cells is associated with risk of lung cancer and the rs2736100 (CLPTM1L-TERT) polymorphism in a prospective cohort study among women in China. PLoS ONE 2013; 8(3): e59230.

Langan JE, Cole CG, Huckle EJ, Byrne S, McRonald FE, Rowbottom L, et al. Novel microsatellite markers and single nucleotide polymorphisms refine the tylosis with oesophageal cancer (TOC) minimal region on 17q25 to 42.5 kb: sequencing does not identify the causative gene. Hum Genet 2004; 114(6): 534-40.

Largaespada DA, Kaehler DA, Mishak H, Weissinger E, Potter M, Mushinski JF, et al. A retrovirus that expresses v-abl and c-myc oncogenes rapidly induces plasmacytomas. Oncogene 1992; 7(4): 811-9.

Lastowska M, Chung YJ, Cheng Ching N, Haber M, Norris MD, Kees UR, et al. Regions syntenic to human 17q are gained in mouse and rat neuroblastoma. Genes Chromosomes Cancer 2004; 40: 158-63.

Lei M, Podell ER, Cech TR. Structure of human POT1 bound to telomeric single-stranded DNA provides a model for chromosome end-protection. Nat Struct Mol Biol 2004; 11: 1223-9.

Li B, Oestreich S, de Lange T. Identification of human Rap1: Implications for telomere evolution. Cell 2000; 101: 471–83.

Li Q, Dang CV. c-Myc overexpression uncouples DNA replication from mitosis. Mol Cell Biol 1999; 19(8): 5339-51.

Li Z, Vam Calcar S, Qu C, Cavenee WK, Zhang MQ, Ren B. A global transcriptional regulatory role for c-Myc in Burkitt's lymphoma cells. Proc Natl Acad Sci USA 2003; 100: 8164-9.

Li Z, Owonikoko T, Ramalingam SS, Doetsch PW, Xiao Z, Khuri F, et al. c-Myc Suppression of DNA double-strand break repair. Neoplasia 2012; 14: 1190–202.

Liang X, Nan K, Li Z, Xu Q. Overexpression of the LKB1 gene inhibits lung carcinoma cell proliferation partly through degradation of c-myc protein. Oncology Reports 2009; 21: 925-31.

Liao B, Lin C, Yang JC. First-line management of EGFR-mutated advanced lung adenocarcinoma: recent developments. Drugs 2013; DOI 10.1007/s40265-013-0020-8.

Littlewood TD, Hancock DC, Danielian PS, Parker MG, Evan GI. A modified oestrogen receptor ligand-binding domain as an improved switch for the regulation of heterologous proteins. Nucleic Acids Res 1995; 23(10): 1686-90.

Liu B, Wang J, Chan K, Tjia W, Deng W, Guan X, et al. Genomic instability in laminopathy-based premature aging. Nat Med 2005; 11: 780-5.

Liu D, O'Connor MS, Qin J, Songyang Z. Telosome, a mammalian telomere-associated complex formed by multiple telomeric proteins. J Biol Chem 2004a; 279: 51338-42.

Liu D, Safari A, O'Connor MS, Chan DW, Laegeler A, Qin J, et al. PTOP interacts with POT1 and regulates its localization to telomeres. Nat Cell Biol 2004b; 6: 673–80.

Loayza D, Parsons H, Donigian J, Hoke K, de Lange T. DNA binding features of human POT1: A nonamer 5-TAGGGTTAG-3 minimal binding site, sequence specificity, and internal binding to multimeric sites. J Biol Chem 2004; 279: 13241–8.

Lockwood WW, Wilson IM, Coe BP, Chari R, Pikor LA, Thu KL, et al. Divergent genomic and epigenomic landscapes of lung cancer subtypes underscore the selection of different oncogenic pathways during tumor development. PLoS One 2012; 7(5): e37775.

Louis SF, Vermolen BJ, Garini Y, Young IT, Guffei A, Lichtensztejn Z, et al. c-Myc induces chromosomal rearrangements through telomere and chromosome remodeling in the interphase nucleus. Proc Natl Acad Sci USA 2005; 102(27): 9613-9618.

Mac Partlin M, Homer E, Robinson H, McCormick CJ, Crouch DH, Durant ST, et al. Interactions of the DNA mismatch repair proteins MLH1 and MSH2 with c-MYC and MAX. Oncogene 2003; 22(6): 819-25.

Machiela MJ, Hsiung CA, Shu XO, Seow WJ, Wang Z, Matsuo K, et al. Genetic variants associated with longer telomere length are associated with increased lung cancer risk among never-smoking women in Asia: a report from the female lung cancer consortium in Asia. Int J Cancer 2015; 137(2): 311-9.

Mai S. Overexpression of c-myc precedes amplification of the gene encoding dihydrofolate reductase. Gene 1994; 148(2): 253-60.

Mai S, Fluri M, Siwarski D, Huppi K. Genomic instability in MycER-activated Rat1A-MycER cells. Chromosome Res 1996a; 4(5): 365-71.

Mai S, Hanley-Hyde J, Fluri M. c-Myc overexpression associated DHFR gene amplification in hamster, rat, mouse and human cell lines. Oncogene 1996b; 12(2): 277-88.

Mai S, Hanley-Hyde J, Rainey GJ, Kuschak TI, Paul JT, Littlewood TD, et al. Chromosomal and extrachromosomal instability of the cyclin D2 gene is induced by Myc overexpression. Neoplasia 1999; 1(3): 241-52.

Mai S, Mushinski JF. c-Myc-dependent genomic instability. J Environ Path Toxicol Oncol 2003; 22: 179-99.

Mai S, Garini Y. Oncogenic remodeling of the three-dimensional organization of the interphase nucleus: c-Myc induces telomeric aggregates whose formation precedes chromosomal rearrangements. Cell Cycle 2005; 4(10): 1327-31.

Mai S, Garini Y. The significance of telomeric aggregates in the interphase nuclei of tumor cells Journal of cellular biochemistry 2006; 97: 904-15.

Mai S. Initiation of telomere-mediated chromosomal rearrangements in cancer. J Cell Biochem 2010; 109(6): 1095-102.

Makarov VL, Hirose Y, Langmore JP. Long G tails at both ends of human chromosomes suggest a C strand degradation mechanism for telomere shortening. Cell 1997; 88: 657-66.

Mandlekar S, Hebbar V, Christov K, Kong AN. Pharmacodynamics of tamoxifen and its 4-hydroxy and N-desmethyl metabolites: activation of caspases and induction of apoptosis in rat mammary tumors and in human breast cancer cell lines. Cancer Res 2000; 60(23): 6601-6.

Manju K, Muralikrishna B, Parnaik VK. Expression of disease-causing lamin A mutants impairs the formation of DNA repair foci. J Cell Sci 2006; 119: 2704-14.

Marella NV, Seifert B, Nagarajan P, Sinha S, Berezney R. Chromosomal rearrangements during human epidermal keratinocyte differentiation. J Cell Physiol 2009; 221(1): 139-46.

Marinkovic D, Marinkovic T, Mahr B, Hess J, Wirth T. Reversible lymphomagenesis in conditionally c-Myc expressing mice. Int J Cancer 2004; 110(3): 336-42.

Matsutani N, Yokozaki H, Tahara E, Tahara H, Kuniyasu H, Haruma K, et al. Expression of telomeric repeat binding factor 1 and 2 and TRF1-interacting nuclear protein 2 in human gastric carcinomas. Int J Oncol 2001; 19: 507–12.

McClintock B. The stability of broken ends of chromosomes in zea mays. Genetics 1941; 26: 234-82.

McRonald FE, Liloglou T, Xinarianos G, Hill L, Rowbottom L, Langan JE, et al. Down-regulation of the cytoglobin gene, located on 17q25, in tylosis with oesophageal cancer (TOC): evidence for trans-allele repression. Hum Mol Genet 2006; 15(8): 1271-7.

Mehta IS, Amira M, Harvey AJ, Bridger JM. Rapid chromosome territory relocation by nuclear motor activity in response to serum removal in primary human fibroblasts. Genome Biology 2010; 11: R5.

Mehta IS, Kulashreshtha M, Chakraborty S, Kolthur-Seetharam U, Rao BJ. Chromosome territories reposition during DNA damage-repair response. Genome Biology 2013; 14(12): R135.

Minuti G, D'Incecco A, Landi L, Cappuzzo F. Protein kinase inhibitors to treat non-small-cell lung cancer. Expert Opin Pharmacother 2014; 15(9): 1203-13.

Mitani S, Kamata H, Fujiwara M, Aoki N, Tango T, Fukuchi K, et al. Analysis of c-myc DNA amplification in non-small cell lung carcinoma in comparison with small cell lung carcinoma using polymerase chain reaction. Clin Exp Med 2001; 2: 105-11.

Mok TS, Wu YL, Thongprasert S, Yang CH, Chu DT, Saijo N, et al. Gefitinib or carboplatin-paclitaxel in pulmonary adenocarcinoma. N Engl J Med 2009; 361(10): 947-57.

Montagna C, Lyu MS, Hunter K, Lukes L, Lowther W, Reppert T, et al. The Septin 9 (MSF) gene is amplified and overexpressed in mouse mammary gland adenocarcinomas and human breast cancer cell lines. Cancer Res 2003; 63(9): 2179-87.

Moon IK, Jarstfer MB. The human telomere and its relationship to human disease, therapy, and tissue engineering. Front Biosci 2007; 12: 4595-620.

Morris CM, Haataja L, McDonald M, Gough S, Markie D, Groffen J, et al. The small GTPase RAC3 gene is located within chromosome band 17q25.3 outside and telomeric of a region commonly deleted in breast and ovarian tumours. Cytogenet Cell Genet 2000; 89(1-2):18-23.

Morrish F, Isern N, Sadilek M, Jeffrey M, Hockenbery DM. c-Myc activates multiple metabolic networks to generate substrates for cell-cycle entry. Oncogene 2009; 28(27): 2485-2491.

Morrish F, Hockenbery D. Myc and mitochondrial biogenesis. Cold Spring Harb Perspect Med 2014; 4(5). pii: a014225.

Mousley CJ, Tyeryar KR, Vincent-Pope P, Bankaitis VA. The Sec14-superfamily and the regulatory interface between phospholipid metabolism and membrane trafficking. Biochim Biophys Acta 2007; 1771(6): 727-36.

Mueller HJ. The remarking of chromosomes. Collecting Net 1938; 13: 181-98.

Murnane JP, Sabatier L. Chromosome rearrangements resulting from telomere dysfunction and their role in cancer. Bioessays 2004; 26(11): 1164-74.

Neel BG, Gasic GP, Rogler CE, Skalka AM, Ju G, Hishinuma F, et al. Molecular analysis of the c-myc locus in normal tissue and in avian leukosis virus-induced lymphomas J Virol 1982; 44: 158–66.

Nera B, Huang H, Lai T, Xu L. Elevated levels of TRF2 induce telomeric ultrafine anaphase bridges and rapid telomere deletions. Nature Com 2015; 6: 10132.

Nickerson JA, Krockmalnic G, Wan KM, Penman S. The nuclear matrix revealed by eluting chromatin from a cross-linked nucleus. Proc Natl Acad Sci USA 1997; 94(9): 4446-50.

Nikitina T, Woodcock CL. Closed chromatin loops at the ends of chromosomes. J Cell Biol 2004; 166: 161-5.

Noguchi K, Yamana H, Kitanaka C, Mochizuki T, Kokubu A, Kuchino Y. Differential role of the JNK and p38 MAPK pathway in c-Myc- and s-Myc-mediated apoptosis. Biochem Biophys Res Commun 2000; 267(1): 221-7.

Nora GJ, Buncher NA, Opresko PL. Telomeric protein TRF2 protects Holliday junctions with telomeric arms from displacement by the Werner syndrome helicase. Nucleic Acids Res. 2010; 38(12): 3984-98.

Nurwidyan F, Takahashi F, Murakami A, Kobayashi I, Kato M, Shukuya T, et al. Acquired resistance of non-small cell lung cancer to epidermal growth factor receptor tyrosine kinase inhibitors. Respir Investig 2014; 52: 82–91.

Ohno S, Babonits M, Wiener F, Spira J, Klein G, Potter M. Non-random chromosome changes involving Ig gene chromosomes (Nos.12 and 6) in pristane induced mouse plasmacytoma. Cell. 1979; 16: 1001-7.

Ohno S, Migita S, Wiener F, Babonits M, Klein G, Mushinski JF, et al. Chromosomal translocation activating myc sequences and transduction of v-abl are critical events in the rapid induction in plasmacytomas by pristane and Abelson virus. J Exp Med 1984; 159: 1762-77.

Ooi AT, Gower AC, Zhang KX, Vick JL, Hong LS, Nagao B, et al. Molecular profiling of premalignant lesions in lung squamous cell carcinomas identifies mechanisms involved in stepwise carcinogenesis. Cancer Prev Res (Phila) 2014; 7(5): 487-95.

Orian A, van Steensel B, Delrow J, Bussemaker HJ, Li L, Sawado T, et al. Genomic binding by the Drosophila Myc, Max, Mad/Mnt transcription factor network. Genes Dev 2003; 17(9): 1101-14.

O'Shea JM, Ayer DE. Coordination of nutrient availability and utilization by MAX- and MLX-centered transcription networks. Cold Spring Harb Perspect Med 2013; 3(9): a014258.

Park SS, Kim JS, Tessarollo L, Owens JD, Peng L, Han SS, et al. Insertion of c-Myc into Igh induces B-cell and plasma-cell neoplasms in mice. Cancer Res 2005; 65(4): 1306-15.

Park ES, Shaughnessy JD, Gupta S, Wang H, Lee JS, Woo HG, et al. Gene expression profiling reveals different pathways related to Abl and other genes that cooperate with c-Myc in a model of plasma cell neoplasia. BMC Genomics 2007; 8: 302.

Pear WS, Wahlström G, Nelson SF, Axelson H, Szeles A, Wiener F, et al. 6;7 chromosomal translocation in spontaneously arising rat immunocytomas: evidence for c-myc breakpoint clustering and correlation between isotypic expression and the c-myc target. Mol Cell Biol 1988; 8(1): 441-51.

Pederson T. Half a century of "the nuclear matrix". Mol Biol Cell 2000; 11(3): 799-805.

Pelengaris S, Khan M, Evan G. c-Myc: more than just a matter of life and death. Nat Rev Cancer 2002; 2(10): 764-76.

Pelengaris S, Khan M. The many faces of c-Myc. Arch Biochem Biophys 2003; 416(2): 129-36.

Ponzielli R, Katz S, Barsyte-Lovejoy D, Penn LZ. Cancer therapeutics: targeting the dark side of Myc. Eur J Cancer 2005; 41(16): 2485-501.

Poon SS, Martens UM, Ward RK, Lansdorp PM. Telomere length measurements using digital fluorescence microscopy. Cytometry 1999; 36(4): 267-78.

Potter M, Wiener F. Plasmacytoma genes in mice: model of neoplastic development dependent upon chromosomal translocation. Carcinogenesis 1992; 13: 1681-97.

Poulet A1, Buisson R, Faivre-Moskalenko C, Koelblen M, Amiard S, Montel F, et al. TRF2 promotes, remodels and protects telomeric Holliday junctions. EMBO J 2009; 28(6): 641-51.

Prescott J, Wentzensen IM, Savage SA, De Vivo I. Epidemiologic evidence for a role of telomere dysfunction in cancer etiology. Mutat Res 2012; 730(1-2): 75-84.

Presneau N, Dewar K, Forgetta V, Provencher D, Mes-Masson AM, Tonin PN. Loss of heterozygosity and transcriptome analyses of a 1.2 Mb candidate ovarian cancer tumor suppressor locus region at 17q25.1-q25.2. Mol Carcinog 2005; 43(3): 141-54.

Rahl PB, Lin CY, Seila AC, Flynn RA, McCuine S, Burge CB, et al. c-Myc regulates transcriptional pause release. Cell 2010; 141: 432-45.

Rapp UR, Korn C, Ceteci F, Karreman C, Luetkenhaus K, Serafin V, et al. MYC is a metastasis gene for non-small-cell lung cancer. PLoS One 2009; 4(6): e6029.

Raz V, Vermolen BJ, Garini Y, Onderwater JJ, Mommaas-Kienhuis MA, Koster AJ, et al. The nuclear lamina promotes telomere aggregation and centromere peripheral localization during senescence of human mesenchymal stem cells. J Cell Sci 2008; 121(Pt 24): 4018-28.

Razin SV, Borunova VV, Iarovaia OV, Vassetzky YS. Nuclear matrix and structural and functional compartmentalization of the eucaryotic cell nucleus. Biochemistry (Mosc) 2014; 79(7): 608-18.

Ridler TW, Calvard S. Picture thresholding using an iterative selection method. IEEE Trans Syst Man Cybernetics 1978; 8: 630-32.

Risk JM, Evans KE, Jones J, Langan JE, Rowbottom L, McRonald FE, et al. Characterization of a 500 kb region on 17q25 and the exclusion of candidate genes as the familial Tylosis Oesophageal Cancer (TOC) locus. Oncogene 2002; 21(41): 6395-402.

Risser R, Potter M, Rowe WP. Abelson virus-induced lymphomagenesis in mice. J Exp Med 1978; 148(3): 714-26.

Robin JD, Ludlow AT, Batten K, Magdinier F, Stadler G, Wagner KR, et al. Telomere position effect: regulation of gene expression with progressive telomere shortening over long distances. Genes Dev 2014; 28: 2464-76.

Robinson K, Asawachaicharn N, Galloway DA, Grandori C. c-Myc accelerates S- phase and requires WRN to avoid replication stress. PloS one 2009; 4(6): e5951.

Rockwood LD, Torrey TA, Kim JS, Coleman AE, Kovalchuk AL, Xiang S, et al. Genomic instability in mouse Burkitt lymphoma is dominated by illegitimate genetic recombinations, not point mutations. Oncogene 2002; 21(47): 7235-40.

Rosenbaum H, Harris AW, Bath ML, McNeall J, Webb E, Adams JM, et al. An E mu-v-abl transgene elicits plasmacytomas in concert with an activated myc gene. EMBO J 1990; 9(3): 897-905.

Russell SE, McIlhatton MA, Burrows JF, Donaghy PG, Chanduloy S, Petty EM, et al. Isolation and mapping of a human septin gene to a region on chromosome 17q, commonly deleted in sporadic epithelial ovarian tumors. Cancer Res 2000; 60(17): 4729-34.

Rust MJ, Bates M, Zhuang X. Sub-diffraction-limit imaging by stochastic optical reconstruction microscopy (STORM). Nat Methods 2006; 3(10): 793-5.

Saha B, Zitnik G, Johnson S, Nguyen Q, Risques RA, Martin GM, et al. DNA damage accumulation and TRF2 degradation in atypical Werner syndrome fibroblasts with LMNA mutations. Front Genet 2013; 4: 129.

Sakamuro D, Prendergast GC. New Myc-interacting proteins: a second Myc network emerges. Oncogene 1999; 18(19): 2942-54.

Sanchez-Espiridion B, Chen M, Chang JY, Lu C, Chang DW, Roth JA, et al. Telomere length in peripheral blood leukocytes and lung cancer risk: a large case-control study in Caucasians. Cancer Res 2014; 74(9): 2476-86.

Sarkar R, Guffei A, Vermolen BJ, Garini Y, Mai S. Alterations of centromere positions in nuclei of immortalized and malignant mouse lymphocytes. Cytometry A 2007; 71(6): 386-92.

Schaefer LH, Schuster D, Herz H. Generalized approach for accelerated maximum likelihood based image restoration applied to three-dimensional fluorescence microscopy. J Microsc 2001; 204(Pt 2): 99-107.

Schmälter AK, Kuzyk A, Righolt CH, Neusser M, Steinlein OS, Müller S, et al. Distinct nuclear orientation patterns for mouse chromosome 11 in normal B lymphocytes. BMC Cell Biol 2014; 15: 22-31.

Schmälter AK, Righolt CH, Kuzyk A, Mai S. Changes in nuclear orientation patterns of chromosome 11 during mouse plasmacytoma development. Transl Oncol 2015; 8(5): 417-23.

Schmitt CA, Lowe SW. Bcl-2 mediates chemoresistance in matched pairs of primary E(mu)-myc lymphomas in vivo. Blood Cells Mol Dis 2001; 27(1): 206-16.

Seow WJ, Cawthon RM, Purdue MP, Hu W, Gao YT, Huang WY, et al. Telomere length in white blood cell DNA and lung cancer: a pooled analysis of three prospective cohorts. Cancer Res 2014; 74(15): 4090-8.

Sewastianik T, Prochorec-Sobieszek M, Chapuy B, Juszczyński P. Myc deregulation in lymphoid tumors: molecular mechanisms, clinical consequences and therapeutic implications. Biochimica et Biophysica Acta 2014; 1846: 457-67.

Shen M, Cawthon R, Rothman N, Weinstein SJ, Virtamo J, Hosgood HD 3rd, et al. A prospective study of telomere length measured by monochrome multiplex quantitative PCR and risk of lung cancer. Lung Cancer 2011; 73(2): 133-7.

Shen Z. Genomic instability and cancer: an introduction. J Mol Cell Biol 2011; 3(1): 1-3.

Shimi T, Pfleghaar K, Kojima S, Pack CG, Solovei I, Goldman AE, et al. The A- and B-type nuclear lamin networks: microdomains involved in chromatin organization and transcription. Genes Dev 2008; 22: 3409-21.

Shumaker DK, Dechat T, Kohlmaier A, Adam SA, Bozovsky MR, Erdos MR, et al. Mutant nuclear lamin A leads to progressive alterations of epigenetic control in premature aging. Proc Natl Acad Sci USA 2006; 103(23): 8703-8.

Simonet T, Zaragosi LE, Philippe C, Lebrigand K, Schouteden C, Augereau A, et al. The human TTAGGG repeat factors 1 and 2 bind to a subset of interstitial telomeric sequences and satellite repeats. Cell Res 2011; 21: 1028-38.

Smith ED, Kudlow BA, Frock RL, Kennedy BK. A-type nuclear lamins, progerias and other degenerative disorders. Mech Ageing Dev 2005; 126: 447-60.

Smith KA, Stark MB, Gorman PA, Stark GR. Fusions near telomeres occur very early in the amplification of CAD genes in Syrian hamster cells. Proc Natl Acad Sci USA 1992; 89: 5427-31.

Smogorzewska A, de Lange T. Different telomere damage signaling pathways in human and mouse cells. EMBO J 2002a; 21: 4338–48.

Smogorzewska A, Karlseder J, Holtgreve-Grez H, Jauch A, de Lange T. DNA ligase IV-dependent NHEJ of deprotected mammalian telomeres in G1and G2. Curr Biol 2002b; 12: 1635-44.

Stansel RM, de Lange T, Griffith JD. T-loop assembly in vitro involves binding of TRF2 near the 3' telomeric overhang. EMBO J 2001; 20: E5532-40.

Sugiyama H, Weber G, Silva S, Babonits M, Wiener F, Klein G. Studies on the accelerating role of Abelson leukemia virus in murine plasmacytoma development: in vitro infection of spleen cells generated donor type tumors after transfer to pristane treated BALB/c mice. Int J Cancer 1989; 44: 348-53.

Sugiyama H, Silva S, Wang Y, Weber G, Babonits M, Rosén A, et al. Abelson murine leukemia virus transforms preneoplastic Emu myc transgene carrying cells of the B lymphocyte lineage into plasmablastic tumors. Int J Cancer 1990; 46: 845-52.

Sunpaweravong P, Thu KL, Lam WL, Mai S. Assessment of the clinical relevance of 17q25.3 copy number and three-dimensional telomere organization in non-small lung cancer patients. J Cancer Res Clin Oncol 2016; 142(4): 749-56.

Swarnalatha M, Singh AK, Kumar V. The epigenetic control of E-box and Myc- dependent chromatin modifications regulate the licensing of lamin B2 origin during cell cycle. Nucleic Acids Res 2012; 40(18): 9021-35.

Sy SM, Wong N, Mok TS, Tsao MS, Lee TW, Tse G, et al. Genetic alterations of lung adenocarcinoma in relation to smoking and ethnicity. Lung Cancer 2003; 41, 91-9.

Tetko IV, Haberer G, Rudd S, Meyers B, Mewes HW, Mayer KF. Spatiotemporal expression control correlates with intragenic scaffold matrix attachment regions (S/MARs) in Arabidopsis thaliana. PLoS Comput Biol 2006; 2(3): e21. Erratum in PLoS Comput Biol 2006; 2(6): e67.

Thu KL, Vucic EA, Chari R, Zhang W, Lockwood WW, English JC, et al. Lung adenocarcinoma of never smokers and smokers harbor differential regions of genetic alteration and exhibit different levels of genomic instability. PLoS One. 2012; 7(3): e33003.

Thomassen M, Tan Q, Kruse TA. Gene expression meta-analysis identifies chromosomal regions and candidate genes involved in breast cancer metastasis. Breast Cancer Res Treat 2009; 113(2): 239-49. Erratum in: Breast Cancer Res Treat 2009; 113(2): 251-2.

Tran PT, Bendapudi PK, Lin HJ, Choi P, Koh S, Chen J, et al. Survival and death signals can predict tumor response to therapy after oncogene inactivation. Sci Transl Med 2011; 3(103): 103ra99.

Tu WB, Helander S, Pilstal R, Hickman KA, Lourenco C, Jurisica I, et al. Myc and its interactors take shape. Biochim Biophys Acta 2015; 1849(5): 469-83.

Uppal S, Aviv H, Patterson F, Cohen S, Benevenia J, Aisner S, et al. Alveolar soft part sarcoma--reciprocal translocation between chromosome 17q25 and Xp11. Report of a case with metastases at presentation and review of the literature. Acta Orthop Belg 2003; 69(2): 182-7.

Vafa O, Wade M, Kern S, Beeche M, Pandita TK, Hampton GM, et al. c-Myc can induce DNA damage, increase reactive oxygen species, and mitigate p53 function: a mechanism for oncogene-induced genetic instability. Mol Cell 2002; 9(5): 1031-44.

van Belzen N, Diesveld MP, van der Made AC, Nozawa Y, Dinjens WN, Vlietstra R, et al. Identification of mRNAs that show modulated expression during colon carcinoma cell differentiation. Eur J Biochem 1995; 234(3): 843-8.

van Steensel B, Smogorzewska A, de Lange T. TRF2 protects human telomeres from end-to-end fusions. Cell 1998; 92: 401-13.

Varadi A, Grant A, McCormack M, Nicolson T, Magistri M, Mitchell KJ, et al. Intracellular ATP-sensitive K+ channels in mouse pancreatic beta cells: against a role in organelle cation homeostasis. Diabetologia 2006; 49(7): 1567-77.

Vennstrom B, Sheiness D, Zabielski J, Bishop JM. Isolation and characterization of c-myc, a cellular homolog of the oncogene (v-myc) of avian myelocytomatosis virus strain 29. J Virol 1982; 42: 773-9.

Vermolen BJ, Garini Y, Mai S, Mougey V, Fest T, Chuang TC, et al. Characterizing the three-dimensional organization of telomeres. Cytometry A 2005; 67(2): 144-50. Erratum in: Cytometry A 2007; 71(5): 345.

Vourc'h C, Taruscio D, Boyle AL, Ward DC. Cell cycle-dependent distribution of telomeres, centromeres, and chromosome-specific subsatellite domains in the interphase nucleus of mouse lymphocytes. Exp Cell Res 1993; 205(1): 142-51.

Wahlstrom T, Henriksson MA. Impact of Myc in regulation of tumor cell metabolism. Biochim Biophys Acta 2015; 1849(5): 563-9.

Walter J, Schermelleh L, Cremer M, Tashiro S, Cremer T. Chromosome order in HeLa cells changes during mitosis and early G1, but is stably maintained during subsequent interphase stages. J Cell Biol 2003; 160(5): 685-97

Watt R, Nishikura K, Sorrentino J, ar-Rushdi A, Croce CM, Rovera G. The structure and nucleotide sequence of the 5'end of the human c-myc oncogene. Proc Natl Acad Sci USA 1983; 80(20): 6307-11.

Weissinger EM, Mischak H, Goodnight J, Davidson WF, Mushinski JF. Addition of constitutive c-myc expression to Abelson murine leukemia virus changes the phenotype of the cells transformed by the virus from pre-B-cell lymphomas to plasmacytomas. Mol Cell Biol 1993; 13(4): 2578-85.

Wiener F, Babonits M, Spira J, Klein G, Potter M. Cytogenetic studies on the IgA/lambda producing murine plasmacytomas: regular occurrence of T(12;15) translocation. Somatic Cell Genet 1980; 6: 731-8.

Wiener F, Coleman A, Mock BA, Potter M. Non random chromosomal change (trisomy 11) in murine plasmacytomas induced by an ABL MYC retrovirus. Cancer Res 1995; 55: 1181-6.

Wiener F, Schmälter AK, Mowat MR, Mai S. Duplication of subcytoband 11E2 of chromosome 11 is regularly associated with accelerated tumor development in v-abl/myc-induced mouse plasmacytomas. Genes Cancer 2010; 1(8): 847-58.

Wojnarowicz PM, Provencher DM, Mes-Masson AM, Tonin PN. Chromosome 17q25 genes, RHBDF2 and CYGB, in ovarian cancer. Int J Oncol 2012; 40(6): 1865-80.

Wolf E, Lin CY, Eilers M, Levens DL. Taming of the beast: shaping Myc-dependent amplification. Trends Cell Biol 2015; 25(4): 241-8.

Wood AM, Rendtlew Danielsen JM, Lucas CA, Rice EL, Scalzo D, Shimi T, et al. TRF2 and lamin A/C interact to facilitate the functional organization of chromosome ends. Nat Commun 2014; 5: 5467.

Wu CY, Tseng RC, Hsu HS, Wang YC, Hsu MT. Frequent down-regulation of hRAB37 in metastatic tumor by genetic and epigenetic mechanisms in lung cancer. Lung Cancer 2009; 63(3): 360-7.

Xiong C, Zheng F, Wan J, Zhou X, Yin Z, Sun X. The E23K polymorphism in Kir6.2 gene and coronary heart disease. Clin Chim Acta 2006; 367(1-2): 93-7.

Yang D, Xiong Y, Kim H, He Q, Li Y, Chen R, et al. Human telomeric proteins occupy selective interstitial sites. Cell Res 2011; 21: 1013-27.

Ye JZ, Donigian JR, Van Overbeek M, Loayza D, Luo Y, Krutchinsky AN, et al. TIN2 binds TRF1 and TRF2 simultaneously and stabilizes the TRF2 complex on telomeres. J Biol Chem 2004a; 279: 47264-71.

Ye JZ, Hockemeyer D, Krutchinsky AN, Loayza D, Hooper SM, Chait BT, et al. POT1-interacting protein PIP1: A telomere length regulator that recruits POT1 to the TIN2/TRF1 complex. Genes Dev 2004b; 18(14): 1649-54.

Young KH. Yeast two-hybrid: So many interactions, (in) so little time. Biol Reprod 1998; 58(2): 302-11.

Yu D, Thomas-Tikhonenko A. A non-transgenic mouse model for B-cell lymphoma: in vivo infection of p53-null bone marrow progenitors by a Myc retrovirus is sufficient for tumorigenesis. Oncogene 2002; 21(12): 1922-7.

Yu M, Ohira M, Li Y, Niizuma H, Oo ML, Zhu Y, et al. High expression of ncRAN, a novel non-coding RNA mapped to chromosome 17q25.1, is associated with poor prognosis in neuroblastoma. Int J Oncol 2009; 34(4): 931-8.

Zack TI, Schumacher SE, Carter SL, Cherniack AD, Saksena G, Tabak B, et al. Pan-cancer patterns of somatic copy number alteration. Nat Genet 2013; 45(10): 1134-40.

Zbarskii IB, Debov SS. Protein fractions in the cell nuclei. Biokhimiia 1951; 16(5): 390-5.

Zhong Z, Shiue L, Kaplan S, de Lange T. A mammalian factor that binds telomeric TTAGGG repeats in vitro. Mol Cell Biol 1992; 12: 4834–43.

Zink D, Cremer T. Cell nucleus: chromosome dynamics in nuclei of living cells. Curr Biol 1998; 8(9): R321-4.